THE AERONAUTICAL QUARTERLY

A Journal devoted to Aeronautics and the Allied Sciences

Volume XI NOVEMBER 1960 Part 4

CONTENTS

Graphite: A Future Structural Material — *A. J. Kennedy*

Boundary Layers over Infinite Yawed Wings — *J. C. Cooke*

A Small-Bore Pick-Up for the Measurement of Fluctuating Pressures — *R. E. Franklin and R. B. Archbold*

The Aerodynamic Forces Associated with Harmonic Motion of Slender Wings on Stationary Bodies of Revolution — *R. D. Milne*

The Reliability of Multiple Rocket Engines — *Gillian Ruston*

The Quasi-Cylinder of Specified Thickness and Shell Loading in Supersonic Flow — *H. Portnoy*

Review of "Progress in Solid Mechanics," Vol. I, edited by I. N. Sneddon and R. Hill — *W. S. Hemp*

Index to Vol. XI

LONDON

ROYAL AERONAUTICAL SOCIETY

4 HAMILTON PLACE W1

15/-

THE AERONAUTICAL QUARTERLY

Editorial Board

Dr. A. M. BALLANTYNE, T.D., B.Sc., Ph.D., F.R.Ae.S., Hon.F.C.A.I. F.I.A.S. (*Chairman*)

Mr. HAYNE CONSTANT, C.B., C.B.E., M.A., F.R.S., F.R.Ae.S.

Sir HAROLD ROXBEE COX, D.Sc., D.I.C., Ph.D., F.R.Ae.S., F.I.A.S.

Sir WILLIAM FARREN, C.B., M.B.E., M.A., D.Sc., F.R.S. Hon.F.R.Ae.S., Hon.F.I.A.S.

Sir ARNOLD HALL, M.A., F.R.S., F.R.Ae.S.

Sir BENNETT MELVILL JONES, C.B.E., A.F.C., M.A., F.R.S., Hon.F.R.Ae.S., Hon.F.I.A.S.

Sir ALFRED PUGSLEY, O.B.E., D.Sc., F.R.S., F.R.Ae.S.

Sir GEOFFREY TAYLOR, M.A., D.Sc., F.R.S., Hon.F.R.Ae.S.

Dr. P. B. WALKER, C.B.E., M.A., F.R.Ae.S.

Editor—E. C. PIKE, M.A., A.F.R.Ae.S.

Editorial Referees

Aerodynamics

(a) General

Sir LEONARD BAIRSTOW
Mr. D. KEITH-LUCAS
Prof. W. A. MAIR
Mr. L. F. NICHOLSON
Dr. R. C. PANKHURST
Mr. E. F. RELF
Prof. E. J. RICHARDS
Dr. B. THWAITES

(b) Fluid Motion

Dr. G. K. BATCHELOR
Mr. A. FAGE
Dr. D. W. HOLDER
Prof. L. HOWARTH
Dr. W. P. JONES
Dr. J. W. MACCOLL
Prof. J. H. PRESTON
Prof. H. B. SQUIRE
Prof. G. TEMPLE
Prof. G. N. WARD
Prof. A. D. YOUNG

(c) Stability and Control

Mr. L. W. BRYANT
Mr. S. B. GATES
Mr. H. B. IRVING
Mr. G. H. LEE
Mr. M. B. MORGAN
Mr. H. H. B. M. THOMAS

Helicopters and Propellers

Prof. J. A. J. BENNETT
Mr. P. BRETT
Mr. L. G. FAIRHURST
Mr. R. HAFNER
Dr. G. S. HISLOP
Capt. R. N. LIPTROT

Instruments and Electrical Equipment

Dr. G. E. BAIRSTO
Sir GEORGE GARDNER
Dr. C. S. HUDSON
Mr. C. N. JAQUES
Mr. F. W. MEREDITH

Aircraft Design

Mr. R. BOORMAN
Mr. R. M. CLARKSON
Mr. A. N. CLIFTON
Mr. H. H. GARDNER
Mr. H. KNOWLER
Mr. W. E. W. PETTER
Mr. F. H. FOLLICUTT
Dr. A. E. RUSSELL
Mr. R. S. STAFFORD
Mr. W. H. STEPHENS

Radio and Radar

Mr. J. F. ATHERTON
Mr. B. G. GATES
Dr. R. L. SMITH ROSE
Dr. A. M. UTTLEY
Sir ROBERT WATSON-WATT

Aviation Medicine

Dr. K. G. BERGIN
Dr. A. BUCHANAN BARBOUR

Meteorology

Sir DAVID BRUNT
Mr. J. K. HARDY
Prof. P. A. SHEPPARD

Sound

Mr. W. MAKINSON
Mr. F. B. GREATREX
Mr. N. FLEMING

Aircraft Propulsion

Mr. A. D. BAXTER
Mr. A. V. CLEAVER
Sir A. H. ROY FEDDEN
Dr. S. HOOKER
Mr. A. R. HOWELL
Mr. W. H. LINDSEY
Mr. P. LLOYD
Dr. A. W. MORLEY
Dr. E. S. MOULT
Mr. N. S. MUIR
Mr. F. NIXON
Mr. F. M. OWNER
Mr. H. PEARSON
Mr. H. SAMMONS
Prof. O. A. SAUNDERS
Prof. A. G. SMITH

Air Transport

Mr. A. C. CAMPBELL ORDE
Mr. P. G. MASEFIELD
Mr. N. E. ROWE
Mr. B. S. SHENSTONE
Mr. W. TYE

Aircraft Accessories

Mr. A. E. BINGHAM
Mr. W. C. CLOTHIER
Mr. H. G. CONWAY
Sir GEORGE DOWTY
Mr. R. GRAHAM
Mr. C. D. HOLLAND

Performance

Mr. H. DAVIES
Mr. D. R. NEWMAN
Mr. A. H. YATES

Flight Testing

Mr. R. R. DUDDY
Mr. P. A. HUPTON
Mr. E. T. JONES
Mr. S. SCOTT HALL
Mr. H. L. STEVENS

Structures

Prof. J. H. ARGYRIS
Mr. A. J. BARRETT
Mr. A. C. BROWN
Mr. H. L. COX
Mr. D. J. FARRAR
Prof. W. S. HEMP
Prof. R. HILL
Mr. H. B. HOWARD
Col. H. T. JESSOP
Mr. E. D. KEEN
Mr. F. A. KERRY
Dr. D. M. A. LEGGETT
Mr. R. L. LICKLEY
Prof. A. J. SUTTON PIPPARD
Prof. S. C. REDSHAW
Mr. R. H. SANDIFER
Sir RICHARD SOUTHWELL

Fuels and Oils

Mr. E. L. BASS
Dr. J. W. DRINKWATER
Prof. F. H. GARNER
Prof. W. E. GARNER
Dr. K. E. W. RIDLER
Dr. C. G. WILLIAMS

Materials

Dr. L. AITCHISON
Dr. N. P. ALLEN
Mr. G. FORREST
Prof. N. F. MOTT
Mr. L. ROTHERHAM
Dr. H. SUTTON
Dr. C. SYKES

Vibration and Flutter

Mr. E. G. BROADBENT
Prof. A. R. COLLAR
Prof. W. J. DUNCAN
Mr. H. TEMPLETON
Mr. M. O. W. WOLFE

Graphite: A Future Structural Material

A. J. KENNEDY, Ph.D., A.M.I.E.E., F.I.M., F.Inst.P.

(The College of Aeronautics, Cranfield)

SUMMARY: Graphite is a material with unique high-temperature properties. Its strength and modulus increase with temperature up to about 2000-2500° C., in which range it exhibits a higher strength than any known material. The development of new types of graphite (such as pyrolytic graphite, deposited from the vapour) and impregnated graphites, are both significant to future technology. The highly-oriented pyrolytic graphites in particular, with their marked thermal and mechanical anisotropy, and their superior mechanical properties (60×10^3 lb./in.^{2} strength at 2750° C., with 60 per cent ductility) offer distinct possibilities, particularly in composite structures. Graphite sublimes directly from the solid to vapour phase at 3700° C. at atmospheric pressure. As the sublimation energy is high, it is, at least in theory, a very efficient ablating material. It also has a high creep resistance. Surface reactions limit its value, particularly in oxidising environments, and coatings, or other methods of surface protection, are of high importance. The modulus of graphite is low, being about one-half of that for lead at room temperature, increasing with temperature to a maximum in the region of 2200° C. The properties vary in detail from one type of graphite to another, and with the direction in which measurements are made. Graphite has a low density (about 2·0) and is comparatively cheap, so that its low temperature limitations (zero ductility at room temperature) may be offset, at least in part, by a re-appraisal of the design factors. It can be joined and fabricated fairly readily, and appears to be a material of great value to advanced high-temperature projects in the future, where composite assemblies of various kinds will be essential.

1. Introduction

Until very recent times, temperature questions were not of any very serious concern in aircraft structures. Materials for structural applications were evolved largely on the basis of strength/weight ratios and stiffness, although higher speeds, and increased dynamic stressing, brought fatigue resistance into such prominence that this factor has exercised, in latter years, a decisive influence on both design and materials utilisation. While fatigue has also been of concern in the development of propulsion units, deformation of engine components by creep at the operating temperatures has been the controlling materials factor, and the need for materials capable of sustaining working stresses at temperatures around 1000° C. has provided a considerable incentive to recent metallurgical research and development in this direction.

Received August 1960.

[The Aeronautical Quarterly, Vol. XI, November 1960]

THE AERONAUTICAL QUARTERLY

Editorial Board

Dr. A. M. BALLANTYNE, T.D., B.Sc., Ph.D., F.R.Ae.S., Hon.F.C.A.I. F.I.A.S. (*Chairman*)

Mr. HAYNE CONSTANT, C.B., C.B.E., M.A., F.R.S., F.R.Ae.S.

Sir HAROLD ROXBEE COX, D.Sc., D.I.C., Ph.D., F.R.Ae.S., F.I.A.S.

Sir WILLIAM FARREN, C.B., M.B.E., M.A., D.Sc., F.R.S. Hon.F.R.Ae.S., Hon.F.I.A.S.

Sir ARNOLD HALL, M.A., F.R.S., F.R.Ae.S.

Sir BENNETT MELVILL JONES, C.B.E., A.F.C., M.A., F.R.S., Hon.F.R.Ae.S., Hon.F.I.A.S.

Sir ALFRED PUGSLEY, O.B.E., D.Sc., F.R.S., F.R.Ae.S.

Sir GEOFFREY TAYLOR, M.A., D.Sc., F.R.S., Hon.F.R.Ae.S.

Dr. P. B. WALKER, C.B.E., M.A., F.R.Ae.S.

Editor—E. C. PIKE, M.A., A.F.R.Ae.S.

Editorial Referees

Aerodynamics

(a) *General*

Sir LEONARD BAIRSTOW
Mr. D. KEITH-LUCAS
Prof. W. A. MAIR
Mr. L. F. NICHOLSON
Dr. R. C. PANKHURST
Mr. E. F. RELF
Prof. E. J. RICHARDS
Dr. B. THWAITES

(b) *Fluid Motion*

Dr. G. K. BATCHELOR
Mr. A. FAGE
Dr. D. W. HOLDER
Prof. L. HOWARTH
Dr. W. P. JONES
Dr. J. W. MACCOLL
Prof. J. H. PRESTON
Prof. H. B. SQUIRE
Prof. G. TEMPLE
Prof. G. N. WARD
Prof. A. D. YOUNG

(c) *Stability and Control*

Mr. L. W. BRYANT
Mr. S. B. GATES
Mr. H. B. IRVING
Mr. G. H. LEE
Mr. M. B. MORGAN
Mr. H. H. B. M. THOMAS

Helicopters and Propellers

Prof. J. A. J. BENNETT
Mr. P. BRETT
Mr. L. G. FAIRHURST
Mr. R. HAFNER
Dr. G. S. HISLOP
Capt. R. N. LIPTROT

Instruments and Electrical Equipment

Dr. G. E. BAIRSTO
Sir GEORGE GARDNER
Dr. C. S. HUDSON
Mr. C. N. JAQUES
Mr. F. W. MEREDITH

Aircraft Design

Mr. R. BOORMAN
Mr. R. M. CLARKSON
Mr. A. N. CLIFTON
Mr. H. H. GARDNER
Mr. H. KNOWLER
Mr. W. E. W. PETTER
Mr. F. H. POLLICUTT
Dr. A. E. RUSSELL
Mr. R. S. STAFFORD
Mr. W. H. STEPHENS

Radio and Radar

Mr. J. F. ATHERTON
Mr. B. G. GATES
Dr. R. L. SMITH ROSE
Dr. A. M. UTTLEY
Sir ROBERT WATSON-WATT

Aviation Medicine

Dr. K. G. BERGIN
Dr. A. BUCHANAN BARBOUR

Meteorology

Sir DAVID BRUNT
Mr. J. K. HARDY
Prof. P. A. SHEPPARD

Sound

Mr. W. MAKINSON
Mr. F. B. GREATREX
Mr. N. FLEMING

Aircraft Propulsion

Mr. A. D. BAXTER
Mr. A. V. CLEAVER
Sir A. H. ROY FEDDEN
Dr. S. HOOKER
Mr. A. R. HOWELL
Mr. W. H. LINDSEY
Mr. P. LLOYD
Dr. A. W. MORLEY
Dr. E. S. MOULT
Mr. N. S. MUIR
Mr. F. NIXON
Mr. P. M. OWNER
Mr. H. PEARSON
Mr. H. SAMMONS
Prof. O. A. SAUNDERS
Prof. A. G. SMITH

Air Transport

Mr. A. C. CAMPBELL ORDE
Mr. P. G. MASEFIELD
Mr. N. E. ROWE
Mr. B. S. SHENSTONE
Mr. W. TYE

Aircraft Accessories

Mr. A. E. BINGHAM
Mr. W. C. CLOTHIER
Mr. H. G. CONWAY
Sir GEORGE DOWTY
Mr. R. GRAHAM
Mr. C. D. HOLLAND

Performance

Mr. H. DAVIES
Mr. D. R. NEWMAN
Mr. A. H. YATES

Flight Testing

Mr. R. R. DUDDY
Mr. P. A. HUFTON
Mr. E. T. JONES
Mr. S. SCOTT HALL
Mr. H. L. STEVENS

Structures

Prof. J. H. ARGYRIS
Mr. A. J. BARRETT
Mr. A. C. BROWN
Mr. H. L. COX
Mr. D. J. FARRAR
Prof. W. S. HEMP
Prof. R. HILL
Mr. H. B. HOWARD
Col. H. T. JESSOP
Mr. E. D. KEEN
Mr. F. A. KERRY
Dr. D. M. A. LEGGETT
Mr. R. L. LICKLEY
Prof. A. J. SUTTON PIPPARD
Prof. S. C. REDSHAW
Mr. R. H. SANDIFER
Sir RICHARD SOUTHWELL

Fuels and Oils

Mr. E. L. BASS
Dr. J. W. DRINKWATER
Prof. F. H. GARNER
Prof. W. E. GARNER
Dr. K. E. W. RIDLER
Dr. C. G. WILLIAMS

Materials

Dr. L. AITCHISON
Dr. N. P. ALLEN
Mr. G. FORREST
Prof. N. F. MOTT
Mr. L. ROTHERHAM
Dr. H. SUTTON
Dr. C. SYKES

Vibration and Flutter

Mr. E. G. BROADBENT
Prof. A. R. COLLAR
Prof. W. J. DUNCAN
Mr. H. TEMPLETON
Mr. M. O. W. WOLFE

Graphite: A Future Structural Material

A. J. KENNEDY, Ph.D., A.M.I.E.E., F.I.M., F.Inst.P.

(The College of Aeronautics, Cranfield)

SUMMARY: Graphite is a material with unique high-temperature properties. Its strength and modulus increase with temperature up to about 2000-2500°C., in which range it exhibits a higher strength than any known material. The development of new types of graphite (such as pyrolytic graphite, deposited from the vapour) and impregnated graphites, are both significant to future technology. The highly-oriented pyrolytic graphites in particular, with their marked thermal and mechanical anisotropy, and their superior mechanical properties (60×10^3 lb./in.^{2} strength at 2750°C., with 60 per cent ductility) offer distinct possibilities, particularly in composite structures. Graphite sublimes directly from the solid to vapour phase at 3700°C. at atmospheric pressure. As the sublimation energy is high, it is, at least in theory, a very efficient ablating material. It also has a high creep resistance. Surface reactions limit its value, particularly in oxidising environments, and coatings, or other methods of surface protection, are of high importance. The modulus of graphite is low, being about one-half of that for lead at room temperature, increasing with temperature to a maximum in the region of 2200°C. The properties vary in detail from one type of graphite to another, and with the direction in which measurements are made. Graphite has a low density (about 2·0) and is comparatively cheap, so that its low temperature limitations (zero ductility at room temperature) may be offset, at least in part, by a re-appraisal of the design factors. It can be joined and fabricated fairly readily, and appears to be a material of great value to advanced high-temperature projects in the future, where composite assemblies of various kinds will be essential.

1. Introduction

Until very recent times, temperature questions were not of any very serious concern in aircraft structures. Materials for structural applications were evolved largely on the basis of strength/weight ratios and stiffness, although higher speeds, and increased dynamic stressing, brought fatigue resistance into such prominence that this factor has exercised, in latter years, a decisive influence on both design and materials utilisation. While fatigue has also been of concern in the development of propulsion units, deformation of engine components by creep at the operating temperatures has been the controlling materials factor, and the need for materials capable of sustaining working stresses at temperatures around 1000°C. has provided a considerable incentive to recent metallurgical research and development in this direction.

Received August 1960.

[The Aeronautical Quarterly, Vol. XI, November 1960]

The construction of aircraft capable of speeds in the region of Mach 2-3 raises a whole series of new issues as far as materials are concerned, the most obvious being the achievement of skin temperatures of about 100-150°C. This is precisely the temperature range in which the strengths of the conventional aluminium alloys fall off. Creep also starts to become a significant consideration at these temperatures. It may well be possible, by the best use of materials, together with suitable cooling techniques, to retain aluminium alloys as the principal structural materials for such aircraft, but there is no doubt that future technology must be prepared to embark upon quite new ventures in materials if advanced machines, aeronautical or astronautical, are to be successfully brought into being. Were it not for the temperature factor, it is highly likely that the present range of available materials would be adequate, even though improvements are naturally always desirable. The existence of high temperatures, and of rapid rates of heating, transforms the whole scene, not merely because temperature-resistant materials are now required where conventional alloys once sufficed, but because of a whole range of secondary issues which involve weight, compatibility, joining, deformation, conductivity and expansion considerations, as well as many others.

Examination of the range of possible materials, including those elements which are not, as yet, available as practical alloys, shows certain important general trends. Firstly, the higher the melting point, the higher, generally, is the density. This tendency is illustrated by Fig. 1, which also shows the general trend in elastic modulus. Secondly, there is a close relation between melting point and the activation energy for those metallurgical processes dependent on atomic mobility, such as diffusion or high-temperature creep (Fig. 2). The exact significance of this second point would require a fairly detailed metallurgical discussion but it does mean, generally speaking, that for any given set of experimental conditions the rate of the relevant process, such as creep, is slower in those materials with a higher activation energy. Thus much is to be gained, it would seem, by moving to materials with higher melting points, the greatest penalties being those of weight, oxidation resistance and, usually, fabricability. It is not necessary, in the present context, to pursue these questions in detail; they have, anyway, been discussed elsewhere[1]. The main point is that, from a survey of the materials situation in this light, two elements emerge as strong non-conformists: beryllium and the graphitic form of carbon. Both materials have a low density (beryllium 1·82 and graphite approximately 2·0); they both show limited ductility at temperatures low compared with their melting points—at room temperature, beryllium has a ductility of less than one per cent and graphite a zero ductility. Both have hexagonal-type structures, but with important differences, and both are materials of serious significance to advanced engineering. An important distinction between them at the present time is that, while beryllium is extremely expensive, graphite is relatively cheap—at least in conventional form. Even the newer types of graphite, which are certainly technically superior to those manufactured in the traditional manner, are unlikely to be ruled out on grounds of cost. There is also a very great distinction between the two in the matter of temperature resistance: indeed, graphite might be regarded, from one point of view, as the ultimate high-temperature material. The energy required to remove a carbon atom from a layer plane in the graphite lattice is very high—higher than that required for any other

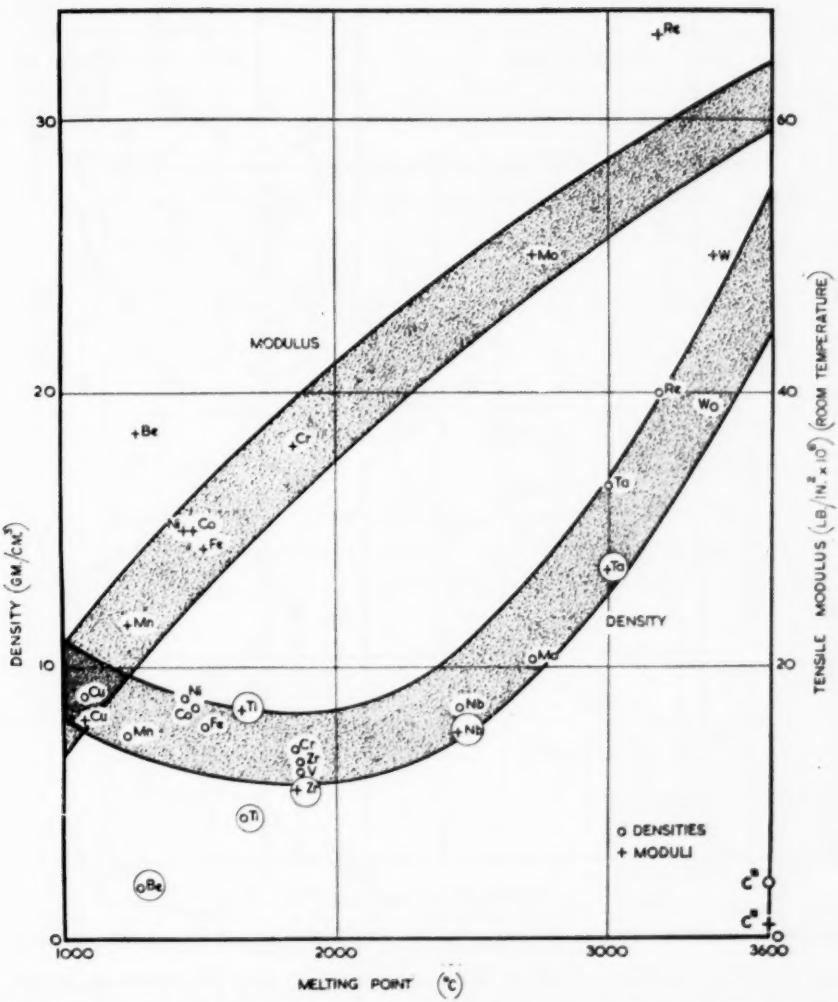

FIGURE 1. The trend of the room-temperature modulus and density of the elements with melting point. Beryllium and graphite are distinct exceptions to the general trend. Graphite (indicated by C★) has no melting point at atmospheric pressure, sublimating directly to the vapour phase at approximately 3,600–3,700°C.

known lattice—and consequently, as graphite sublimes to the vapour phase without any intermediate liquid phase at normal pressures (at about 3700°C.), very large amounts of energy can be removed by ablation. This is of very great advantage, as those materials which melt are liable to be carried away from the surface in the liquid phase, and only the latent heat of melting is utilised. Unfortunately there are factors

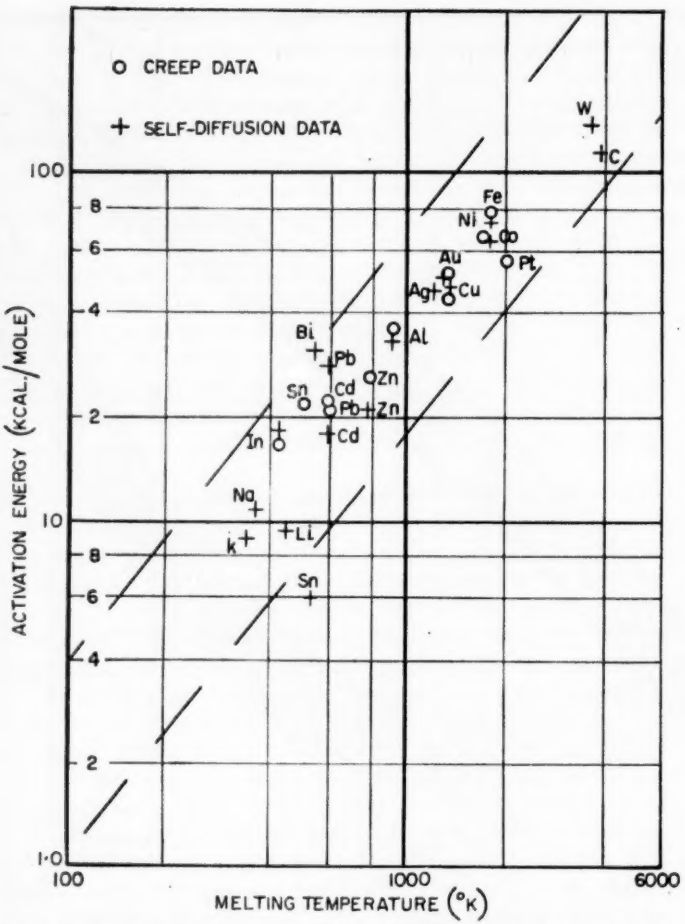

FIGURE 2. Activation energies for creep and for self-diffusion plotted against melting point.

which make it difficult (at least at the present time) to take full advantage of the possibilities that graphite theoretically offers. An assessment of these necessarily requires some appreciation of the fundamental nature of graphite. This is now considered.

2. The Fundamental Nature of Graphite

Graphite is a particular form of carbon structure, the atoms being arranged in planes made up of carbon rings, the carbon atoms in the rings being spaced at a distance of 1·45 Å. In the more common form of graphite, these planes are stacked in the ABABA . . . . sequence, that is, every other plane is in alignment, as Fig. 3 shows. The spacing between the planes is 3·348 Å and the interplanar bonding is fulfilled by

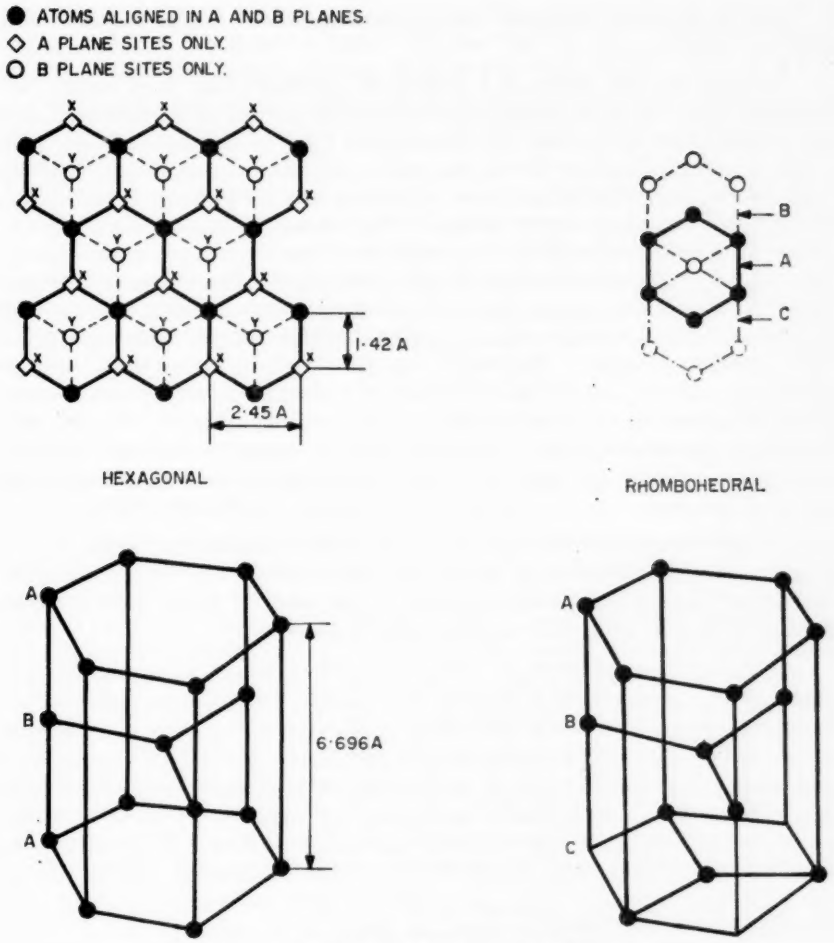

FIGURE 3. The crystal structure of graphite.

van der Waal's forces. In the hexagonal metals, each layer plane is close-packed (each atom has six nearest neighbours, which is equivalent geometrically to adding an extra atom to the centre of each carbon ring) and these planes are arranged in the stacking sequence ABABA . . . . as with the common hexagonal modification of graphite. There is X-ray evidence for the existence of a rhombohedral form of graphite, which is identical in its layer plane structure, the difference being that the planes are stacked in the ABCABC . . . . sequence. This is illustrated by Fig. 3. Such a stacking sequence is characteristic of the face-centred cubic metals. The rhombohedral form is unstable at high temperatures, and can be annealed, as it were, to the hexagonal form at temperatures above 1300°C., at least in artificial graphites.

Like many metals, graphite exhibits twinning, which can be initiated fairly easily.

Graphite certainly differs in a number of significant ways from metals: the character of its interplanar bonding is an obvious example of such a difference. It is also distinguished by the fact that intermediate types of structure, between what might be called amorphous carbon and perfect graphite, exist and indeed represent stages in the graphitisation processes. Such structures are probably best described as ones in which a high degree of order within planes has been achieved—that is, carbon ring formation—without any highly developed ordering in their stacking. This type of arrangement has been termed "turbostratic". These certainly represent important differences, because they do mean that conventional graphites may (and almost invariably do) contain regions which are highly disordered. Such regions have no counterpart in metals: the nearest parallel would be the structure of grain boundaries, but this is not a valid comparison, as such structures are merely highly localised atomic accommodations between two grain orientations. Indeed, such boundaries also exist in graphite. The fact is, then, that materials which are commonly described as graphites may really be no more than highly graphitic, containing regions which are not graphitic at all, with, in addition, considerable flaws and holes.

Another important difference (with real practical applications) is that the graphite lattice is more anisotropic than that of any known metal. This anisotropy covers mechanical, thermal and electrical properties, and arises, of course, from the quite different types of bonding within and between the layers.

In spite of these differences, however, the graphite structure, as such, is one which is amenable to consideration in terms of metal physics. Indeed, at the present time a very great deal can be gained by adapting dislocation theory to the case of the graphite lattice. Such a theory can go a long way, for example, in accounting for the twinning and stacking fault observations[2, 3], and developments in this direction will probably prove of high importance in elucidating the mechanical properties of graphite, as well as the kinetics of the graphitisation process itself. The situation might be summed up by saying that graphite should be accepted as a metal with polymeric tendencies.

3. Graphite Technology

Details of methods of graphite production need hardly be described in a paper of this type. However, some consideration must be given to the manufacturing questions if advances in graphite technology are to be given any just assessment.

First of all, graphite does exist as a natural mineral and often relatively large and pure pieces can be mined—for example in Ceylon. Deposits exist in, among other places, Madagascar, Mexico, Korea, China and Germany, each having its own characteristics and each being utilised, in one way or another, by the graphite industry. As they stand, the natural products are of no commercial use, and must be converted into useful compacts. This can be done by mixing with a suitable binder material and graphitising the whole aggregate or, in one special case, actually compacting small graphitic particles, from which all impurities have been removed, by pressure at high temperatures. The resulting material is very highly oriented and has a

high density of about 2·1, compared with the theoretical density of the graphite lattice of 2·26. This figure is higher than that for the more common artificial graphites, which usually have a density of about 1·8 - 1·9.

Natural graphite can be a useful addition to industrial mixes, but is not in itself the primary source of commercial material. Briefly, the essential production process is as follows.

Carbon artefacts are prepared from the products of the distillation of petroleum and coal. The hard cokes derived from petroleum residues or from the pitch of the coal-distillation process are crushed to powder form, calcined to remove the volatile constituents, and graded into powders with suitable particle size distributions. Lamp black, carbon black or natural graphite fines may, or may not, be blended in. A binder material, which is usually ground pitch, is then added in suitable proportions and the whole is mixed. The mixture is then pressed or extruded. These "green" mixes are then baked at between 900 and 1300°C. under non-oxidising conditions, with the object of achieving the maximum carbon with the minimum of mechanical damage. The blocks of carbon so prepared are then packed into carbon powder and heated to not less than 2500°C. by direct current heating, during which the process of graphitisation proper occurs.

This process of graphitisation is one which has been subjected to much research, but it cannot be said that any real understanding of the controlling factors has yet been achieved, even though a fair amount of knowledge of the character of the structural changes has been acquired[4]. As graphitisation proceeds, the linear dimensions of the graphite crystallites start at about 10-20 Å, but increase rapidly for temperatures over about 1000°C. (which is the temperature at which a rapid evolution of hydrogen occurs). Growth, therefore, seems to be associated with the re-combination of edge atoms made available for bonding by the removal of their attached hydrogen or hydrocarbon groups. For carbon black, the dimensions parallel to the planes, L_a, may reach 100 Å or more (i.e. about 40 rings), depending on the particular material and that normal to the planes, L_c, may reach 50 Å or more (i.e. about 15 planes). This alignment occurs at first without any rotational adjustment, so that orientations about the plane normals are random. As the temperature is raised, pairs of neighbouring planes assume the graphite relation, the actual temperature at which this occurs depending again on the specific material—it can be over 2800°C, although usually rotations begin at about 2000°C. There does seem to be some correlation with L_a in this respect, as nearest neighbour graphitic ordering appears to start when L_c reaches about 100 Å. It has also been possible to detect second neighbour ordering and this has shown that, in the early stages, groups in the ABA and ABC sequences are of equal probability. The retention of bands in the ABCABC . . . . sequence would, of course, result in rhombohedral stacking faults. For prolonged heating, more and more layers orient themselves into the graphitic sequence.

The graphite structure is obviously anisotropic and the coefficient of thermal expansion in the *c*-direction (normal to the layer planes) is about thirty times greater than in the *a*-direction. In cooling, after graphitisation, very great internal stresses can theoretically arise and these could be large enough to break the bonds and form voids. It is argued that the restraints imposed on polycrystalline graphite in this respect are

largely responsible for the inability to achieve the "perfect" graphite density of 2·26, although, of course, the effect may be mitigated, or obscured, by the fact that the starting compacts already contain voids which may not be filled by the graphitisation treatment. This could lead to anomalies. However, it may be important to recognise, in this connection, that the idea of void-creation by anisotropic shrinkage is tenable only if no stress-relieving (recovery) mechanisms operate. In particular, if dislocations are accepted, then the necessary geometrical adaptions during cooling could be readily provided by dislocation generation and movement. It seems likely that some such adaptation does, in fact, take place.

The conventional methods of graphite manufacture necessarily involve the creation of micropores in the material. Considerable research has been devoted, in more recent times, to producing impermeable graphites, particularly for nuclear applications. It might be convenient to divide the pores into two broad types; those which arise at the particle boundaries in the baking processes, due to the loss of the volatile constituents, and those on a smaller scale which make up the misfit boundaries between adjoining crystallites of different relative orientation. While the former may, theoretically, be processed out, there is a limit to the latter contribution, set by the crystallite size. The larger the crystallites, and the greater the degree of preferred orientation, the less the microporosity. This has been confirmed by experiment, showing the crystallite boundary micropores to be about 3 to 8 Å in width. This compares with interparticle voids of, say, 10,000 Å or more.

To sum up: the processes of graphitisation have certain general features which can be recognised and measured, but in detail they depend greatly on the materials used and on the exact graphitising conditions. This variability has made it difficult to establish a proper quantitative theory. The reasons why some carbons graphitise far more readily than others is not understood. For example, an anthracene low temperature char graphitises much more readily than chars from simple benzene derivatives, but, if the conditions are adjusted, graphitisable carbons can be prepared from benzene itself. Not only do the size of the crystallite parameters vary from one type of carbon to another, but so also do the spacings.

It is possible to build up less and less defective graphite by polymerising smaller aromatic molecules at progressively higher temperatures. X-ray studies show that the progress of polymer formation takes place more rapidly with some than with others: carbon polymer from polyvinyl chloride gives a density of 2·25, whereas from polyvinylidene chloride the density limit is 1·59, even after 3000°C. heating.

It does seem that certain types of crystallite boundary are extremely stable, even at very high temperatures, so that if the initial structure is such that these types are developed, then further growth ceases. This is clearly true for lamp black particles where the crystallites grow to the maximum size consistent with the retention of layer-plane surfaces. Surface planes which contain edge-atoms of the layer planes are therefore of high-energy. Growth which involves their creation is therefore impeded unless the energy can be derived from, say, an internal stress field.

The processes of graphite manufacture described here have been evolved to meet the demand for a cheap material for use in electrical and chemical plant. There has

been no commercial incentive, until recent times, for any very high quality, and possibly expensive, product. The situation was changed, in the first place, by the need for an impermeable nuclear-grade material and this stimulated quite new researches, many of which were undertaken, and developed successfully, outside the established graphite industry. The most important of these may be classed as "impregnated graphites", which are considered separately in the following section. It may be observed here that a new stimulus to graphite research and development is now afforded by high-temperature technology, particularly, at present, by rocketry and by re-entry vehicles. Unfortunately, the market for such applications is negligible compared with the huge demands of industrial plant, so that the graphite industry has little incentive to undertake the expensive research and development work necessary if a radical change in the quality and properties of graphite is to be achieved. Much fundamental work is in hand within the industry and this is of the highest quality, but the results are not freely available and, certainly in matters in any way relevant to the processes of production, the closest secrecy is maintained. In an industry where success depends upon specialised techniques, developed to their present state by prolonged experience, such caution is understandable, but it may well be questioned whether it is, in the long term, altogether wise. For one of the consequences of this impenetrable barrier which the industry has set up around itself has been to compel groups with special interests to undertake, on their own account, new lines of work which have yielded advances of great consequence and promise. It can hardly be said to be a credit to the established graphite industry, with its unparalleled resources for research in the field, that the two major advances in graphite technology over the past few years have sprung into prominence because of work carried out in organisations external to that industry. These two particular developments concern impregnation techniques, and the consequent achievement of highly impermeable materials, and pyrolytic graphites, produced by the thermal breakdown of gaseous compounds, such as benzene, methane and propane. This situation is even less understandable when it is realised that the graphite industry has conducted successful research in these fields for many years and has certainly been in a position to launch out with new ventures, but, presumably for economic reasons, has not done so. The result is that at present the materials which seem most promising for aeronautical and space projects are being developed in newly-created organisations which lack the enormous background of knowledge and experience which the major graphite companies have acquired over the years.

4. Pyrolytic Graphite

Carbon deposited from a suitable vapour at sufficiently high temperatures (say 2000°C. and above) can be highly graphitic in structure, with negligible permeability, and strongly oriented crystallographically, the layer planes lying parallel to the deposition surface[5-7]. Such graphite sheets, termed "pyrolytic", are therefore extremely anisotropic, with low conductivity normal to the plane of the sheet and a high conductivity in the plane. Some of the principal properties of products now commercially available are listed in Table I.

TABLE I

SOME PROPERTIES OF PYROLYTIC GRAPHITE

In pyrolytic graphite the ratio of crystallites oriented parallel to the layer planes (*a* direction) to those oriented perpendicular to the layer planes (*c* direction) can be varied from 100 to at least 1000 to 1.

THERMAL PROPERTIES

Thermal conductivity (dependent on process variables) (B.t.u. ft./hr. ft.^{2} °C.)

	a direction	*c* direction
Room temperature	415	3·64
200°C.	395	1·57
400°C.	344	0·63
600°C.	—	0·48
800°C.	—	0·30

Specific heat (B.t.u./lb.°C.)

Room temperature	0·42
250°C.	0·54
500°C.	0·67
750°C.	0·77
1000°C.	0·87

Emissivity

500°C.	0·70
1000°C.	0·77
1500°C.	0·84
1750°C.	0·90

Thermal Expansion Coefficient

a direction	0–140°C.	$-0{\cdot}225\times10^{-6}$/°C.
	400–1050°C.	$2{\cdot}05\times10^{-6}$/°C.
c direction	10–600°C.	$23{\cdot}5\times10^{-6}$/°C.
	600–1050°C.	$25{\cdot}5\times10^{-6}$/°C.

ELECTRICAL PROPERTIES

Resistivity (dependent on process variables), room temperature.

a direction	240 micro-ohm. cm.
c direction	0·5 ohm. cm.

MECHANICAL PROPERTIES

Ultimate Tensile Strength (dependent on process variables) lb./in.^{2}

a direction	Room temperature	16,000–19,000
	2500°C.	33,000
	2700°C.	50,000
c direction	No data	

Young's Modulus (dependent on process variables) lb./in.^{2}

a direction	Room temperature	$1{\cdot}1\times10^6$
	600°C.	$1{\cdot}5\times10^6$

Ultimate Shear (dependent on process variables) lb./in.^{2}

a direction	Room temperature	5,300

Compressive Strength (dependent on process variables) lb./in.^{2}

No data

Transverse Bend Strength (dependent on process variables) lb./in.^{2}

a direction	Room temperature	15,000
	1000°C	30,000
c direction	Not measured	

PHYSICAL AND CHEMICAL PROPERTIES

Density (dependent on process variables)	87·4–140 lb./ft.^{3}
Sublimation Temperature	3700°C.
Latent Heat of Sublimation	56·8 B.t.u./lb.
Triple Point	4200°C; 1250 lb./in.^{2}
Imperviousness	Helium leak tight, 10^{-6} mm. Hg.
Purity	Total impurities 0·1 p.p.m.
Surface Finish (micro-inches)	
As produced	100–500
Polished	1–10
Oxidation Resistance (lb./in.^{2}/mm.) (in air)	
Below 900°C.	1×10^{-5}
Above 2000°C.	1×10^{-4}
Hardness (mohs.)	
a direction	1·0
c direction	4·5

The successful development of techniques for producing large, shaped pieces of pyrolytic graphite has been one of the noteworthy advances of the past year or so. Control of all the process variables, to the required degree, is not easy. For successful products, the conditions of deposition should be constant throughout, which means that the surface at which the hydrocarbons are being broken down and deposited should be held at constant temperature. As the deposit grows, it acts as a layer of low thermal conductivity between the wall and the deposition surface (usually being oriented so that the *c*-direction is normal to the growth face) and this upsets the thermal distribution. The cross sections of the deposits, when examined microscopically, reveal a cone-like growth from the base material. The nature of the deposit is, incidentally, affected by the nature of the substrate, ceramic bases being coated with a compact carbon, while metals and metal oxides give a powdery deposit. It does now seem that fine-cone structures are associated with a high resistance to what is called delamination, or splitting along the layer planes, and the deliberate attempts to produce such materials has resulted in a striking improvement. It has also been a commonplace assumption that higher graphite strength is necessarily associated with a higher density material. This does not seem to be well borne out by some of the pyrolytic work. It is possible to increase the density of such graphites by high temperature annealing, but the resultant strength can be less by a factor of two or so.

5. Impregnation—Filling

The porosity which exists in conventional fine-grain artificial graphites takes the form of interconnecting macropores, about 1 μ in radius, forming a network between the original particles. The possibility of improving the properties of standard commercial grade graphites by attempting to fill these pores is no new idea. It is not, however, so easy to achieve a radical improvement by this means as might be thought. The character of the initial graphite is important, and so also are the details of the impregnation process. Obviously the main interest in this development has been in connection with the use of impermeable graphite in nuclear engineering[8, 9]. The improvements in physical properties generally are of significance, however, in other applications and Fig. 4 shows the extent of these improvements compared with the original starting material.

Technically, the long periods of treatment necessary for the production of impregnated graphites are a disadvantage, but if it were proved that these graphites were particularly outstanding for nozzle applications, then the time factor might well be accepted. It is understood that some new methods of manufacture are now being attempted by gas-cracking in beds of carbonised matted fibres.

The principal method of liquid impregnation depends upon the use of furfuryl alcohol ($C_5H_6O_2$) plus a suitable catalyst, so that polymerisation occurs, yielding a solid resin which is carbonised at 1000°C. to give about 50 per cent carbon. During the carbonisation the resin shrinks uniformly without becoming liquid. As the impermeability is unaffected by high-temperature treatment, the method may be applied to carbons which can subsequently be graphitised. Fine-grained materials appear most suited to this kind of treatment, and it is usual to carry out two impregnations. In the case of tubes, a common one for reactor applications, one impregnation is made

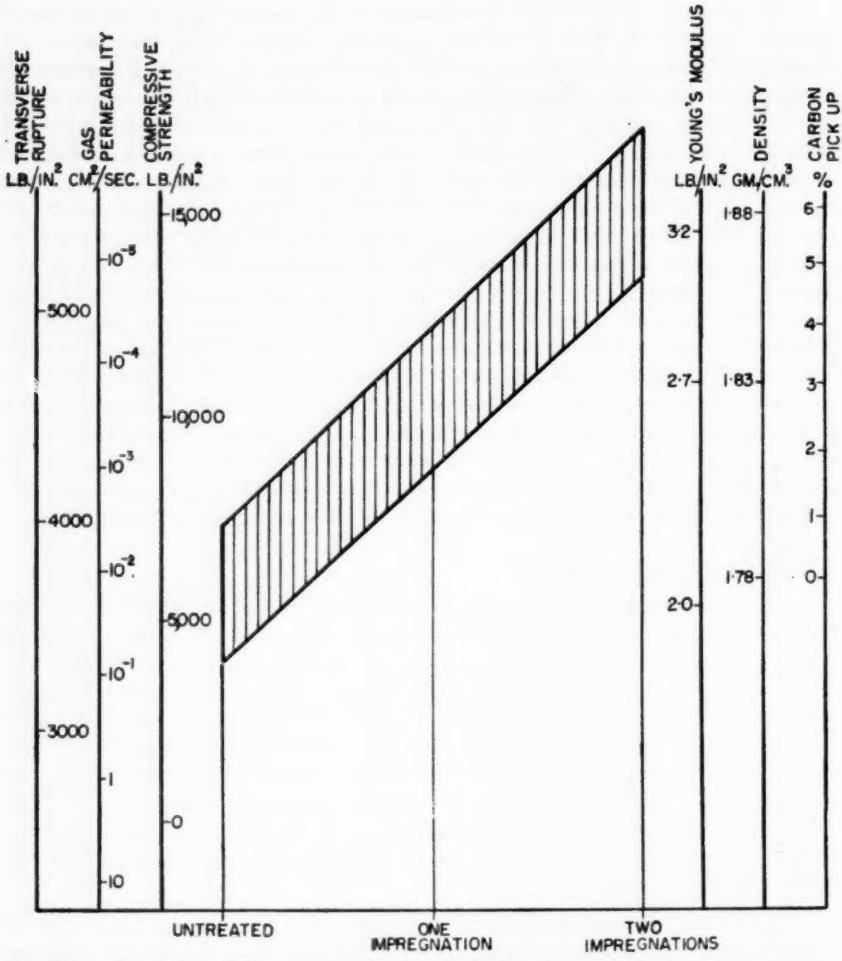

FIGURE 4. The degree of improvement in the properties of conventional graphites brought about by impregnation.

from each side. Considerable improvements in mechanical properties, such as strength and modulus, result from this kind of treatment, as indicated by Fig. 4. The successful use of furfuryl alcohol has naturally led to its being considered as a binder material. Quite large section bars of graphite have been produced with such a binder, and the permeability of the product normal to the extrusion direction was fifty times lower than that of a conventional low-permeability graphite.

Impregnation can also be carried out using normal pitch binder material, but a large number of treatments is required to change the permeability by a factor of a

thousand or so and the process of decomposition is in any case necessarily slow. Impregnation by a concentrated solution (7 per cent by weight) of sugar has proved highly effective. On heating slowly to about 1000°C., the sugar decomposes to leave a residue of carbon in the pores; four to five impregnations can reduce the permeability by a factor of about 10^6. About six or seven such impregnations, followed by one or two impregnations of furfuryl alcohol, result in an approximate doubling of both modulus and strength.

It is also possible to carry out what is virtually a gas impregnation technique, although this might well be classified as a pyrolytic deposition method, particularly as coatings can be applied successfully by this means. In the particular impregnation technique of most interest the pyrolysis is so controlled that it occurs only within the pores of the material, the sealing-up action therefore takes place wholly internally and no surface coating problems arise. With a nitrogen-benzene vapour atmosphere, the transition from surface to internal deposition occurs between 750°C. and 800°C. The weight can increase by about 9 per cent without any dimensional changes, and permeabilities of $1{\cdot}5 \times 10^{-9}$ cm.^{2}/sec. can be achieved.

This temperature range applies to graphites with a mean pore size of about 0·5 micron. A wider temperature range would be needed to make use of a coarser graphite of larger pore size.

One factor of some interest to the high temperature field is that the oxidation rate of the finally graphitised products of this type is about one-twentieth of the original graphite, although these figures relate only to performance at a relatively low temperature (550°C.).

6. Coatings

Graphite is readily oxidised at high temperatures and for successful operation some form of protective coating is required, such as an impervious layer of carbide[10-12]. A large number of research organisations are now engaged in examining methods of coating graphite and, because of the commercial implications, few details can be ascertained. One method is based upon the vaporisation of halides ($NbCl_5$, $TaBr_5$, $ZrBr_4$, for example) at temperatures in the region of 2000°C., at low pressure—a few centimetres of mercury. The carbide coatings deposited (NbC, TaC, and ZrC in the cases quoted) bond well to the graphite, being locked into the porous structure, and they can be made in thicknesses of the order of 1 mm. They appear resistant to thermal cycling and, by using the base carbon to form the carbide, the rate of growth is controlled by diffusion and is, therefore, largely insensitive to the vapour flow conditions.

Profound disagreement exists at present regarding the improvements that the available coatings offer. In the case of silicon carbide (SiC), some quite striking improvements in resistance have been reported for 30 seconds exposures to a stagnation temperature of 3000°K: the actual surface temperature of the carbide may not rise above 2000°C. Other workers in the field have expressed the view that this is an optimistic estimate and, if anything, a coating of 60W 25Cr $15Al_2O_3$ is superior in this temperature range. At the lower temperatures, improvements are easier to obtain

using coatings such as silicon nitride (SiN) and boron nitride (BN). Boron nitride oxidises at 800°C. and silicon nitride oxidises rapidly above 1400°C. Expert views in the matter of coatings research differ very sharply. Many believe that the main weight of research should be concentrated on developing graphite itself to its most resistant form. There is now some sign that this view might be well founded in that pyrolytic graphite has advanced technically very markedly over the past year. Another view is that admixtures of carbides with graphite will prove far more profitable than coatings, as such. Finally, another body of opinion feels that the whole science of coatings is in its very early stages and that continued research in this direction will ultimately pay high dividends.

There seems no reason at present to assume that improvements along each of these three lines could not be exploited to advantage by future technology. There is little doubt that the oxidation resistance of graphite is an important factor, even though for many applications the atmosphere is reducing and not oxidising. If research were to be seriously influenced by this last consideration, then the results might be unfortunate, as it may well be necessary in the future to take up the subject again if highly oxidising fuels are brought into use.

7. Graphite as a Future Structural Material

The foregoing survey has drawn attention to some of the special features which distinguish graphite from other materials, and has indicated the principal classes of graphite at present available: these may be grouped as (*a*) natural, (*b*) conventional artificial, (*c*) impregnated and (*d*) pyrolytic.

If any just assessment is to be made of the part that graphite might play in future technology, then some special examination is required of its mechanical properties[13-19].

The ductility of graphite at temperatures up to about 1500°C. may be taken to be zero. At 2500°C. it is about 5 per cent; at 2700°C., 10 per cent, and about 20 per cent at 3000°C. The basic mechanics of the crystal lattice of graphite, and the exact role that boundaries play in deformation, are so little understood at present that it would be unwise to draw the conclusion that ductility is an inescapable limitation. The stage has now been reached in graphite studies where a real advance in understanding is possible, rather on the lines of that which has taken place in metal physics over the past twenty years or so. It should be remembered, however, that the progress of fundamental studies in crystal mechanics has been made possible, to a large degree, by measurements and observations on the behaviour of single, isolated, metal crystals, and on limited aggregates of crystals. Unfortunately, the successful production of graphite crystals, large enough and perfect enough for serious experiment, has not yet been achieved. The importance of this course of fundamental research cannot be over-emphasised.

One of the interesting facts about the conventional graphites is that their strengths and elastic moduli increase with temperature—at least up to a limit, above which they fall off (Fig. 5). The tensile strength, for example, can approximately double from, say, 3×10^3 lb./in.^{2} at room temperature to 6×10^3 lb./in.^{2} at about 2500°C. The reason

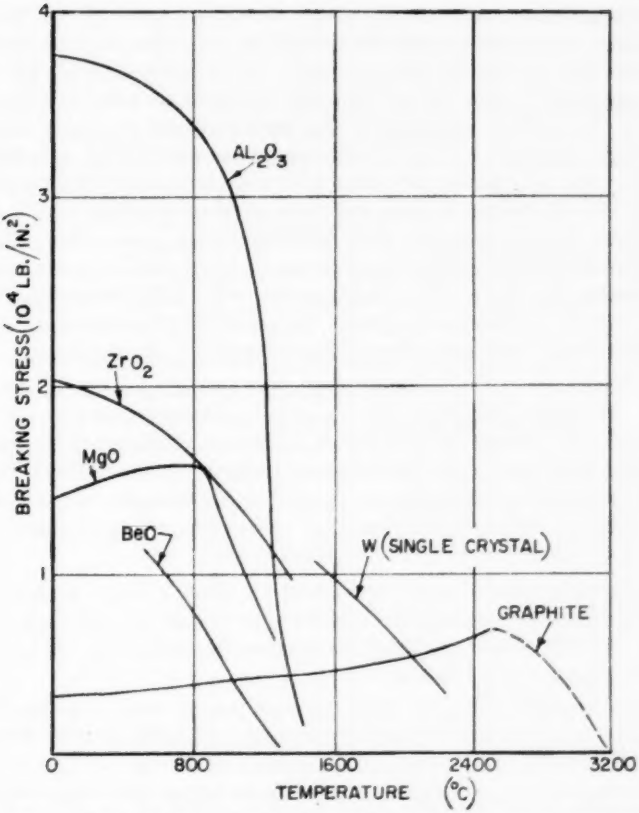

FIGURE 5. The variation of the strength of graphite with temperature compared with that of other materials.

for this increase is not established. It is tempting to think that it is a secondary effect, due to the enhanced plasticity at the higher temperatures, which in turn reduces the severity of any stress concentrations present. In other words, the ability of the material to work-harden at the higher temperatures more than compensates for any true thermal weakening. The same sort of effect is, indeed, observed with other substances, such as the ceramic oxides. It might be expected, then, that the more perfect the graphite, the less evident this strength increase with temperature should be. Such an expectation is not borne out by experiments on pyrolytic graphites, which are highly oriented, and more perfect, and show an increase in strength from about 18×10^3 lb./in.^{2} at room temperature measured parallel to the highly oriented layer planes (this figure being six times higher than that for conventional graphite) to about 33×10^3 lb./in.^{2} at 2500°C. and 50×10^3 lb./in.^{2} at 2700°C. This strength at 2700°C. puts graphite into a class of its own, far higher than the strengths of the refractory metals, rhenium, molybdenum, tantalum and niobium. Few tests have,

in fact, been reported on metals at this temperature, but even at 2000°C. the highest metal strengths, under short-duration loading, are less than 10×10^3 lb./in.^{2} and there is no recorded strength as high, even, as 5×10^3 lb./in.^{2} at 2700°C. The strength of pyrolytic graphite is, then, at least an order of magnitude better at these extreme temperatures. It should be remembered that such graphites are highly anisotropic, and the strength perpendicular to the layer planes is much lower. Although, then, more perfect types of graphite still show the temperature-strengthening effect, the original idea that this results in some way from increased plasticity need not be discarded outright. It does mean that gross inhomogeneities, macropores and the like, are not responsible, and it must be supposed that there are features in the lattice itself which can confer brittleness at low temperatures while being decreasingly effective in this respect as the temperature is raised. The problem is therefore likely to involve dislocations and much must await the outcome of studies in this direction.

The increase in the elastic modulus of graphite with temperature is also a useful feature as far as design is concerned, but is even less well understood than the strength increase. Again, the amount of the change in modulus is a function of the direction in which it is measured—that is, parallel or perpendicular to the layer planes in pyrolytic graphite, or, with conventional graphite, parallel or perpendicular to the direction of extrusion. With pyrolytic graphite ("parallel" measurements) the modulus increases from about $1{\cdot}0 \times 10^6$ lb./in.^{2} to $1{\cdot}5 \times 10^6$ lb./in.^{2} at 600°C.

Conventional graphites, which have about the same Young's modulus parallel to the extrusion direction, increase by about the same amount over the range 0-2000°C. The rigidity modulus of such graphites also increases by nearly 50 per cent up to about 1500-2000°C., above which it falls off.

The creep of graphite exhibits much the same general features as that of metals and appears to be capable of a physical treatment on similar lines[20]. Some creep curves are illustrated by Fig. 6 and an examination of this type of data in terms of activation energy (that is, by plotting creep rate on a logarithmic scale against the reciprocal of absolute temperature for a constant stress) leads to results of the kind shown in Fig. 7. Without entering into any detailed discussion of the physical factors which affect the creep behaviour, it is perhaps worth noting that the values of creep activation energy can be very high—around 200 kcal./mole, approximating to the energy for self-diffusion. Graphite is, then, relatively creep-resistant, in the sense that a high energy is required to activate the elementary creep process. Some caution is required in interpreting this factor, for a high activation energy alone does not necessarily imply a low absolute creep rate. However, in general, resistance to creep at any given temperature is strongly related to the activation energy, and high values are certainly desirable.

Another factor related to that of the creep activation energy is the energy associated with ablation. As was noted previously, the sublimation energy (for the direct solid-vapour transition) of graphite is high, and consequently absorbs a large amount of any heat developed aerodynamically, provided that this heating is sufficient to promote the process in the first place. Depending on the material, actual burning, or depolymerisation, or melting, are all, of course, processes capable of contributing to this energy absorption, but none is theoretically as efficient as the

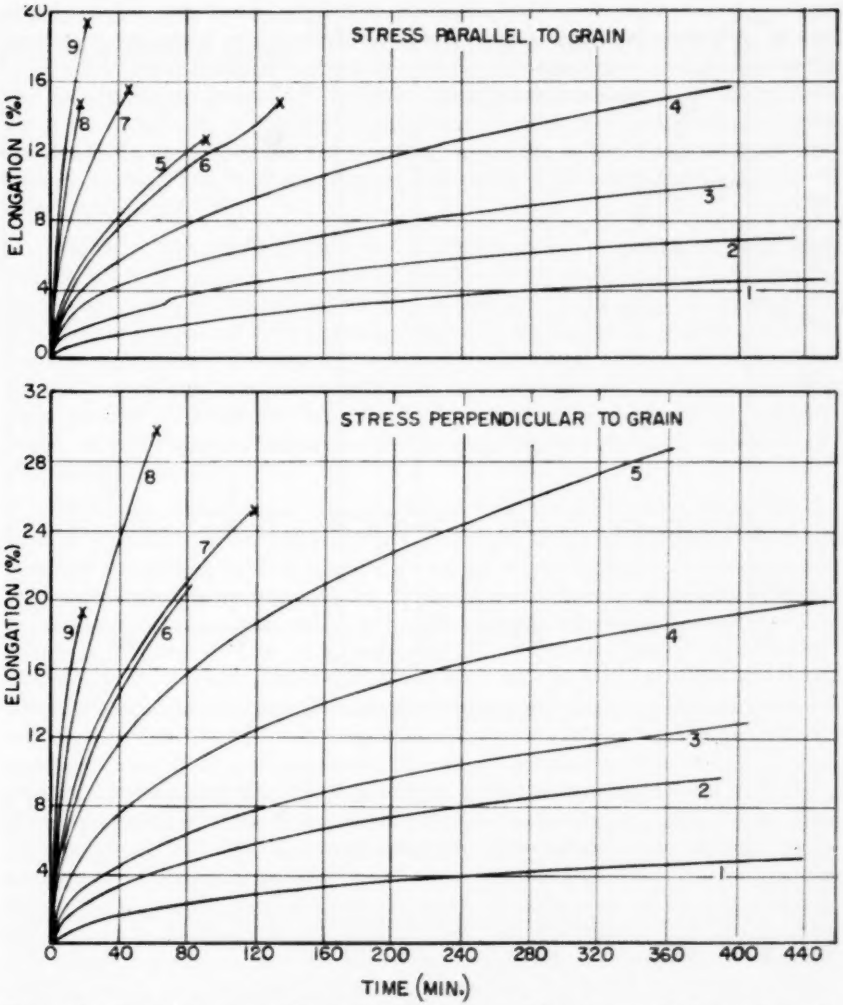

FIGURE 6. Creep tests on graphite at 2,000 lb./in.² parallel and perpendicular to the grain at the following temperatures:—

1. 2443°C. 2. 2504°C. 3. 2565°C. 4. 2621°C. 5. 2682°C.
6. 2738°C. 7. 2809°C. 8. 2854°C. 9. 2916°C.

sublimation of graphite, which is capable of absorbing about 20,000 B.t.u./lb., compared with figures of about 5,000 B.t.u./lb. for plastics, 1,000 B.t.u./lb. for beryllium and 200 B.t.u./lb. for copper. Unfortunately, conventional graphite is a relatively good conductor, with an average coefficient of thermal conductivity, at the lower temperatures, equivalent to magnesium or beryllium. This decreases very

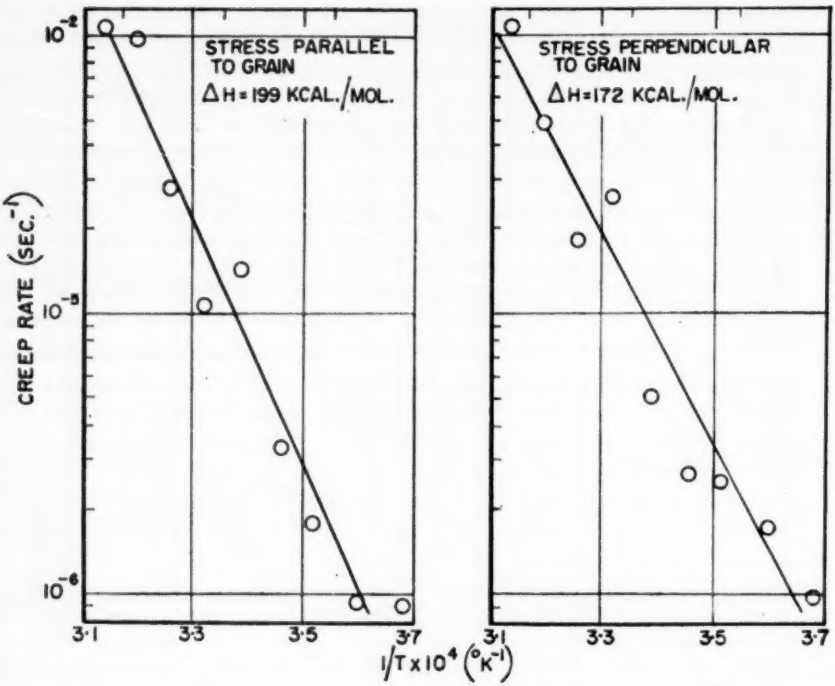

FIGURE 7. Creep rate plotted against $1/T$, as derived from the curves of Fig. 6.

usefully as the temperature is raised, so that at 800°C. the conductivity in the low-conductivity direction (perpendicular to the layer planes) is down to about one-tenth of its value at room temperature. At temperatures of 2000-3000°C. the value is probably as low as one-hundredth of the room-temperature conductivity. In pyrolytic graphite, formed as, say, a casing material, with the layer planes parallel to the surface, this low conductivitv will usefully limit the transmission of heat to the interior. The conductivity parallel to the surface for such graphites is higher by a factor of over 100. This anisotropy in the conductivity may not be of critical importance in thermal protection systems, but raises special design problems for more general structures. The anisotropy in thermal expansion is more troublesome. In the approximate temperature range 0-200°C., the thermal expansion coefficients differ by a factor of 100 in the "parallel" and "perpendicular" directions; at higher temperatures, the ratio approaches 10. Expansion is greater perpendicular to the layer planes ($\simeq 25{\cdot}0\times10^{-6}$/°C.) than it is in the parallel direction ($\simeq 0{\cdot}2\times10^{-6}$/°C. at 150°C., $\simeq 2{\cdot}0\times10^{-6}$/°C. at 1000°C.), and if the graphite were deposited on a metal substrate, the differential expansion parallel to the surface could be serious, steel and beryllium being about 12×10^{-6}/°C., and aluminium and magnesium around 25×10^{-6}/°C. Tungsten, however, is usefully low—about 4×10^{-6}/°C. It should

also be noted that similar differential expansion problems would arise if pyrolytic graphite were coated on a conventional graphite base. Indeed, experiments on such materials in plasma jets have shown that the surface deposit can be fractured by the thermal stresses so created. If, however, the degree of orientation in the graphite could be varied with depth, the surface layers being highly oriented (layer planes parallel to the surface) giving a low conductivity in the perpendicular direction, and with the material becoming gradually more isotropic in the interior, then real benefits might be achieved.

Although high-purity graphite is an abrasive as far as cutting tools are concerned, it can be machined fairly easily, and this is the usual way of manufacturing components. Graphite-graphite bonding is possible, using either a conventional binder or a substance such as furfuryl alcohol, and finally re-graphitising, or by brazing techniques[21]. Copper-silver eutectic alloys have been used in the latter method, by heating *in vacuo* at 950°C., as have titanium and zirconium heated *in vacuo* to 1850°C. Metals can also be joined to graphite by some such brazing technique, so that complex, bonded assemblies are certainly possible, even if technical difficulties still remain.

With such evident virtues it might well be asked why it is that graphite has not been very seriously considered as a high-temperature structural material, even though it is now accepted as the best material for certain specific applications—for example, rocket nozzles. The main reasons are, firstly, that its properties at low temperatures are not acceptable for primary structures, in particular its negligible ductility. The pyrolytic graphites are no better in this respect, although they are somewhat superior[22] above 1650°C. Secondly, conventional graphites show a notorious variation in their properties and no kind of specification exists at the present time. This situation will certainly be improved by the development of the newer types. Thirdly, and perhaps most significant of all, graphite reacts with gases at high temperature and, in particular, burns away in an oxygen environment. If the gas stream impinges on the surface at a high velocity, then erosion also occurs and it is this combined process which really causes most concern at present. Very little is really understood about the mechanics of erosion itself, so that the part that the particular characteristics of the chemical attack might play in the case of graphite are even more difficult to assess. Much fundamental work is now going on, and it is too early to attempt any prediction of the way in which a radical practical improvement might be brought about, but, as this is certainly a major question, a special review will be made of the underlying factors in the following section. Before doing this, it may be timely to comment on the frequently-expressed view that, as the environment in rocket nozzles is usually reducing, not oxidising, the attempts to decrease the oxidation rate at the surface are mis-guided. The main purpose of fundamental surface studies is to elucidate the basic mechanisms of the reactions, and oxidation, apart from its intrinsic interest, provides a clue to some of the more general characteristics of such reactions in graphite. In any case, it would surely be short-sighted to abandon the search for a means of reducing oxidation merely because, at this particular time, in the evolution of a particular technology, oxidation is not the primary problem.

8. Surface Reactions: Some Fundamental and Practical Factors

In the conditions of the rocket nozzle, graphite is eroded by the burning gases. This is particularly severe with the newer high-temperature fuels, such as those containing aluminium. Opinion on the exact mechanism of this erosion, and the factors influencing it, is divided. A microscopic study of certain graphites, which have been widely used in nozzles, after exposure to rocket conditions, has resulted in the conclusion that the attack occurs preferentially at the interfaces of the original particles—that is, in the binder material. Another view is that the presence of metallic particles may seriously accelerate the wear by abrasive action. Yet another is that the effect is worse with the metallic propellants, simply because they operate at higher temperatures and for no other reason. This view is almost equally counterbalanced by the opposite, evidence being cited for the high resistance to erosion of graphite under the action of high-aluminium fuels. This dissension really underlines the fact that erosion is a chemically-activated process and not a question of wear mechanics, at least in the early stages, and that it is very sensitive to the exact combustion conditions.

The possibilities of silicon carbide-silicon boride coatings have been previously noted, attention being drawn to the disagreements which exist at present regarding the temperature range over which such coatings may prove beneficial. In fact the non-uniformity of the attack, once the carbide coating has been eroded through locally, results in a distortion of the nozzle profile which is more deleterious than that brought about by a more uniform wear. Silicon carbide coated graphites fail by the conversion of the silicon carbide to silicon dioxide, which liquifies at 1600°C., and is driven off by the gas stream.

As with all chemical kinetics, the rate of attack, other things being equal, will increase with temperature. The temperature factor alone, however, cannot explain the wear rate, and this explanation may be discarded at the outset. The constituents of the fuels are, however, of great importance, as has been demonstrated by experiments in which magnesium and aluminium fuels were used in similar nozzles at very nearly the same temperature. Only the aluminium-containing fuel eroded the graphite to any serious extent, and this suggests that the important factor is a chemical reaction between some constituent, such as Al_2O_3, and the graphite.

Fundamental studies are clearly required for a proper assessment and certain results recently presented on work which is still in progress [23] are drawn upon here. The nature of the chemical attack on graphite surfaces in reactions with CO_2, O_2, O_3, and O, at temperatures below 1000°C. has been studied by optical and electron microscopy. Hennig finds that metallic particles of Fe, Au, Ag, and W do not act individually in catalysing the reactions, but only when aggregated into larger colloidal particles of about 200 Å diameter. The attack is not on the basal plane but only on the edges of the steps, and then only in certain preferred directions, so that a sort of channelling results. If vacancies are present, however (as produced by irradiation, for example), then the layer planes are attacked at once and pitting results—presumably this accords with the previous observation, the attack being at the edges of the vacancy clusters. Whatever the detailed interpretation of these and other related effects may be, it is clear that the crystallographic nature of the surface, and the

constituents of the gases, are of fundamental importance. The most beneficial surface structure appears to be that presented by the layer plane face, at least for the case of O_2; in fact, chemisorbed O_2 protects the layer planes. On the other hand, O_3 attacks the layer planes direct. The presence of chlorine, bromine and carbon monoxide affects the nature of the attack and slows it down. Grinding, on the other hand, accelerates chemisorption, whereas subsequent annealing retards it.

It is very likely that the binder material (or, more properly, the boundaries) offers sites for preferred attack by O_2, because such boundaries may have a locally more disoriented structure, with a higher concentration of faults and vacancies, and with exposed layer edges. An aspect of this dependence has been demonstrated by natural graphite, of micron size, moulded without a binder up to densities of 2·0. Heat treatment at temperatures up to 3000°C. results in a gradual decrease in the reactivity, at a given temperature, to carbon dioxide; the factor is about 30. The activation energy remains the same (42 kcal./mole), so there is no question of a differing mechanism, the result being due to the reduction in the extent of the vulnerable material by processes of growth and boundary diffusion, and with the consequent dissolution of stress concentrations built up in the moulding process.

The chemical considerations alone are still inadequate, however, in judging the behaviour when the erosion is superimposed upon conditions of thermal shock. Differential expansions in the surface may readily result in the development of microfeatures which are susceptible to attack: the creation of surface steps by slip is an example. This is a field where the crystal mechanics of graphite are relevant, and this part of the fundamental theory is still in its infancy. The actual surface chemistry of graphite is indeed much better developed and paramagnetic resonance techniques have enabled a number of theoretical possibilities to be examined. The details of this work would lead into special technicalities which cannot be pursued here but it should be recorded that these researches are of high importance, and of great relevance to the high-temperature field. As with all properties, the rate of attack and its nature varies greatly between graphites of different origin and pre-treatment. This is consistent with the view that such attack is strongly related to the microstructural detail.

Graphite has a good resistance to thermal shock, a coarse-grained graphite being better in this respect than the finer grades, which usually have better strength characteristics. Decreasing the amount of filler component decreases the thermal shock resistance, so that it would appear that the boundary material is largely responsible for absorbing the anisotropic thermal stresses.

The degree of oxidation-pitting that occurs is dependent on the local concentration of impurity in the graphite, being worse for titanium, vanadium and calcium than with iron and other impurities, at least up to about 1000°C. Va (giving Va_2O_5) plus NaF is a particularly serious catalyst, and the attack (say 2·5 p.p.m. of each) is worse than the sum of the individual rates of each separately. The purity of the graphite is therefore important.

The rate of reaction of carbon with gases is influenced also by the porosity and the amount of internal surface material, and by the diffusivity of the gaseous reactants. At low temperatures the dominant reaction is simply that of chemical attack at all

surfaces, internal and external, and the slower the rate the lower the concentration gradients. This would apply to the phenomena already discussed. As the temperature increases, the reactivity rate increases, the diffusion of the gas through the pores becomes a controlling factor, the effective rate decreases, and the overall activation energy, as measured, decreases. For even higher temperatures, the mass transfer through the boundary gas layer becomes important, this layer decreasing in thickness with increasing gas velocity. It is therefore to be expected that porosity is of importance as a rate-determining factor in oxidation, but this is not significant for temperatures below about 600°C. or so.

Returning to the nature of the burning of graphite, it has been observed that very special surface features are developed. All the layers of the steps which are attacked do not burn off at the same rate and, as a result, a sort of undercutting occurs because of the fact that some planes burn more slowly—these are spaced at about $0{\cdot}5\mu$ with a very regular periodicity even in the most perfect graphite crystals obtainable: again, these experiments are at temperatures below 1000°C.

In measurements made at very high temperatures (2400°C) with gas velocities in the region 20-60 metres/sec. in gases containing about 50 per cent H_2O, there is some evidence that the rate is proportional to the square root of the velocity. The latest series of measurements indicate that the rate of reaction is in the region $3{\cdot}5$ to $5{\cdot}0 \times 10^{-3}$ gm./cm.^{2} sec. at gas velocities of about 50 metres/sec., this rate decreasing with graphite density. The difference between graphitised carbons and simple carbons appears to be small, at least at temperatures of about 2000°C. On the other hand, there is experimental evidence available which shows that pyrolytically deposited carbons have a significantly lower rate of reactivity than either commercial carbons or graphite, by a factor of about 3. In combustion tests of this kind small incandescent grains have been observed in the combustion gases and these appear to be eroded by the burn-up of the interparticle bonds. Incidentally, it is curious that the degree of parallel stacking appears to increase with oxidation; the effect being partly reversed when the oxygen is removed. No very convincing explanation of the effect has been deduced.

There is an almost total lack of correlation between reactivity and many of the bulk measurements such as, resistivity, ash content, degree of crystallinity, so that only direct measurements have any real value.

Pyrolytically-coated graphites have shown about the best resistance to erosion so far obtained but, at the very extreme temperatures, about 3000°C., they simply flake off if there is not a proper thermal matching to the under surface.

Impregnation can be beneficial in a quite different way, in offering a means of energy extraction by vaporisation: for example impregnation with ammonium iodide can hold down the surface temperature for several minutes at a quite high rate of heating. Materials with higher boiling points are, however, required. Impregnation with metals appears unlikely to be of great value. Firstly, the rapid differential thermal expansion at the start of the combustion could result in the fragmentation of the surface layers and, secondly, the metal may well be swept out in the liquid phase, giving little benefit where it is most needed. For a reasonable quantity of such

coolant to be introduced, a fair pore size is required, so that the metal can be absorbed in the graphite structure—at least in the boundaries.

Rare earth additions have been experimented with, such as cerium oxide and aluminium fluoride, but for operation above 2000°C. no really noteworthy advance has been achieved. One difficulty in drawing conclusions from the test results is that they differ greatly with the exact test conditions, so that materials which appear to show improvement in one jet torch are disappointing (and even worse than unimpregnated graphite) when tested in another. The possibilities of impregnation are, however, scantily investigated, as yet, and some real advantages may yet be attained by such means.

The actual admixture of carbides to the graphite mixes has also been investigated, with promising results. Combinations of graphite with B_4C and SiC have resisted temperatures around 1600°C. for some 80 min. without failure by burning. No improvement has been achieved to date by metallic impregnation—for example, with copper.

The actual sublimation of carbon itself, in the graphite form, is the most obvious mechanism to use to advantage. The difficulty is to arrange that such erosion is truly atomic, and not in the form of particles, as it most certainly is at present.

9. Conclusions

It will be evident from the foregoing that graphite offers certain quite unique possibilities as a material in high-temperature structures. These possiblities will not be fully realised unless a number of quite fundamental issues are better understood and unless those designing in graphite appreciate to the full its very special characteristics. The recent improvements achieved in graphites should encourage a certain optimism regarding its ultimate utilisation as a serious structural material, although in the immediate future there are several more limited applications where it could be of real value—as a turbine blade material, for example. In the longer term, it will certainly play an important part in the composite assemblies required to meet the specifications of advanced projects in the future.

References

1. Murphy, A. J. and Kennedy, A. J. Temperature Effects on Material Characteristics. Fourth AGARD Combustion and Propulsion Colloquium, Milan, 1960. Pergamon Press, London.

2. Kennedy, A. J. Dislocations and Twinning in Graphite. *Proceedings of the Physical Society*, 75, 607, 1960.

3. Tsuzuku, T. Dislocations in Graphite Crystals. *Proceedings of the Third International Conference on Carbon*, Buffalo, 1957. Pergamon Press, London, 1959.

4. Bowman, J. C. Imperfections in the Graphite Structure. *Proceedings of the First and Second International Conferences on Carbon*, Buffalo. University of Buffalo, 1956.

5. Bradshaw, F. J. and Wheeler, C. Some Interesting Properties of Pyrolytic Carbon: Deformation of Deposited Carbon. *Journal of Less Common Metals*, Vol. 1, p. 101, 1959.

6. Brown, A. R. G., Clark, D., and Easterbrook, J. Some Interesting Properties of Pyrolytic Carbon: Structure and Density. *Journal of Less Common Metals*, Vol. 1, p. 94, 1959.

7. KEON, E. F. The Preparation and Properties of Pyrolytic Graphite. Paper No. 74. *Proceedings of the Fourth International Conference on Carbon*, Buffalo, 1959.

8. BOYLAND, D. A. The Reduction of the Permeability of Graphite. *G.E.C. Atomic Energy Review*, Vol. 2, March 1959.

9. WATT, W., BICKERDIKE, R. L., BROWN, A. R. G., JOHNSON, W., and HUGHES, G. Production of Impermeable Graphite. *Nuclear Power*, February, 1959.

10. ALLEN, J. M., and HARP, J. L. Development of Testing Properties Procedures and Evaluation of Refractory Materials. Wright Air Development Center Technical Report No. 58-682, 1959.

11. JANES, M. Graphite-based Materials for High Temperature Applications. Wright Air Development Center Technical Report No. 57-602, 1958.

12. NUDELMAN, H. B. Zirconium and Boron Carbide Coatings for Graphite. WAL 371'48, Watertown Arsenal Laboratories, U.S.A., June 1957.

13. ADAMS, R. E., and NELSON, H. R. Tensile and Creep Properties of Graphite. Battelle Memorial Institute Report No. BMJ-N-45, May 1950.

14. BINNING, M. S. and BILLING, B. F. The Mechanical Properties in Tension and Compression at Room Temperature and 1000°C. of Three Moulded Carbon Materials. R.A.E. Technical Note Met. 271, 1957.

15. DAVIDSON, H. W., and LOSTY, H. H. W. Elastic and Plastic Properties of Carbon and Graphite. *Mechanical Properties of Non-Metallic Brittle Materials*, p. 219. Butterworths Scientific Publications, 1959.

16. GREEN, L., JR. High-Temperature Compression Testing of Graphite. *Journal of Applied Mechanics*, Vol. 20, p. 289, 1953.

17. MALSTROM, C., KEEN, R., and GREEN, L., JR. Some Mechanical Properties of Graphite at Elevated Temperatures. *Journal of Applied Physics*, Vol. 22, p. 593, 1951.

18. MARTENS, H. E., JAFFE, L. D., and JEPSON, J. E. High Temperature Tensile Properties of Graphites. California Institute of Technology Jet Propulsion Laboratory Report No. 20-326, 1957.

19. MROZOWSKI, S. Mechanical Strength, Thermal Expansion and Structure of Cokes and Carbons. *Proceedings of the First and Second International Conferences on Carbon*. University of Buffalo, 1956.

20. MARTENS, H. E., JAFFE, L. D., and BUTTON, D. D. High-Temperature Short-Time Creep of Graphite. California Institute of Technology Jet Propulsion Laboratory Report No. 20-373, 1958.

21. AVES, R., BAINES, D., JAQUES, T. A. J., and WADE, F. High Temperature Graphite Joints. Atomic Energy Research Establishment. R/M 165, 1958.

22. MARTENS, H. E., and KOTLEVSKY, W. V. Tensile Behaviour of Pyrolytic Graphite at 2,750°C. *Nature*, Vol. 186, p. 960, 1960.

23. HENNIG, G. R. Electron Microscope Studies of Graphite Crystals. *Proceedings of the Fourth International Conference on Carbon*, Buffalo, 1959. (In the press).

Boundary Layers over Infinite Yawed Wings

J. C. COOKE

(Royal Aircraft Establishment, Farnborough)

SUMMARY: A method of calculating turbulent boundary layers on infinite yawed wings is given, making use of a method of calculating turbulent boundary layers due to Spence and of an analogy between three-dimensional and axi-symmetric boundary layers. It is also shown that the displacement thickness is equal to that computed using chordwise components and that the streamwise momentum thickness is approximately equal to the chordwise momentum thickness. Shock-free flow and small boundary layer cross-flow are assumed.

1. Introduction

In dealing with the boundary layers of infinite yawed wings[1, 2] use has generally been made of the " independence principle," by which the chordwise flow may be calculated as though no spanwise flow were present. This only applies for incompressible or isothermal compressible laminar boundary layers. This paper gives a method of calculating the flow in the turbulent incompressible or compressible cases where the independence principle does not apply. It is based on an axially symmetric analogy[9] for general three-dimensional flow.

It is first shown that, in spite of the fact that the independence principle does not always apply, the " displacement thickness " calculated by means of chordwise components is the true displacement thickness in the case of infinite yawed wings.

Assuming small cross-flow in the boundary layer, which in effect means small incidence, the flow is calculated by the axially symmetric analogy, following a streamline of the external flow. For infinite yawed wings it is possible to modify the details of the analysis so that, in effect, the solution proceeds across the span normal to the leading edge. An equation for the momentum thickness is thus obtained and this is very little more complicated than the corresponding two-dimensional equation of Spence[7]. Other properties such as displacement thickness and streamwise skin friction follow.

No attempt is made here to calculate the cross-flow component of flow. This is of little interest when one is assessing the effects of boundary layer on the properties of a wing whose incidence is low enough for the cross-flow to be small. This cross-flow component would of course be required to determine separation, but the method probably becomes less valid as separation is approached.

Received May 1960.

NOTATION

a velocity of sound

B defined in equation (12)

c chord

c_p pressure coefficient

c_f skin friction coefficient

$F(M), G(M)$ defined in equation (12)

$h_{x'}, h_{y'}$ defined in Section 3

H form parameter, $=\delta_{x'}/\theta$

$K = T_e/T_\infty$

M Mach number

p pressure

R Reynolds number

r in Section 6, recovery factor $= 0{\cdot}89$

r radius of analogous axi-symmetric body

s arc measured along a streamline

T temperature

u, v velocity components along axes of x and y

u', v' velocity components along axes of x' and y'

$v_e = U_\infty \sin \Lambda$

U_e velocity outside the boundary layer

$u_e = U_e^2 - U_\infty^2 \sin^2 \Lambda$

x, y, z co-ordinates: x normal to leading edge along the surface, y spanwise, z normal to surface

x', y', z' co-ordinates: x' along the external streamline, z' normal to surface, y' normal to x' and z'

β angle between x and x' co-ordinate axes

δ_x given by equation (1)

$\delta_{x'}$ displacement thickness given by equation (1*a*)

δ^* true displacement thickness

$\theta, \theta_{x'}$ streamwise momentum thickness

$\Theta = \theta (U_e \theta/\nu)^{0{\cdot}2}$

Λ angle of sweep

ν kinematic viscosity

ρ density

$\bar{\rho}$ defined in Section 4

τ_w skin friction

$\phi(H), \psi(H), \chi(H)$ defined in Section 5

Suffixes

e main stream values

0 values at a reference station

∞ values at infinity

r recovery values

m values at a "mean" position

i incompressible values

s values at an isentropic stagnation point

T values at transition.

2. The Independence Principle

In laminar incompressible flow the independence principle is well known for infinite yawed wings. It is that *the chordwise flow may be calculated as if no spanwise flow were present*. It is sometimes thought that the independence principle may be stated as " everything is independent of y," where y is measured along the span, *i.e.* along the generators. It is important to realise that these are *not* the same. It is well known that the independence principle does not hold in turbulent or compressible flow[1, 2] in general, yet if the wing were truly infinite one might expect the second statement "everything is independent of y" to hold even if the first does not. If steady flow is possible at all then the second principle must hold, and there seems to be no reason why steady flow should not be possible. It is assumed that the second statement, called here " Principle II ", holds.

3. Displacement Thickness

In some circumstances it is necessary to know the displacement thickness δ^* in order to assess the effect of the boundary layer on the external flow. δ^* is defined to be the amount by which the body must be deformed or "thickened" in order that the potential flow about such a deformed body will give the same flow outside the boundary layer as the actual flow. We define δ_z by

$$\delta_z = \int_0^\infty \left(1 - \frac{\rho u}{\rho_e u_e}\right) dz, \qquad . \quad . \quad . \quad . \quad (1)$$

u and u_e being the *chordwise* components of the velocity inside and outside the boundary layer, ρ and ρ_e the corresponding densities, and z the distance measured normal to the surface.

We now show that the displacement thickness δ^* is equal to δ_z. The proof follows that of Lighthill for the general three-dimensional case. Lighthill[3]

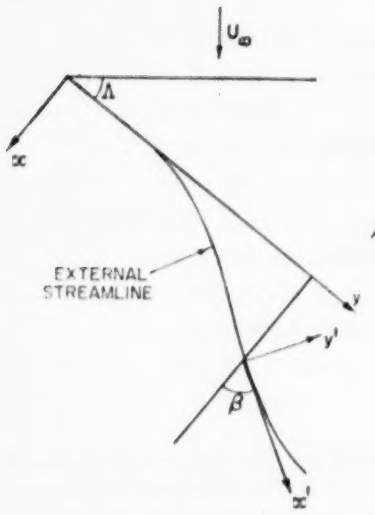

FIGURE 1.

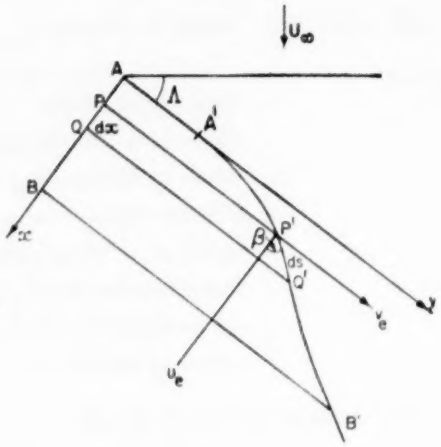

FIGURE 2.

took an element of fluid in the streamwise direction and showed that, if x' and y' are measured along and perpendicular to the external streamlines (*see* Fig. 1),

$$\delta_{x'} = \int_0^\infty \left(1 - \frac{\rho u'}{\rho_e U_e}\right) dz, \qquad . \quad . \quad . \quad . \quad (1a)$$

is not the true displacement thickness, because in obtaining it by flow through a control surface no allowance was made for the fluid flowing into the surface through its sides. When this was accounted for he found that the displacement thickness became

$$\delta^* = \delta_{x'} - \frac{1}{\rho_e U_e h_{y'}} \frac{\partial}{\partial y'} \int_0^x \rho_e U_e \delta_y h_x dx', \qquad . \quad . \quad . \quad (2)$$

where $h_{x'}$ and $h_{y'}$ are determined from the line element in the surface, that is

$$ds^2 = h_{x'}^2 dx'^2 + h_{y'}^2 dy'^2.$$

If axes x and y are taken normal to and along the generators, respectively, then the displacement thickness, as before, can be seen to be δ_x together with a correction term analogous to that in equation (2). However, so long as everything is independent of y the correction term will vanish, since the fluid coming in on one side of the control surface is exactly balanced by the fluid going out the other side. An

analytical proof, starting from equation (2) and transforming the co-ordinates to chordwise and spanwise, can also be given.

Hence, so long as Principle II holds, the displacement thickness δ^* is equal to δ_x, as defined in equation (1). This is so even in turbulent flow and compressible flow, for which the independence principle does *not* apply.

4. Infinite Yawed Cylinders in Incompressible Turbulent Flow

To investigate the development of the boundary layer over infinite yawed wings when the flow is turbulent, it is first necessary to calculate the laminar boundary layer up to transition. For this part, comprehensive accounts have been given by Rott and Crabtree[1] and by Crabtree[2]. The Appendix gives an alternative method.

After transition the independence principle no longer holds. Cooke[4], however, has given reasons for believing that the flow in the *streamwise* direction behaves much as in two dimensions and, on that basis, has derived a momentum equation which applies if taken along an external streamline. He showed that, if θ is the momentum thickness in the streamwise direction, and

$$\Theta = \theta\,(U_e\theta/\nu)^{1/5},$$

then, provided that the cross-flow is small,

$$\frac{\partial}{\partial s}\left\{\frac{\Theta U_e^{14/5}}{\bar{\rho}^{9/5}}\right\} = 0{\cdot}0106\,\frac{U_e^{14/5}}{\bar{\rho}^{9/5}},$$

where U_e is the external velocity along the streamlines, ds is an element of streamline length and $\bar{\rho}$ is a function determined by the external flow conditions.

For an infinite yawed wing, Zaat[5] has shown that

$$\bar{\rho} = \frac{A^2}{u_e^2},$$

where A is a constant and

$$u_e^2 = U_e^2 - U_\infty^2 \sin^2 \Lambda,$$

U_∞ being the velocity at infinity and Λ the angle of sweep.

Hence
$$\frac{\partial}{\partial s}\{\Theta U_e^{14/5} u_e^{6/5}\} = 0{\cdot}0106 U_e^{14/5} u_e^{6/5} \quad . \quad . \quad (3)$$

along a streamline.

As long as Principle II holds, the integral along the curve $A'B'$ (Fig. 2) can be replaced by the integral along AB, since any quantity which has a certain value at P' has the same value at P.

In Fig. 2, $dx = ds \cos \beta$, where $\tan \beta = v_e/u_e$, $v_e = U_\infty \sin \Lambda$, $U_e^2 = u_e^2 + v_e^2$.

$$\text{Hence} \quad \frac{\partial}{\partial s} = \frac{u_e}{U_e} \frac{\partial}{\partial x}. \qquad (4)$$

Integrating (3) with respect to x, and expressing U, u_e, θ and x non-dimensionally in terms of U_∞ and c, we have

$$U_e^3 u_e^{1\cdot2} \theta^{1\cdot2} = \frac{0\cdot0106}{R^{0\cdot2}} \int U_e^{3\cdot8} u_e^{0\cdot2}\, dx + \text{constant}, \qquad (5)$$

where $R = U_\infty c/\nu$.

In this equation x is distance along the *surface* of the wing normal to the generators.

The equation depends on the assumption that the streamwise skin friction takes the same form as that used in two dimensions, namely

$$\frac{\tau_w}{\rho_e U_e^2} = 0\cdot0088 \left(\frac{U_e \theta}{\nu}\right)^{-1/5}.$$

Doubts have sometimes been expressed as to the validity of applying this assumption to three-dimensional flow and these may possibly be justified in general. However the method has been applied[4] to some unpublished experiments by

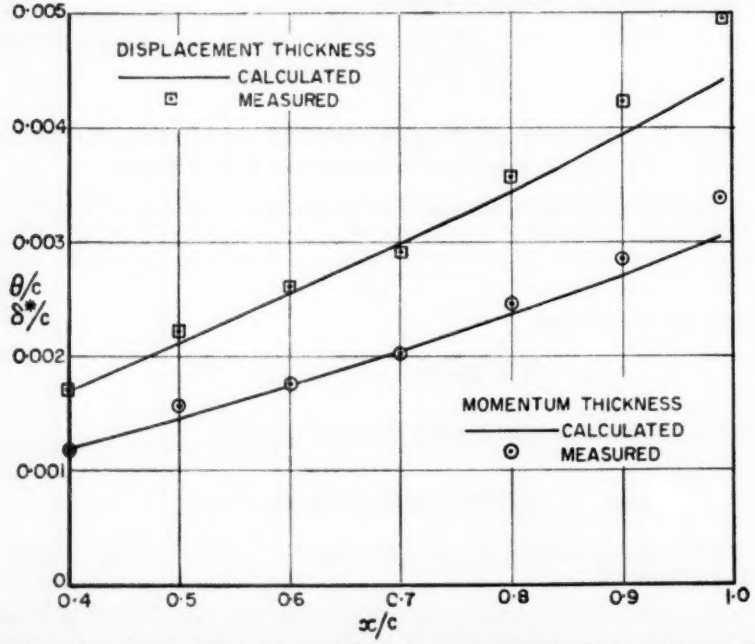

FIGURE 3. Momentum and displacement thickness for swept wing R.A.E. 101, thickness/chord ratio 0·045, angle of sweep 55° (Brebner).

Brebner on the turbulent boundary layer at mid-semi-span of an untapered wing with a sweep angle of 55°. Fig. 3 shows reasonably good agreement between experiments and calculation by the present method for this wing and lends support for the assumptions made in deriving equation (5).

Equation (5) will determine the streamwise momentum thickness at any point, starting from transition, assuming that its value there is known from the laminar calculations and that it is continuous at transition.

Equation (5) may also be obtained by the use of the axisymmetric analogy as applied in Section 6.

5. The Determination of H

If it is required to find the displacement thickness in turbulent flow it is necessary to find H, where

$$H = \delta_{x'}/\theta.$$

Cooke[4] found that, in an example resembling an infinite swept wing, H could be determined from the equation

$$\Theta \frac{dH}{ds} = \phi(H)\left(-\frac{\Theta}{U_e}\frac{dU}{dx}\right) - \psi(H), \qquad . \quad . \quad . \quad (6)$$

the same equation as used by Spence[6] in two dimensions. In this equation

$$\psi(H) = 0{\cdot}00307\,(H-1)^2,$$

$$\phi(H) = 9{\cdot}525\,(H-1{\cdot}21)\,(H-1).$$

Integration of equation (6) gives

$$U_e^3\chi(H) = \text{constant} - 0{\cdot}00135\int^x \frac{U_e^2\,ds}{\Theta},$$

$$\text{where} \quad \chi(H) = 2{\cdot}105 - \frac{0{\cdot}442}{H-1}. \qquad . \quad . \quad . \quad . \quad . \quad (7)$$

Use of equation (4), as before, gives

$$U_e^3\chi(H) = \text{constant} - 0{\cdot}00135\int^x \frac{U_e^3}{u_e\Theta}\,dx. \qquad . \quad . \quad . \quad (8)$$

The initial value of H, at transition, is usually taken as 1·4. If the flow is such that separation is nowhere approached it may be sufficiently accurate to take H as constantly equal to 1·5, instead of attempting to calculate its variation.

6. Infinite Yawed Cylinders in Compressible Turbulent Flow

In the compressible flow case shock-free flow is assumed, except possibly at the leading edge. It is also assumed that μ varies as the absolute temperature raised to the power 8/9.

Spence[7] has given a method of solution in two-dimensional flow, based on these assumptions and that

$$H+1=\frac{T_r}{T_e}(H_i+1), \qquad . \quad . \quad . \quad . \quad (9)$$

where the suffix "i" refers to a corresponding incompressible case, and

$$T_r=T_e\{1+\tfrac{1}{2}r(\gamma-1)M^2\},$$

T_r being the recovery temperature and r the recovery factor, which is taken as 0·89, and M the external Mach number.

Alternatively, from a curve given by Young[6], we may take

$$H=0{\cdot}4M^2+1{\cdot}5, \qquad . \quad . \quad . \quad . \quad . \quad (10)$$

which fits Young's curve well for values of M between 1 and 4. Equation (10) agrees with equation (9) if r is taken as 0·8 and H_i as 1·5.

The skin friction at the surface (τ_w) is given by

$$\frac{\tau_w}{\rho_e U_e^2}=D\frac{\rho_m}{\rho_e}\left(\frac{\rho_e U_e\theta}{\mu_m}\right)^{-1/N}, \qquad . \quad . \quad . \quad . \quad (11)$$

where D and N have their incompressible values, the suffix "m" refers to a "mean" condition relating compressible to incompressible flow, and the suffix "e" refers to flow outside the boundary layer. Spence takes

$$T_m=\tfrac{1}{2}(T_e+T_r)+0{\cdot}22(T_r-T_e)=0{\cdot}28T_e+0{\cdot}72T_r$$

in the case of zero heat transfer, and so

$$T_m=T_e(1+0{\cdot}128M^2).$$

Spence also takes $N=5$, $D=0{\cdot}0088$ and assumes that in the compressible momentum equation H_i may be taken as constant and equal to 1·5.

Spence's[7] equation then becomes

$$\left(\frac{\theta}{c}\right)^{1{\cdot}2}M^{B+0{\cdot}2}G(M)=0{\cdot}0106\left(\frac{a_0 c}{\nu}\right)^{-0{\cdot}2}\int M^B F(M)\,d\left(\frac{x}{c}\right)+\text{constant}, \qquad . \quad . \quad (12)$$

where the suffix 0 refers to an isentropic stagnation point. In this equation it may,

TABLE I

	Zero Heat Transfer	*Constant Wall Temperature* T_w
B	4	$1{\cdot}8\,(T_w/T_e)+2{\cdot}2$
$F(M)$	$\left(\frac{T_e}{T_0}\right)^{3{\cdot}343}\left(\frac{T_m}{T_e}\right)^{-0{\cdot}822}$	$\left(\frac{T_e}{T_0}\right)^{3{\cdot}344}\left(\frac{T_m}{T_e}\right)^{-0{\cdot}822}$
$G(M)$	$(T_e/T_0)^{3{\cdot}765}$	$(T_e/T_0)^{3{\cdot}666}$
T_m/T_e	$1+0{\cdot}128\,M^2$	$\frac{1}{2}\left\{1+0{\cdot}078M^2+\frac{T_w}{T_e}(1+0{\cdot}2M^2)\right\}$
T_e/T_0	$\frac{1+0{\cdot}2M_0^{\,2}}{1+0{\cdot}2M^2}$	

however, refer to any point in the external flow that can be reached isentropically from just outside the boundary layer. a_0 is the velocity of sound at the reference station and B, F and G are found from Table I.

In this table T_e is the temperature at an isentropic stagnation point.

If we write $M=U_e/a_e$ and note that

$$a_e/a_0=(T_e/T_0)^{1/2},$$

Spence's equation becomes, in the case of zero heat transfer,

$$\left(\frac{\theta}{c}\right)^{1{\cdot}2}U_e^{4{\cdot}2}\left(\frac{T_e}{T_0}\right)^{1{\cdot}665}=0{\cdot}0106\left(\frac{c}{\nu_0}\right)^{-0{\cdot}2}\int U_e^4\left(\frac{T_e}{T_0}\right)^{1{\cdot}343}\left(\frac{T_m}{T_e}\right)^{-0{\cdot}822}d\left(\frac{x}{c}\right)+\text{constant},$$

or, expressing U_e, θ and x non-dimensionally in terms of U_0 and c,

$$U_e^{4{\cdot}2}\,\theta^{1{\cdot}2}\left(\frac{T_e}{T_0}\right)^{1{\cdot}665}=\frac{0{\cdot}0106}{R^{0{\cdot}2}}\int U_e^4\left(\frac{T_e}{T_0}\right)^{1{\cdot}343}\left(\frac{T_m}{T_e}\right)^{-0{\cdot}822}dx+\text{constant},$$

where $R=U_0c/\nu_0$.

The axi-symmetric analogy of Cooke[9] asserts that three-dimensional flow along a streamline may be calculated as though it were flow about an axially symmetric body of radius r, provided that the cross-flow in the boundary layer is small. r is connected with $\bar{\rho}$ of Section 4, the relation being

$$r^2=\frac{1}{\bar{\rho}U_e^2},$$

and so, in this case,

$$r=A\frac{u_e}{U_e}.$$

The momentum equation used by Spence, namely

$$\frac{d\theta}{dx} + (H+2-M^2)\frac{\theta}{u_e}\frac{du_e}{dx} = \frac{\tau_w}{\rho_e u_e^2},$$

becomes, in axi-symmetric flow over a body of radius r,

$$\frac{d\theta}{dx} + (H+2-M^2)\frac{\theta}{u_e}\frac{du_e}{dx} + \frac{\theta}{r}\frac{dr}{dx} = \frac{\tau_w}{\rho_e u_e^2}.$$

The effect of this is to add an extra multiplier $r^{1\cdot2}$ in the left-hand side of equation (12) and also in the right-hand side inside the integral, while $d(x/c)$ must be replaced by $d(s/c)$, since the integral is along a streamline.

Using equation (4), we thus obtain

$$U_e^3 u_e^{1\cdot2}\theta^{1\cdot2}\left(\frac{T_e}{T_0}\right)^{1\cdot665} = \frac{0\cdot0106}{R^{0\cdot2}}\int U_e^{3\cdot8}u_e^{0\cdot2}\left(\frac{T_e}{T_0}\right)^{1\cdot343}\left(\frac{T_m}{T_e}\right)^{-0\cdot822}dx + \text{constant}, \qquad (13)$$

where U_e, u_e, θ and x are expressed non-dimensionally in terms of U_0 and c. This should be compared with equation (5).

If there is heat transfer and the wall has a constant temperature T_w, equation (13) is altered by the changed values of B, $F(M)$ and $G(M)$. The result is written in full in Section 8, namely equations (21), (22) and (23).

If it may be assumed that there is no leading edge shock, which should be the case if the sweep is such that the leading edge is subsonic, then infinity may be taken as the reference condition. If, thus, T_0, ν_0 are replaced by T_∞, ν_∞, it can be shown that, if the pressure coefficient is given by

$$c_p = \frac{p_e - p_\infty}{\frac{1}{2}\rho_\infty U_\infty^2},$$

then

$$\left.\begin{aligned}
&\frac{T_e}{T_\infty} = (1+0\cdot7M_\infty^2 c_p)^{2/7} = K \text{ (say)},\\
&M^2 = \frac{5+M_\infty^2}{K} - 5,\\
&\frac{U_e}{U_\infty} = \frac{\sqrt{[(5+M_\infty^2-5K)]}}{M_\infty},\\
&u_e^2 = U_e^2 - U_\infty^2\sin^2\Lambda = \frac{\sqrt{[(5+M_\infty^2\cos^2\Lambda-5K)]}}{M_\infty}.
\end{aligned}\right\} \qquad (14)$$

7. Momentum Thickness at Transition

In equations (5) and (13) the constants are determined by the assumption that the streamwise momentum thickness at transition is continuous. Hence it is necessary to know this thickness at the end of the laminar part of the flow. As already mentioned, the boundary layer over the laminar part may be calculated by the independence principle together with some method such as that of Thwaites[10], if incompressible, or by Crabtree's method[2] if compressible (*see* the Appendix). In either case a chordwise momentum thickness is calculated fairly simply, but to calculate the streamwise momentum thickness is much more difficult. Fortunately the former will be a sufficiently good approximation to use in order to start the turbulent calculations after transition, if incidence is small, as we shall now show.

By the use of laminar methods, the value of the "chordwise" momentum thickness, namely

$$\theta_x = \int_0^\infty \frac{u}{u_e}\left(1 - \frac{\rho u}{\rho_e u_e}\right) dz, \qquad . \quad . \quad . \quad . \quad . \quad (15)$$

is found, while for the turbulent calculation the "streamwise" momentum thickness

$$\theta = \theta_{x'} = \int_0^\infty \frac{u'}{U_e}\left(1 - \frac{\rho u'}{\rho_e u_e}\right) dz \qquad . \quad . \quad . \quad . \quad . \quad (16)$$

is required.

If the axes (x, y) (x', y') are taken in the same sense (both right-handed or both left-handed) and β is the angle between the two axes of x (*see* Fig. 1), we have

$$u' = u \cos\beta + v \sin\beta \qquad . \quad . \quad . \quad . \quad . \quad (17)$$

$$v' = -u \sin\beta + v \cos\beta. \qquad . \quad . \quad . \quad . \quad . \quad (18)$$

If v' is assumed to be small in the laminar flow, equation (18) gives

$$v \simeq u \tan\beta,$$

and so, substituting in equation (17),

$$u' \simeq u \sec\beta.$$

Also, since $v_e' = 0$,

$$U_e = u_e \sec\beta,$$

an equation which is exactly true.

Hence, from equations (15) and (16),

$$\theta \simeq \theta_x$$

and so the chordwise momentum thickness θ_x may be used as an approximation to the starting value of the streamwise momentum thickness θ, after transition.

The same arguments show that $\delta_{x'} \simeq \delta_x = \delta^*$.

8. Summary of Calculation Methods in Turbulent Flow

Writing equations (5) and (13) in full we have, in the incompressible case,

$$U_e^3 u_e^{1\cdot2}\theta^{1\cdot2} = U_{eT}^3 u_{eT}^{1\cdot2}\theta_T^{1\cdot2} + \frac{0\cdot0106}{R^{0\cdot2}}\int_{x_T}^{x} U_e^{3\cdot8} u_e^{0\cdot2}\,dx. \qquad (19)$$

and in the compressible case, for zero heat transfer,

$$U_e^3 u_e^{1\cdot2}\theta^{1\cdot2}\left(\frac{T_e}{T_0}\right)^{1\cdot665} = U_{eT}^3 u_{eT}^{1\cdot2}\theta_T^{1\cdot2}\left(\frac{T_e}{T_0}\right)_T^{1\cdot665} +$$

$$+ \frac{0\cdot0106}{R^{0\cdot2}}\int_{x_T}^{x} U_e^{3\cdot8} u_e^{0\cdot2}\left(\frac{T_e}{T_0}\right)^{1\cdot343}(1+0\cdot128M^2)^{-0\cdot822}\,dx, \qquad (20)$$

where the suffix "T" refers to transition values, x is measured over the surface of the wing normal to the leading edge, and $R = U_0 c/\nu_0$. U_e, u_e, θ and x are here expressed non-dimensionally in terms of U_0 and c.

If there is no leading edge shock, T_0, U_0 and ν_0 may be replaced by T_∞, U_∞ and ν_∞, and if c_p is known, T_e/T_∞, M, U_e/U_∞ and u_e/U_∞ may be found from equations (14).

For a wall of constant temperature T_w, equation (20) is replaced by

$$U_e^{B-1} u_e^{1\cdot2}\theta^{1\cdot2}\left(\frac{T_e}{T_0}\right)^{1\cdot566} = U_{eT}^{B-1} u_{eT}^{1\cdot2}\theta_T^{1\cdot2}\left(\frac{T_e}{T_0}\right)_T^{1\cdot566} +$$

$$+ \frac{0\cdot0106}{R^{0\cdot2}}\int_{x_T}^{x} U_e^{B-0\cdot2} u_e^{0\cdot2}\left(\frac{T_e}{T_0}\right)^{1\cdot244}\left(\frac{T_m}{T_e}\right)^{-0\cdot822} dx \qquad (21)$$

where $$\frac{T_m}{T_e} = \tfrac{1}{2}\left\{1 + 0\cdot078M^2 + \frac{T_w}{T_e}(1+0\cdot2M^2)\right\} \qquad (22)$$

$$B = 2\cdot2 + 1\cdot8\,T_w/T_e, \quad R = U_0 c/\nu_0. \qquad (23)$$

The suffix "s" here refers to an isentropic stagnation point in the free stream. U_e, u_e, θ and x are expressed, as before, non-dimensionally in terms of U_0 and a length c.

The local streamwise skin friction coefficient c_f may be found from equation (11) once θ has been calculated.

In terms of non-dimensional quantities, as before,

$$c_f = \frac{\tau_w}{\frac{1}{2}\rho_0 U_0^2}$$

$$= 0{\cdot}0177 R^{-1/5} U_e^{9/5} \theta^{-1/5} \left(\frac{T_e}{T_0}\right)^{2{\cdot}178} (1 + 0{\cdot}128 M^2)^{-0{\cdot}822} . \qquad (24)$$

For constant wall temperature T_w, the expression $(1 + 0{\cdot}128M^2)^{-0{\cdot}822}$ is replaced by T_m/T_e from equation (22).

For incompressible flow the last two factors of equation (24) are dropped, but a more accurate value may be found by means of the Ludwieg and Tillman formula

$$\frac{\tau_w}{\frac{1}{2}\rho_0 U_0^2} = 0{\cdot}246 \times 10^{-0{\cdot}678H} (R\theta)^{-0{\cdot}268} U_e^{1{\cdot}732} ,$$

again expressed non-dimensionally, provided that H has been determined by equations (7) and (8).

The local momentum thickness $\delta^\star$ is found approximately from

$$\delta^\star = H\theta ,$$

where H is found from equations (7) and (8), or (9) with $H_1 = 1{\cdot}5$, $r = 0{\cdot}89$, or from equation (10).

9. Discussion

In the methods given here it is assumed that the independence principle may not be used, and so the integration proceeds following a streamline and assuming small cross-flow, so that the axisymmetric analogy[9] may be used. The calculations give the streamwise momentum thickness and the " streamwise displacement thickness." If the cross-flow is small, the latter may be taken as a first approximation to the actual displacement thickness. It is also to be understood that in deriving the equations the skin friction component in the streamwise direction is the same as it would be in two-dimensional flow.

No special equation for H is given in the compressible case, and it is supposed that equations (9) or (10) give a sufficiently accurate value.

In the incompressible case a method for finding H is given, but it seems to be of doubtful validity. However, the method gave fair agreement with experiment in one

case where the flow was approximately of the same nature as that considered in this paper[4] (*see* Fig. 3).

It must again be made clear that this paper applies in the main to flow at small incidence and with small cross-flows. Nowhere must separation be approached.

Appendix

Laminar Compressible Flow

Crabtree[2] has pointed out that an approximate solution of the chordwise equation may be obtained by assuming the independence principle to hold and using the Stewartson-Illingworth transformation as in Ref. 1.

This leads to the equation

$$\theta_x^2 = 0{\cdot}45\nu_0 \left(\frac{T_e}{T_0}\right)^{-3} u_e^{-6} \int_0^x \left(\frac{T_e}{T_0}\right)^{1{\cdot}5} u_e^5 dx,$$

and, if $u_e = 0$ at the start (*e.g.* for a rounded leading edge),

$$\left(\frac{\theta_x^2}{\nu_0}\right)_0 = \frac{0{\cdot}075}{(du_e/dx)_0}\left(\frac{T_e}{T_0}\right)^{-0{\cdot}5} \quad . \quad . \quad . \quad . \quad . \quad (25)$$

Alternatively we may again use the axisymmetric analogy and integrate along a streamline.

Since in axially symmetric flow, as shown in Ref. 1,

$$\theta^2 = 0{\cdot}45\nu_0 \left(\frac{T_e}{T_0}\right)^{-3} r^{-2} U_e^{-6} \int_0^s \left(\frac{T_e}{T_0}\right)^{1{\cdot}5} r^2 U_e^5 ds,$$

we have, putting $r = Au_e/U_e$ and using equation (4),

$$\theta^2 = 0{\cdot}45\nu_0 \left(\frac{T_e}{T_0}\right)^{-3} u_e^{-2} U_e^{-4} \int_0^x \left(\frac{T_e}{T_0}\right)^{1{\cdot}5} u_e U_e^4 dx.$$

Expressed non-dimensionally, as before, this equation may be written

$$U_e^4 u_e^2 \theta^2 \left(\frac{T_e}{T_0}\right)^3 = \frac{0{\cdot}45}{R} \int_0^x U_e^4 u_e \left(\frac{T_e}{T_0}\right)^{1{\cdot}5} dx;$$

it has been written in this form so that it may be compared with equation (20).

REFERENCES

1. ROTT, N. and CRABTREE, L. F. Simplified Laminar Boundary-Layer Calculation for Bodies of Revolution and for Yawed Wings. *Journal of the Aeronautical Sciences*, Vol. 19, p. 553, 1952.

2. CRABTREE, L. F. The Compressible Laminar Boundary Layer on a Yawed Infinite Wing. *The Aeronautical Quarterly*, Vol. V, p. 85, 1954.

3. LIGHTHILL, M. J. On Displacement Thickness. *Journal of Fluid Mechanics*, Vol. IV, p. 383, 1958.

4. COOKE, J. C. A Calculation Method for Three-Dimensional Turbulent Boundary Layers. A.R.C. 21059, Oct. 1958. (To be published in the R. & M. series.)

5. ZAAT, J. A. A Simplified Method for the Calculation of Three-Dimensional Laminar Boundary Layers. N.L.L. Report F.184, April 1956.

6. THWAITES, B. (Editor). *Incompressible Aerodynamics*. Oxford University Press. 1960.

7. SPENCE, D. A. The Growth of Compressible Turbulent Boundary Layers on Isothermal and Adiabatic Walls. A.R.C. 21144, June 1959. (To be published in the R. & M. series.)

8. YOUNG, A. D. The Calculation of the Profile Drag of Aerofoils and Bodies of Revolution at Supersonic Speeds. College of Aeronautics Report No. 73. A.R.C. 15970. April 1953.

9. COOKE, J. C. An Axisymmetric Analogue for General Three-Dimensional Boundary Layers. A.R.C. 21386, June 1959. (To be published in the R. & M. series.)

10. THWAITES, B. Approximate Calculation of the Laminar Boundary Layer. *The Aeronautical Quarterly*, Vol. I, p. 245, 1949.

A Small-Bore Pick-Up for the Measurement of Fluctuating Pressures

R. E. FRANKLIN* and R. B. ARCHBOLD†

SUMMARY: The paper describes the development of a small-bore probe microphone, the frequency response of which is smoothed by arranging that the probe tube is terminated in its characteristic impedance.

1. Introduction

The work described in this paper originated in a programme of research on jet noise at the University of Southampton. Most of the work done at the University of Southampton (and indeed elsewhere) on the noise from model jets has been done with standard microphones. This is not entirely satisfactory for the following reasons. When scaling the results obtained from model jets in an attempt to compare them with results obtained from similar experiments on full-size engines, the fact that the pressure-sensitive device, namely the microphone, is the same size in both cases raises the question of the effect of this on scale factors. Again, the results of an experiment in which the diameter of the microphone diaphragm is almost half that of the jet are immediately suspect, for it is not reasonable to assume that a microphone of this size does not affect the geometry of the sound field, particularly if measurements are carried out quite near to the jet. Ideally the measurements taken should be point measurements of the pressures in the sound field and there is clearly a need for a very small microphone for these model tests. Such a microphone would have wide application outside the field of jet noise work; for example, it would be useful for the study of pressure fluctuations in boundary layers, static pressure fluctuations in turbulent flow, and many problems quite outside the field of aeronautics.

The need for a small diameter microphone was felt most acutely at Southampton University when it was decided to initiate experiments on the space-correlation of the pressures in the near noise field of a model jet. In these measurements two microphones are used, one of which is held stationary at some reference point in the pressure field while the other is tracked past it. For certain field separation distances the signals from the two microphones are multiplied together and the average value of their product is computed. The result of this averaging is called the correlation of the two signals and a graph of this correlation against the separation distance is

*Department of Aeronautics, University of Southampton. Now at the Oxford University Engineering Laboratory.
†Post Office Research Station, Dollis Hill, London N.W.2.
Paper received August 1960.

called the correlation curve. Examination of similar work[1] carried out on a full-size engine confirmed an estimate made from purely dimensional considerations that the correlation was likely to vary rapidly in distances of the order of one jet diameter. As a result of this it was clear that, for reasons of physical size and accuracy of measurement, the largest microphones which could be used with a 2 in. diameter model jet would be of 0·125 in. diameter. An examination of the literature showed that the best solution would be obtained by fitting probe attachments to the standard microphones and the most promising of the attachments described in the literature seemed to be that developed at the Post Office Research Station for use with a moving coil microphone[2, 3].

This paper reports a joint investigation carried out at the University of Southampton and the Post Office Research Station into the construction of a probe attachment for a condenser microphone.

2. Principles of Probe Attachments

The problems of design and construction of very small microphones are considerable and, even if they are overcome, one is confronted with the difficulties associated with very low sensitivity. As an alternative, one thinks of using a small bore tube to pick up the pressure fluctuations and then sensing the pressures at the far end of the tube with a standard microphone. This is the principle of the probe microphone.

The probe attachment introduces the question of the transmission of sound along pipes. In passing down a pipe a sound wave has to overcome the inertia of the air in the pipe and its stiffness or acoustical capacitance. Both of these are continuous functions of position along the pipe and so the pipe is a system with distributed constants. The distributed effective mass, stiffness and resistance to flow combine to form a certain impedance, called the characteristic impedance, which is the impedance at any point along an infinite pipe of the same dimensions. There are no reflections in an infinite pipe; further, if a pipe of finite length is arranged to end, or terminate, in another acoustical element, the impedance of which is equal to the characteristic impedance of the pipe, then to a sound wave approaching the end the pipe is effectively infinite and again no reflections occur. If the pipe is terminated in an impedance different from its characteristic impedance, then reflections occur at this impedance discontinuity, the reflected wave being positive or negative as the terminating impedance is greater or less than the characteristic impedance of the pipe. Under these circumstances standing waves can be set up at certain regular frequencies; these frequencies are the resonant frequencies of the pipe*.

It is now clear that a microphone sensing either the pressure in the wall or that at the far end of a probe tube will, in general, indicate pressures different from those at the open end. This is not in itself a difficulty, since the microphone and probe can be calibrated as a unit in terms of the sound pressure at the open end of the tube.

*A pipe is the acoustical equivalent of an electrical transmission line.

The pressure differences can become troublesome in practice, however, if they manifest themselves as undulations in an otherwise smooth sensitivity/frequency characteristic and this is what usually happens. There are several ways of overcoming this. If the tube is made long and its far end is filled with distributed absorbing material, the wave is absorbed before any reflections occur and the pressure sensed with a microphone in the tube wall will be such that it is simply related to the pressure at the open end of the probe, *i.e.* a smooth characteristic will be obtained. Probes built along these lines are described in Refs. 2, 4 and 5. They are usually of fairly large bore and are not suitable for the applications mentioned in Section 1. Alternatively, if the microphone is used to sense the pressure at the far end of the tube, the resonances which occur may be damped out by placing damping material in the tube. This naturally results in a greater loss of sensitivity than that due to attenuation in the simple tube.

If the standard microphone is to be used to sense the pressure at the far end of the tube, then one has to provide a cavity coupler; the probe tube and microphone are fitted into its opposite faces. The cavity will have a certain impedance depending upon its size and, further, the microphone diaphragm will have a certain equivalent acoustical impedance. It seems possible that, by altering the shape and size of the cavity, the combined impedance of the cavity and microphone might be made equal to the characteristic impedance of the probe tube. This method was the one followed in Ref. 3 with very satisfactory results. The work reported in Ref. 3 was mainly concerned with a moving coil microphone; the present work extends this to the condenser microphone.

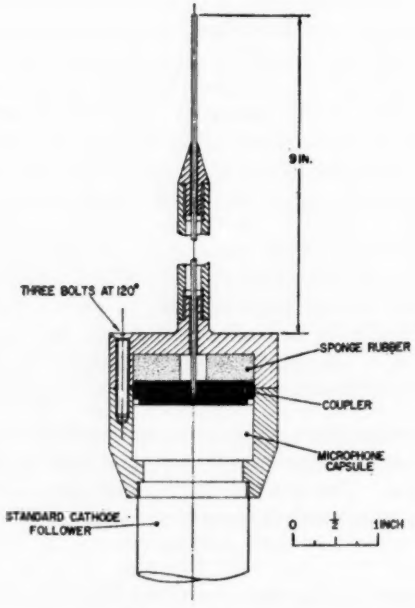

FIGURE 1. Details of probe attachment.

3. Construction of the Probe Attachment

The microphone used at the University of Southampton for standard noise work is the Bruel and Kjaer Condenser Microphone Type 4111, and it was proposed to build a probe attachment to fit this. The final design is as shown in Fig. 1.

In this design the brass body of the attachment has been made fairly thick in order to cut down the transmission of noise through it. For this reason, too, the actual probe tube, which is of stainless steel hypodermic tubing of 0·031 in. inside diameter, is enclosed for most of its length by a thick-walled brass tube; the space between the two tubes may be packed with insulating material, should tests prove this necessary. These precautions are important, in general, because the actual pick-up area of the probe tube is so small; they were particularly important with reference to the application for which the microphones were intended, namely on model jet noise rigs where the ambient noise level is high.

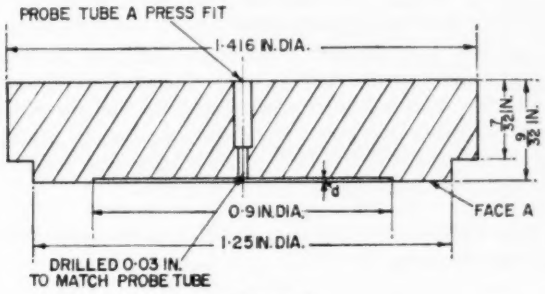

FIGURE 2.

A larger scale sketch of the steel coupler is given in Fig. 2. The Bruel and Kjaer microphone has a flat diaphragm which stands roughly 0·005 in. proud of the capsule. Thus the cavity is cylindrical and of depth d; it is this dimension which is altered (by grinding face A) in adjusting the terminating impedance of the probe tube. The coupler is pressed on to the face of the microphone by the sponge rubber insert shown in Fig. 1, the contact face between coupler and cavity being lightly smeared with Vaseline to prevent air leaks.

4. Calibration of Probes

The probes were calibrated on the Rayleigh Disc Resonance Tube at the Post Office Research Station. In this apparatus the particle velocity at the middle of a resonance tube is measured by the angular deflection of a small, light disc suspended there. One end of the tube is closed by a small loudspeaker and the other by the microphone which is being calibrated. The frequency of the supply to the driving loudspeaker is adjusted until simultaneous maxima of the disc deflection and microphone signal are obtained, indicating that the tube is in resonance. The deflection of the disc then gives the velocity at the velocity anti-node and from this

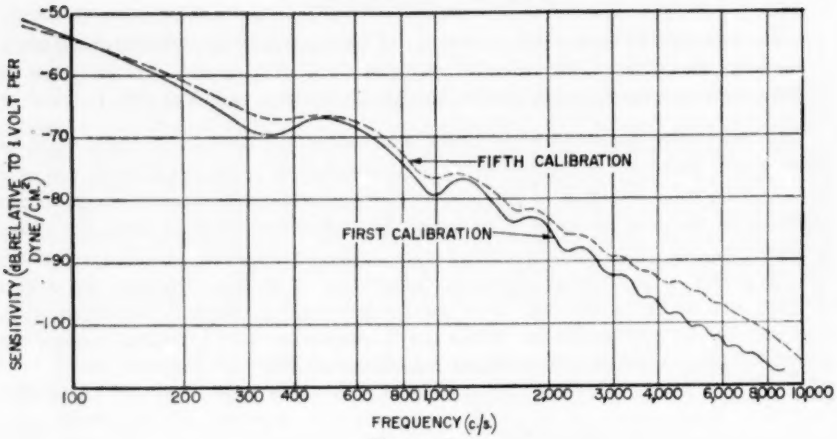

FIGURE 3.

the pressure at the microphone (which is at the pressure anti-node) may be calculated. In practice, once an appropriate frequency has been found, the power to the loudspeaker is adjusted to give a standard deflection of the disc; this results in a standard pressure being applied to the microphone and, from its open circuit e.m.f., the sensitivity of the microphone is known at once.

With this apparatus, the microphone could be calibrated accurately (*i.e.* to within 1/10 dB.) over the range 70–8,000 c./s.

5. Results of Tests

The initial cavity depth was fixed arbitrarily at 0·010 in. and the results of the calibration with this cavity are shown in Fig. 3, where the resonant characteristics of the probe tube may clearly be seen superimposed on a curve which droops because of the friction in the tube and cavity.

The technique was now to reduce the cavity depth by grinding material off face *A* and then to repeat the calibration to determine the effect of the change in dimension. From previous work on the moving coil microphone[3] it was expected that, as the cavity depth was reduced, the peak-to-trough ratio of the resonances would gradually decrease until a smooth curve was obtained, indicating that the probe tube was terminated correctly. In Ref. 3 it is also shown that further decrease in the cavity depth causes the peaks to be replaced by troughs and vice versa (*i.e.* the terminating impedance is reduced to less than the characteristic impedance).

With the condenser microphone it was found that, taking cuts off face *A* of 0·001 in. at a time, the changes from one calibration to the next were very small until the combined impedance of the microphone diaphragm and cavity closely approached the characteristic impedance of the tube. These small changes are probably due to the fact that most of the combined impedance is that of the microphone diaphragm, which is very high, and changes in the cavity impedance have little

effect until the critical stage is reached. As this stage was approached, the cuts taken from face *A* were gradually reduced, finally to 0·0001 in.

The results of the fifth calibration are also plotted in Fig. 3 and illustrate the two main effects of the changes in cavity depth, namely that the peak-to-trough ratio of the resonances is reduced and that the response curve is raised at the higher frequencies.

The final calibration is shown in Fig. 4. For this calibration the cavity depth is estimated at about 0·0015 in., the actual value being difficult to measure because of the danger of puncturing the microphone diaphragm.

With such a drooping characteristic a microphone is unsatisfactory but, if the curve of Fig. 4 is examined, it will be seen that the general slope is about −6 dB. per octave. This may be overcome by designing an amplifier having a gain characteristic rising at +6 dB. per octave to compensate for the fall, and this has been done. The response curve of this amplifier is shown in Fig. 4 and the third curve is the overall response of the probe microphone and amplifier combination. This overall response is almost the same as the frequency response of the original capsule and the gain of the compensating amplifier is conveniently such that the sensitivity is also unaltered.

Finally, it should be noted that the smoothed characteristic of the probe microphone could be appreciably improved at the higher frequencies if a current model of standard microphone were used. It so happened that the model available was specifically designed to have a fall in pressure sensitivity above about 2,000 c./s. in order that the free field sensitivity could be constant with frequency, thus introducing some handicap in the present investigation. With current models advantage could be taken of microphones with constant pressure sensitivity extending over 10,000 c./s.

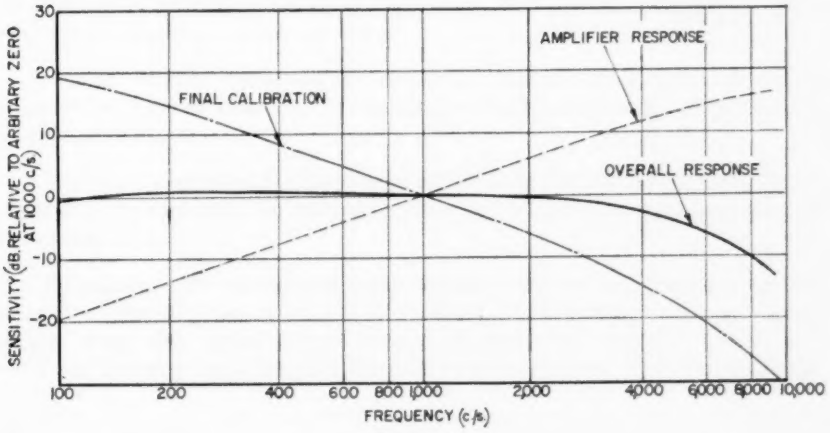

FIGURE 4.

6. Concluding Remarks

It has been shown that a probe attachment of the sort described in Refs. 2 and 3 can be designed for a standard condenser microphone to give a very smooth frequency response, which can be readily equalised to give an overall sensitivity substantially independent of frequency.

For the correlation work mentioned earlier it was necessary to produce a matched pair of probes. This was successfully carried out, the two microphones having responses which differed by less than 0·5 dB. over the useful frequency range.

Acknowledgments

The authors would like to thank Professor E. J. Richards, for the interest he showed in this investigation, and Mr. K. R.McLachlan, who designed the microphone amplifier.

Acknowledgment is also made to the Engineer-in-Chief of the Post Office for permission to make use of information contained in this paper.

References

1. Callaghan, E. E., Howes, W. L. and Coles, D. W. Near Noise Field of a Jet-Engine Exhaust. II. Cross Correlation of Sound Pressures. N.A.C.A. T.N. 3764.

2. West, W. Probe Microphones as Laboratory Standards. *Proceedings of the First International Congress on Acoustics*, Netherlands, 1953.

3. Archbold, R. B. An Experimental Probe Microphone for the Measurement of Sound Pressures. *The Post Office Electrical Engineers' Journal*, Vol. 45, Pt. 4, Jan. 1953.

4. Leonard, R. W. Resistively Terminated Probe Microphone. *Journal of the Acoustical Society of America*, Vol. 24, p. 113 (A), 1952.

5. Goff, K. W. and Mercer, D. M. A. Probe Microphone Analysis and Testing at High Pressures and Intensities. *Journal of the Acoustical Society of America*, Vol. 27, pp. 1004 (A), 1133, 1955.

The Aerodynamic Forces Associated with Harmonic Motion of Slender Wings on Stationary Bodies of Revolution

R. D. MILNE

(Queen Mary College, University of London)

SUMMARY: The slender-body theory is applied to the determination of the unsteady aerodynamic forces on slender wing-body combinations when the body is stationary and the wing is deforming harmonically. The uniform body is circular in cross section, the wings are placed symmetrically and the wing deformation mode is necessarily symmetrical about a vertical plane through the body axis. The frequency parameter is restricted to that range for which the "cross-flow" potential equation is Laplace's equation. The case of an all-moving slender control surface on a body is treated in detail and numerical results are given for the forces and moments on body and control surface when the control plan form is triangular: the presence of a gap is neglected.

1. Introduction

In Ref. 1 the slender body theory is applied to the calculation of the unsteady aerodynamic forces on deforming, slender wings and heaving and pitching, rigid, slender wing-body combinations. This paper deals, in an analogous manner, with the case of the deforming, slender wing on a fixed body of revolution. The necessary conditions on slenderness, frequency parameter and Mach number for which the theory is applicable are briefly set down.

It is an essential restriction of this analysis that the wing motion should be symmetrical in the aeroelastic sense: in addition, in the region of the wings the body is required to be uniform.

Thus for a prescribed harmonic wing deformation the generalised forces on the wings and the associated lift and moment on the wing-body combination may be determined.

By neglecting the presence of a gap between wing root and body the analysis covers the interesting particular case of a combination consisting of the body and a slender wing with hinged control surface or all-moving control. This case is developed in some detail and, for the case of an all-moving control of triangular

Paper received July 1960.

plan form, numerical results are given for the lift and moment on both the combination and on the control due to a harmonic control rotation.

The analysis of this paper, with that of Ref. 1, allows a study of the stability of the general longitudinal motion of a slender wing-body combination with flexible wings and, by an application of the Laplace transform, the calculation of its response characteristics. These applications may be made only to motions which are sufficiently slow that they do not violate the restrictions placed on the frequency parameter.

NOTATION

U free stream velocity

ρ free stream density

a speed of sound in the free stream

M Mach number of the free stream

p_0 free stream pressure

$Oxyz$ right-handed Cartesian co-ordinates

t time

ϕ perturbation velocity potential

ω angular frequency

$\nu = \omega c/U$, frequency parameter

c reference length for the combination

$s(x)$ semi-span of the combination

p local pressure

Δp differential pressure across the wing

$X = y + iz = \zeta e^{i\theta}$, X-plane

$X_1 = y_1 + iz_1 = \zeta_1 e^{i\theta_1}$, X_1-plane

$X_2 = y_2 + iz_2$, X_2-plane

$v, w; v_1, w_1; v_2, w_2$ perturbation velocity components

$f(x, y)$ deformation mode of the wing

R body radius

s_0 semi-span of the combination at the wing trailing edge

$\sigma = R/s_0$

$r = R/s$

$s_1 = s - R^2/s$

$b = s_1/(2R)$

x_a, x_l, x_t x co-ordinates of hinge axis, intersection of wing leading edge and body, and wing trailing edge, respectively

L_{2n+1} coefficients in the series expansion, equation (14)

$n = 0, 1, 2, 3, \ldots\ldots\ldots$

$m^2 = b^2 + 1$

$\beta = \cos^{-1} 1/m$

$\alpha e^{i\omega t}$ instantaneous wing incidence

$S = s_0 c$, area of the "basic" wing

A aspect ratio of the wing

$L_w, M_w; L_B, M_B; L_{w+B}, M_{w+B}$ lift and moment on the wing, body, and combination, respectively

Q_j generalised force associated with the j^{th} wing mode

$f_j(x, y)$ j^{th} wing mode

$L_\alpha, L_{\dot\alpha}, L_{\bar\alpha}$; $M_\alpha, M_{\dot\alpha}, M_{\bar\alpha}$ force and moment derivatives for the combination

$F(\sigma), G(\sigma), H(\sigma), J(\sigma)$ defining functions for the combination derivatives

$l_\alpha, l_{\dot\alpha}, l_{\bar\alpha}$; $m_\alpha, m_{\dot\alpha}, m_{\bar\alpha}$ force and moment derivatives for the wing

$f(\sigma), g(\sigma), h(\sigma), j(\sigma)$ defining functions for the wing derivatives

$F_{2n+1}(b)$ *see* equation (19)

Note: The use of a bar over a symbol denotes that it is the amplitude of the harmonically oscillating quantity represented by the symbol itself.

Lift is defined as positive upwards, moment as positive nose-up, and incidence as positive nose-up.

2. The Slender-Body Theory

The configuration under consideration is shown in Fig. 1 and it is assumed to be immersed in a uniform stream of velocity U and density ρ. Right-handed Cartesian axes are used, with the origin O fixed at a point on the body axis and with the x-axis parallel to the stream and the z-axis upward. The wing is situated symmetrically on the uniform body whose cross section in the region of the wing is circular. The wing is represented as a thin plate oscillating about its mean position in the plane $z=0$ but always lying in the immediate vicinity of the plane. The trailing edge of the wing is straight and conditions downstream of this section are not considered.

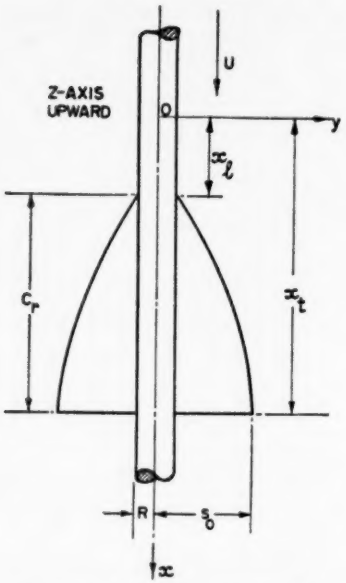

FIGURE 1. Wing-body combination.

The perturbation velocity potential satisfies the equation

$$\nabla^2\phi = \frac{1}{a^2}\left(U\frac{\partial}{\partial x} + \frac{\partial}{\partial t}\right)^2\phi. \quad . \quad . \quad . \quad . \quad . \quad (1)$$

The conditions holding at the surface of the wing-body combination are that the (rigid) body is at zero incidence and the wing is in motion in a specified manner.

When the wing motion is taken to be simple harmonic, of angular frequency ω, equation (1) becomes

$$\nabla^2\bar{\phi} = \frac{1}{a^2}\left(U\frac{\partial}{\partial x} + i\omega\right)^2\bar{\phi}. \quad . \quad . \quad . \quad . \quad . \quad (2)$$

where $$\bar{\phi}(x, y, z)\, e^{i\omega t} = \phi(x, y, z, t). \quad . \quad . \quad . \quad (3)$$

It is now assumed that the wing is slender, in the sense that

$$|M^2 - 1|^{1/2} s/c \ll 1,$$

where s is a characteristic width and c a characteristic length of the configuration. It is further assumed that the frequency of the motion is such that the relation

$$(Ms/c)^2\nu \ll 1$$

is satisfied, where $\nu = \omega c/U$, the frequency parameter, is $O(1)$.

Under these restrictions the potential equation (2) reduces to Laplace's equation in two dimensions[2],

$$\bar{\phi}_{yy}+\bar{\phi}_{zz}=0. \quad . \quad . \quad . \quad . \quad . \quad . \quad (4)$$

The co-ordinate x enters the solution only as a parameter and the boundary conditions are applied in every "cross-flow plane", $x=$constant. The solution in every cross-flow plane is complete in itself so long as the total source strength in each cross section is zero, such as is the case in antisymmetric flow problems.

For the configuration considered (having a uniform body) the pressure is given by the linear relation

$$-\left(\frac{p-p_0}{\rho}\right)=U\phi_x+\phi_t$$

or, for harmonic motion,

$$-\left(\frac{\bar{p}-p_0}{\rho}\right)=U\bar{\phi}_x+i\omega\bar{\phi}. \quad . \quad . \quad . \quad . \quad (5)$$

3. Solution for the Velocity Potential

The cross section in the plane $x=$constant is that of Fig. 2(*a*); this physical plane will be referred to as the X-plane, where $X=y+iz=\zeta e^{i\theta}$.

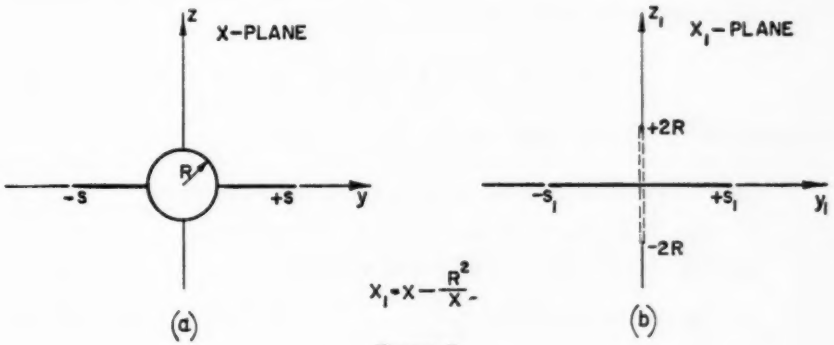

FIGURE 2.

The boundary conditions on the potential $\bar{\phi}$ in the plane $x=$constant are:—

(*a*) $\bar{\phi}$, $\bar{\phi}_z$, $\bar{\phi}_y \longrightarrow 0$ as $\zeta \longrightarrow \infty$, $0 \leqslant \theta \leqslant 2\pi$.

(*b*) On the surface of the body ($\zeta=R$, $0 \leqslant \theta \leqslant 2\pi$) the radial velocity $v_r=0$.

(*c*) At any point on the wing ($z=0$, $R \leqslant |y| \leqslant s(x)$) the prescribed normal velocity must be equal to the normal derivative of $\bar{\phi}$. Let the vertical displacement of the point (x, y) on the wing be represented by $f(x, y)\, e^{i\omega t}$; then

$$\bar{w}(x, y)=we^{-i\omega t}=\bar{\phi}_z(x, y, 0)=i\omega f(x, y)+Uf_x(x, y). \quad . \quad . \quad (6)$$

(*d*) Outside the configuration and outside the wake, $\bar{\phi}(x, y, z)$ must be continuous and, since it is antisymmetric in z, must satisfy the condition

$$\bar{\phi}(x, y, 0)=0, \qquad |y| > s(x).$$

(*e*) The flow is symmetrical about the plane $y=0$, that is

$$f(x,+y)=f(x,-y),$$
$$\bar{\phi}(+y, z)=\bar{\phi}(-y, z)$$
$$\text{and} \quad \bar{v}(0, z)=\bar{\phi}_y(0, z)=0.$$

The transformation $$X_1=X-R^2/X \quad . \quad . \quad . \quad . \quad . \quad (7)$$

is used to map the cross section of Fig. 2(*a*) onto the X_1-plane of Fig. 2(*b*). In this plane the body is represented by the sides of a vertical slit along the z_1-axis and the wings by that part of the real axis for which

$$0 \leqslant |y_1| \leqslant s-(R^2/s)=s_1.$$

The relation (7) maps both the inside and the outside of the circle $\zeta=R$ onto the X_1-plane and in this instance the latter is the required transformation. The appropriate inversion is obtained by making the points at infinity correspond; that is, the positive sign is selected for the square root, giving

$$X=\frac{1}{2}X_1\left\{1+\left[1+\left(\frac{2R}{X_1}\right)^2\right]^{1/2}\right\}. \quad . \quad . \quad . \quad . \quad (8)$$

The points $X_1=\pm 2iR$ are branch points.

The boundary conditions in the X_1-plane are, correspondingly: —

(*a*) $\bar{\phi}, \bar{\phi}_{z_1}, \bar{\phi}_{y_1} \to 0$ as $\zeta_1 \to \infty$, $0 \leqslant \theta_1 \leqslant 2\pi$.

(*b*) $\bar{v}_1=0$ for $y_1=\pm 0$, $0 < |z_1| < 2R$.

(*c*) $$\bar{w}_1(x, y_1)=\bar{w}\left[1+\frac{R^2}{y^2}\right]^{-1}$$
$$=\bar{w}(x, y_1)\left[\left(\frac{2R}{y_1}\right)^2\left\{1+\left[1+\left(\frac{2R}{y_1}\right)^2\right]^{1/2}\right\}^{-2}+1\right]^{-1}$$
$$=\bar{\phi}_{z_1}(x, y_1, 0), \quad 0 \leqslant |y_1| \leqslant s_1(x). \quad . \quad . \quad . \quad (9)$$

(*d*) $\bar{\phi}(x, y_1, 0)=0$ for $|y_1| > s_1$.

(*e*) $\bar{v}_1=0$ for $y_1=0$ and for all z,
$$\bar{\phi}(+y_1, z)=\bar{\phi}(-y_1, z).$$

The condition (*e*) thus contains the condition (*b*), which may therefore be omitted.

The restriction that the flow is symmetrical about the y_1-plane means that $\bar{\phi}$ is determined solely by conditions on the wing in the X_1-plane. To obtain the solution

to this "equivalent wing" problem, it is convenient to introduce the transformation

$$X_1 = s_1 \cosh X_2 = s_1 \cosh (y_2 + iz_2), \quad . \quad . \quad . \quad (10)$$

in which z_2 may be taken to vary between 0 and 2π and y_2 from 0 to ∞. The X_1-plane is thus mapped onto a semi-infinite rectangular region of the X_2-plane of width 2π. The upper and lower surfaces of the wing are represented by the z_2-axis between, respectively, 0 and π, π and 2π, the correspondence between points on the wing being given by

$$y_1 = s_1 \cos z_2, \qquad 0 < |y_1| < s_1, \qquad 0 \leqslant z_2 \leqslant 2\pi.$$

The remainder of the real axis is given by $z_2 = 0,\ \pi,\ 2\pi,\ y_2 = 0 \longrightarrow \infty$. The body occupies those portions of the lines $z_2 = \pi/2,\ 3\pi/2$ for which $0 < y_2 < \sinh^{-1}(2R/s_1)$. The points at infinity correspond.

The boundary conditions in the X_2-plane are, correspondingly:—

(*a*) $\tilde{\phi},\ \tilde{\phi}_{x_2},\ \tilde{\phi}_{y_2} \longrightarrow 0$ as $y_2 \longrightarrow \infty$.

(*c*) $\overline{v}_2(x, z_2) = \overline{w}_1(x, s_1 \cos z_2)\, s_1 \sin z_2 = \tilde{\phi}_{y_2}(x, 0, z_2)$. . . (11)

Combining this with the relation (9),

$$\tilde{\phi}_{y_2}(x, 0, z_2) = \overline{w}(x, s_1 \cos z_2)\, \frac{1}{2} \left\{ 1 + \frac{|b \cos z_2|}{(1 + b^2 \cos^2 z_2)^{1/2}} \right\} s_1 \sin z_2, \quad . \quad . \quad . \quad . \quad (12)$$

where $b = s_1/(2R)$.

(*d*) $\tilde{\phi}(x, y_2, \gamma\pi) = 0, \quad \gamma = 0,\ 1,\ 2.$

(*e*) $\overline{w}_2 = 0$ for $z_2 = \pi/2,\ 3\pi/2,$

$$\tilde{\phi}\left(x, y_2, \frac{(2\gamma+1)\,\pi}{2} + \theta\right) = \tilde{\phi}\left(x, y_2, \frac{(2\gamma+1)\,\pi}{2} - \theta\right), \qquad 0 < \theta < \pi/2.$$

The potential equation in the X_2-plane is

$$\tilde{\phi}_{x_2 x_2} + \tilde{\phi}_{z_2 z_2} = 0, \quad . \quad . \quad . \quad . \quad . \quad (13)$$

for which a general solution is

$$\tilde{\phi} = e^{-Cy_2}(K \cos Cz_2 + L \sin Cz_2) + e^{Cy_2}(M \cos Cz_2 + N \sin Cz_2),$$

where $C^{(2)}$ is a constant of separation. Boundary condition (*a*) requires that $M = N = 0$, while condition (*d*) requires that $K = 0$ and that C is any positive integer. Condition (*e*) restricts C to the odd positive integers. Thus the solution of equation (13) satisfying the boundary conditions (*a*), (*d*) and (*e*) is

$$\tilde{\phi} = \sum_{n=0}^{\infty} e^{-(2n+1)y_2} L_{2n+1} \sin (2n+1)\, z_2, \quad n = 0, 1, 2, 3, \ldots\ldots \quad . \quad (14)$$

and the L_{2n+1} are to be determined from the condition (*c*). Thus, on the wing,

$$-\sum_{n=0}^{\infty} (2n+1)\, L_{2n+1} \sin (2n+1)\, z_2 = \overline{w}_1 s_1 \sin z_2.$$

Multiplying both sides by $\sin(2n+1)z_2$, integrating from 0 to π and noting that $\overline{w}$ is symmetrical about $\pi/2$, we have

$$-(2n+1)L_{2n+1}=\frac{4s_1}{\pi}\int_0^{\pi/2}\overline{w}(x, s_1\cos z_2)\frac{1}{2}\left\{1+\frac{b\cos z_2}{(1+b^2\cos^2 z_2)^{1/2}}\right\}\sin(2n+1)z_2\ \sin z_2 dz_2 \quad . \quad . \quad . \quad . \quad (15)$$

On the wing, $$\bar{\phi}(x, 0, z_2)=\sum_{n=0}^{\infty}L_{2n+1}\sin(2n+1)z_2. \quad . \quad . \quad . \quad . \quad (16)$$

As required, $\bar{\phi}$ is antisymmetric across the wing surface.

4. Lift and Moment due to an Oscillating Rigid Control

4.1. General

The motion to be considered is that due to the whole or a part of the wing pitching harmonically about an axis lying in the plane $z=0$ and normal to the body. Such a motion implies that a variable gap will exist between the wing root and body; the presence of this gap is neglected. An assessment of its effect on the lift in the steady case is given in Ref. 3.

Let the line $x=x_a$ be the hinge axis; then the function $f(x, y)$ takes the form

$$f(x, y)=(x_a-x)\alpha, \quad x_l<x<x_t \quad . \quad . \quad . \quad . \quad (17a)$$

for an all-moving control and

$$\left.\begin{aligned} f(x, y)&=0 && x_l<x<x_a \\ &=(x_a-x)\alpha, && x_a<x<x_t \end{aligned}\right\} \quad . \quad . \quad . \quad (17b)$$

for a flap control, where $\alpha e^{i\omega t}$ is the instantaneous angle of incidence. It is convenient to continue the analysis for the all-moving control only, since the flap control differs from this only in that $\bar{\phi}\equiv 0$ for $x<x_a$.

4.2. The Velocity Potential

The coefficients L_{2n+1} are given by

$$(2n+1)L_{2n+1}=\frac{4s_1}{\pi}U\alpha\left[1+\frac{i\omega}{U}(x-x_a)\right]\times$$

$$\times\int_0^{\pi/2}\frac{1}{2}\left\{1+\frac{b\cos z_2}{(1+b^2\cos^2 z_2)^{1/2}}\right\}\sin(2n+1)\ z_2\sin z_2 dz_2. \quad . \quad (18)$$

The second term of the integrand is evaluated by replacing $\sin(2n+1)z_2$ by a sum of odd powers of $\sin z_2$ and using the substitution $(1+b^2\cos^2 z)=u^2$, which leads to integrals of the type

$$\frac{1}{b^{2n+1}}\int_1^m(m^2-u^2)^{n+\frac{1}{2}}\,du, \quad \text{where } m^2=b^2+1.$$

Writing $$L_{2n+1}=\frac{4s_1}{\pi}U\alpha\left[1+\frac{i\omega}{U}(x-x_a)\right]F_{2n+1}(b), \quad . \quad . \quad . \quad . \quad . \quad (19a)$$

the first three functions F_1, F_3, F_5 are given by

$$F_1=\frac{\pi}{4}\frac{1}{2}\left[1+\frac{2}{\pi b}\left(\frac{m^2\beta}{b}-1\right)\right], \quad . \quad . \quad . \quad . \quad . \quad . \quad . \quad (19b)$$

$$F_3=\frac{1}{6b}\left[1-\frac{3}{2}\frac{1}{b^2}\left(\frac{m^2\beta}{b}-1\right)\right], \quad . \quad . \quad . \quad . \quad . \quad . \quad (19c)$$

$$F_5=\frac{1}{10b}\left[\frac{5}{2}\frac{(1+m^2)}{b^2}\frac{1}{b^2}\left(\frac{m^2\beta}{b}-1\right)-\frac{1}{b^2}\left(b^2+\frac{10}{3}\right)\right] \quad . \quad . \quad . \quad (19d)$$

where $\beta=\cos^{-1}(1/m)$.

It may be noted that $$\lim_{b\to 0}\frac{1}{b^2}\left(\frac{m^2\beta}{b}-1\right)=2/3$$

and $$\lim_{b\to\infty}\frac{1}{b}\left(\frac{m^2\beta}{b}-1\right)=\pi/2.$$

The functions F_3, F_5 are zero for $R/s=0$, 1 and reach their maximum numerical values for $R/s\simeq 0{\cdot}2$. At this value of R/s the relative magnitudes of the F_{2n+1}, and thus of the L_{2n+1}, are

$$L_1:L_3:L_5=100:4:2.$$

It is seen that convergence is very rapid.

As a general point, it is of interest to note that, if the L_{2n+1} are regarded as Fourier coefficients in an expansion for the function $g(z_2)\sin z_2$ (*cf.* equation (15)) in the range $0<z_2<\pi/2$, then, since the coefficients in the series for ϕ are these Fourier coefficients divided by $2n+1$, the potential is relatively insensitive to the harmonics in the Fourier expansion of $g(z_2)\sin z_2$.

4.3. Lift and Moment on the Control

The differential pressure across the control is given by

$$\Delta\bar{p}(x,y)=2\rho U\left(\bar{\phi}_x+\frac{i\omega}{U}\bar{\phi}\right)_{z=+0} \quad . \quad . \quad . \quad . \quad (20)$$

and the lift and moment about the origin for both controls by

$$L_w=2\int_w \Delta\bar{p}\,dydx \quad . \quad . \quad . \quad . \quad . \quad (21a)$$

$$-M_w=2\int_w x\Delta\bar{p}\,dydx, \quad . \quad . \quad . \quad . \quad . \quad (21b)$$

where the integration is over one wing panel.

These integrals are most conveniently evaluated in the X_2-plane; thus,

$$L_w = 2\int_{x_l}^{x_t}\int_0^{\pi/2} \Delta\bar{p}\frac{s_1}{2}\left\{1+\frac{b\cos z_2}{(1+b^2\cos^2 z_2)^{1/2}}\right\}\sin z_2\, dz_2 dx, \quad . \quad . \quad (22)$$

with a similar expression for M_w.

On substituting for $\Delta\bar{p}$ in terms of $\bar{\phi}$ in the series form (16), it is seen that the lift on a spanwise strip depends on integrals of the same type as those determining the L_{2n+1} (equation (18)). As a result, the relative magnitudes of the contributions of the successive terms of the series (16) to the lift on a spanwise strip are in the proportions

$$(L_1)^2 : 3\,(L_3)^2 : 5\,(L_5)^2 : \quad \ldots\ldots\ldots$$

which in numerical terms (for $R/s \simeq 0{\cdot}2$) are

$$100 : 1/2 : 1/5.$$

It is clear that for practical purposes the lift and moment on the wing may be computed using only the first term of the series, when the error is at most $\frac{1}{2}$ per cent.

4.4. Lift and Moment on the Wing-Body Combination

The pressure on the body surface is given by

$$\bar{p}_B - p_0 = \rho U\left(\bar{\phi}_x + \frac{i\omega}{U}\bar{\phi}\right), \quad . \quad . \quad . \quad . \quad . \quad (23)$$

and the lift and moment about the origin by

$$L_B = 4\int_B \bar{p}_B \sin\theta\, R\; d\theta dx \quad . \quad . \quad . \quad (24a)$$

$$-M_B = 4\int_B x\bar{p}_B \sin\theta\, R\, d\theta dx, \quad . \quad . \quad . \quad (24b)$$

where the integration is over that part of the body surface for which $0 < \theta < \pi/2$ and $x_l < x < x_t$.

Calculation of the lift and moment on the combination is facilitated by the following considerations. Let $\bar{\phi}'$ be the potential (amplitude) due to an isolated cylindrical body at incidence $\alpha' e^{i\omega t}$ to the free stream. Then, since $\bar{\phi}$ and $\bar{\phi}'$ are both solutions of Laplace's equation (4), the following relation[5] holds over a closed surface $S(x)$ which is taken to be the surface of the body and that part of the plane $z=0$ occupied by the wing in the plane $x=$ constant: —

$$\int_S \bar{\phi}\frac{\partial\bar{\phi}'}{\partial n}dS = \int_S \bar{\phi}'\frac{\partial\bar{\phi}}{\partial n}dS \quad (x=\text{constant}) \quad . \quad . \quad . \quad (25)$$

where n is the outward normal to $S(x)$.

For the potential $\bar{\phi}'$, the conditions on S are

$$\frac{\partial \bar{\phi}'}{\partial n} = -U\alpha' \sin\theta, \quad \text{on the body } S_B,$$

$$\frac{\partial \bar{\phi}'}{\partial n} = \frac{\partial \bar{\phi}'}{\partial z} = \bar{w}'(y), \quad \text{on the wings } S_w.$$

The downwash $\bar{w}'(y)$ is that due to the potential

$$\bar{\phi}' = \frac{U\alpha' R^2}{r} \sin\theta$$

evaluated on the plane $z=0$; thus

$$\bar{w}'(y) = U\alpha' \frac{R^2}{y^2}. \qquad (26)$$

For the potential $\bar{\phi}$, the conditions on S are those set out in Section 3, namely,

$$\frac{\partial \bar{\phi}}{\partial n} = 0 \quad \text{on the body } S_B$$

and $$\frac{\partial \bar{\phi}}{\partial n} = \frac{\partial \bar{\phi}}{\partial z} = \bar{w}(y) \quad \text{on the wings } S_w.$$

The integral relation (25) taken over body and wings becomes

$$\int_{S_B} \bar{\phi}_B \sin\theta \, dS_B = \int_{S_w} \bar{\phi}_w \frac{R^2}{y^2} dS_w. \quad (x = \text{constant}) \qquad (27)$$

Using this result in the pressure equations (20) and (23), it is clear that the lift and moment on the body may be simply related to those on the wing; thus

$$L_B = 2\int_w \Delta\bar{p} \frac{R^2}{y^2} dydx \qquad (28a)$$

$$-M_B = 2\int_w x \, \Delta\bar{p} \frac{R^2}{y^2} dydx. \qquad (28b)$$

Adding equations (21) and (28), and noting that

$$\left(1 + \frac{R^2}{y^2}\right) dy = dy_1,$$

$$\text{then} \quad L_{w+B} = 2\int_w \Delta\bar{p} \, dy_1 dx = 2\int_{x_1}^{x_2} \int_0^{\pi/2} \Delta\bar{p} \, S_1 \sin z_2 \, dz_2 dx \qquad (29a)$$

$$-M_{w+B} = 2\int_w x \, \Delta\bar{p} \, dy_1 dx = 2\int_{x_1}^{x_2} \int_0^{\pi/2} x \, \Delta\bar{p} S_1 \sin z_2 \, dz_2 dx. \qquad (29b)$$

An immediate consequence of equations (29) is that the lift and moment on the wing-body combination depend only on the coefficient L_1, so that these results are exact within the assumptions of the slender-body theory. The lift and moment on the wing or body separately depend on all the coefficients L_{2n+1}.

5. The Calculation of Generalised Forces

The generalised force Q_j (for two wing panels) associated with the normalised deformation function $f_j(x, y)$ is given by

$$Q_j = \sum_{i=1}^{n} 2 \int_{w} \Delta\bar{p}_i f_j \, dxdy, \quad . \quad . \quad . \quad . \quad (30)$$

where $\Delta\bar{p}_i$ is the pressure differential across the wing due to the normalised deformation function $f_i(x, y)$.

The pressure $\Delta\bar{p}_i$ is determined from the potential whose coefficients $(L_{2n+1})_i$ are given by the relations (15) with $\bar{w}(x, s_1 \cos z_2) = \bar{w}_i(x, s_1 \cos z_2)$.

The lift and moment on the wing-body combination due to the normalised wing deformation $f_j(x, y)$ are clearly given by

$$(L_{w+B})_j = 2 \int_{w} \Delta\bar{p}_j \, dy_1 dx \; . \quad . \quad . \quad . \quad . \quad (31a)$$

$$(-M_{w+B})_j = 2 \int_{w} x \Delta\bar{p}_j \, dy_1 dx, \quad . \quad . \quad . \quad . \quad (31b)$$

the result (27) again being applied.

These forces, together with the generalised forces associated with plunging and pitching of the rigid wing body combination[1], allow a general longitudinal stability analysis to be undertaken for the combination based on a semi-rigid representation of the wing.

6. Numerical Results for a Triangular Control Surface

6.1. Definitions

In this section numerical results are presented for the lift and moment due to a triangular control surface. The origin of co-ordinates is conveniently taken to be at the point of intersection of the leading edges when produced to the body axis. The triangular wing, so formed by these extensions and by the continuation of the trailing edge through the body, will be referred to as the "basic" wing. Let c be the root chord and let s_0 be the semi-span of this "basic" wing: also let $\sigma = R/s_0$.

Then the root chord of the exposed control surface is

$$c_r = c(1 - \sigma)$$

and $$\frac{\text{area of control surface}}{\text{area of "basic" wing}} = (1 - \sigma)^2.$$

Let x_a be the distance of the hinge axis from the origin and x_r the distance of the

hinge axis from the intersection of the wing leading edge and body; then we define

$$\xi_0 = \frac{x_a}{c}, \quad \xi_r = \frac{x_r}{c_r}$$

so that $$\xi_0 = \xi_r + \sigma(1-\xi_r)$$

or $$(1-\xi_0) = (1-\sigma)(1-\xi_r). \quad . \quad . \quad . \quad . \quad (32)$$

Let $S = s_0 c$ be the area of the "basic" wing and let $A = (2s_0)^2/S$ be its aspect ratio; this is also the aspect ratio of the control.

The notation of flutter derivatives rather than that of stability derivatives is used.

6.2. Lift and Moment on the Combination

$$\text{Let} \quad L_{w+B} = \tfrac{1}{2}\rho U^2 S \{L_\alpha + ivL_{\dot\alpha} - \nu^2 L_{\ddot\alpha}\}\alpha \quad . \quad . \quad . \quad (33a)$$

$$\text{and} \quad M_{w+B} = \tfrac{1}{2}\rho U^2 Sc \{M_\alpha + ivM_{\dot\alpha} - \nu^2 M_{\ddot\alpha}\}\alpha \quad . \quad . \quad . \quad (33b)$$

$$\left.\begin{aligned} \text{Then} \quad L_\alpha &= (\pi/2)(1-\sigma^2)^2 F(\sigma) A \\ L_{\dot\alpha} &= (\pi/2)[(1-\xi_0)(1-\sigma^2)^2 F(\sigma) + G(\sigma)] A \\ L_{\ddot\alpha} &= (\pi/2)[H(\sigma) - \xi_0 G(\sigma)] A \\ -M_\alpha &= (\pi/2)[(1-\xi_0)(1-\sigma^2)^2 F(\sigma) - G(\sigma)] A \\ -M_{\dot\alpha} &= (\pi/2)(1-\xi_0)^2 (1-\sigma^2)^2 F(\sigma) A \\ -M_{\ddot\alpha} &= (\pi/2)[J(\sigma) - 2\xi_0 H(\sigma) + \xi_0^2 G(\sigma)] A \end{aligned}\right\} \quad . \quad . \quad (34)$$

$$\left.\begin{aligned} \text{where} \quad F(\sigma) &= F_1(r)_{r=\sigma}, \qquad H(\sigma) = \sigma^4 \int_\sigma^1 \frac{(1-r^2)^2}{r^5} F_1(r)\, dr \\ G(\sigma) &= \sigma^3 \int_\sigma^1 \frac{(1-r^2)^2}{r^4} F_1(r)\, dr, \qquad J(\sigma) = \sigma^5 \int_\sigma^1 \frac{(1-r^2)^2}{r^6} F_1(r)\, dr. \end{aligned}\right\} \quad . \quad (35)$$

In these expressions $r = R/s$. In order to carry out the indicated integrations the function $F_1(r)$ was replaced by the quadratic approximation.

$$F_1(r) = 1 - 0{\cdot}914r + 0{\cdot}414r^2; \quad . \quad . \quad . \quad . \quad (36)$$

the maximum error in the integrals is estimated to be 1·5 per cent. The functions G, H, J are shown in Fig. 3.

The movement of the aerodynamic centre of the combination with variation in σ is shown in Fig. 5, together with the aerodynamic centre position for both wing and body at incidence. The function $F(\sigma)$ is the ratio of the lift on the wing-body combination when the body is at zero incidence to that when the body is at the incidence of the wing: this relation, which is independent of wing plan form, is shown in Fig. 5 and agrees with a curve derived by Mirels[4] from the complete complex potential.

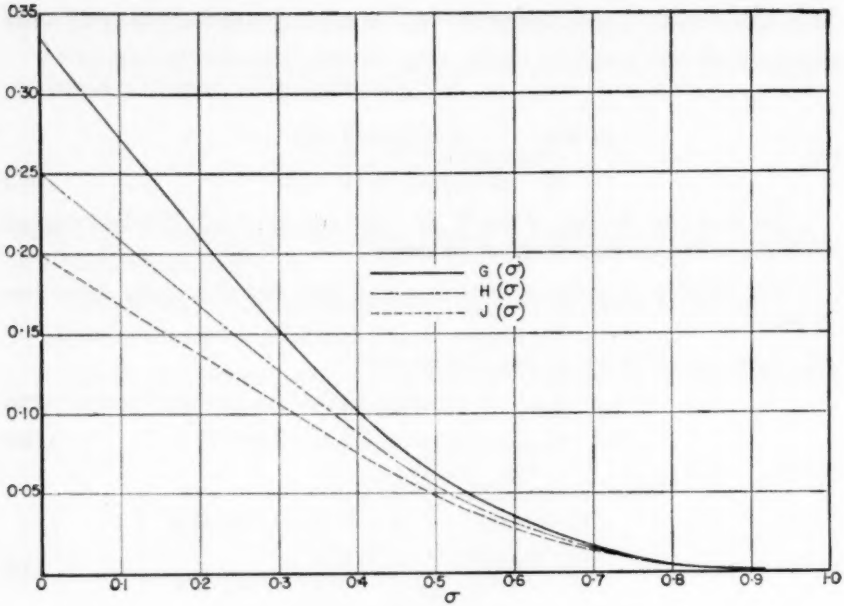

FIGURE 3.

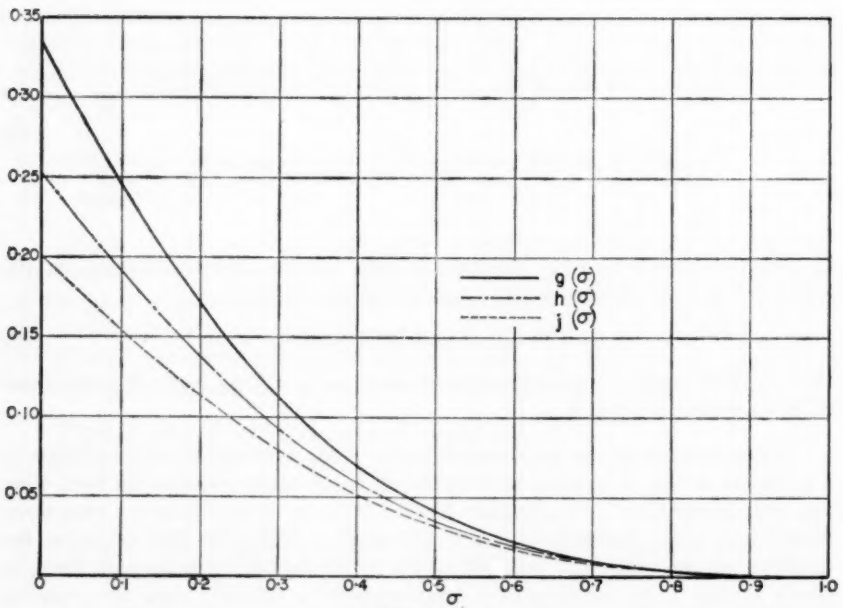

FIGURE 4.

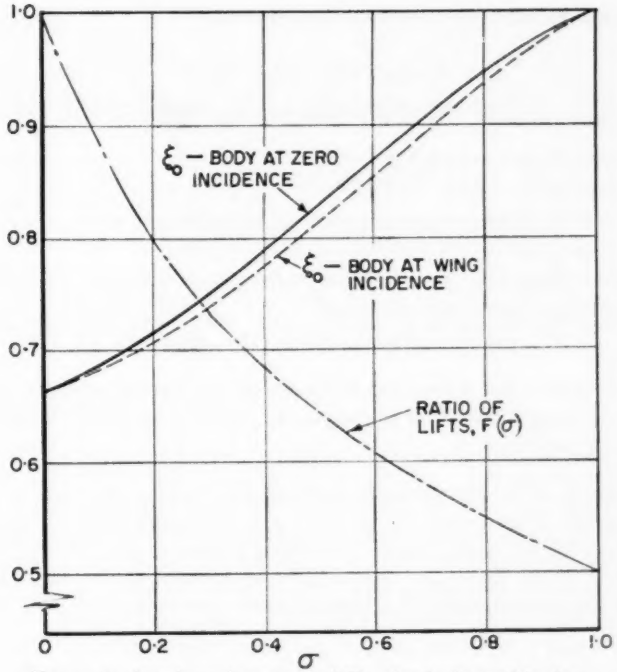

FIGURE 5. Aerodynamic centre and lift, wing-body combination.

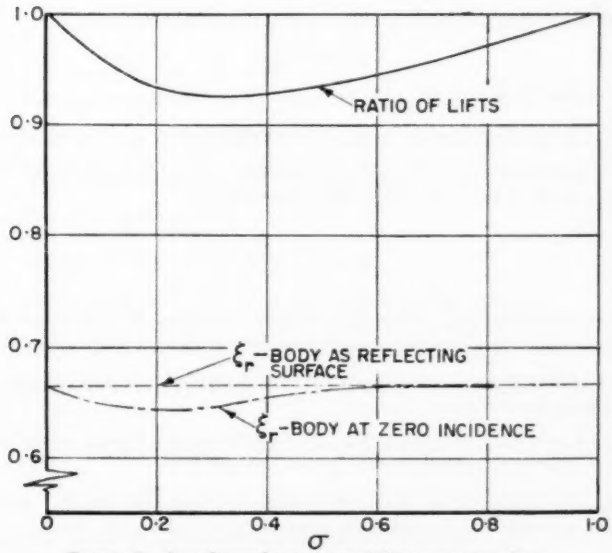

FIGURE 6. Aerodynamic centre and lift, control surface.

6.3. Lift and Moment on the Control Surface

$$\text{Let} \quad L = \tfrac{1}{2}\rho U^2 S\{l_a + ivl_{\dot{a}} - v^2 l_{\ddot{a}}\}\,\alpha \quad . \quad . \quad . \quad . \quad (37a)$$

$$\text{and} \quad M = \tfrac{1}{2}\rho U^2 Sc\{m_a + ivm_{\dot{a}} - v^2 m_{\ddot{a}}\}\,\alpha. \quad . \quad . \quad . \quad (37b)$$

$$\left.\begin{aligned}
\text{Then} \quad l_a &= (\pi/2)(1-\sigma^2)^2 f(\sigma) A \\
l_{\dot{a}} &= (\pi/2)[(1-\xi_r)(1-\sigma^2)^2(1-\sigma) f(\sigma) + g(\sigma)] A \\
l_{\ddot{a}} &= (\pi/2)[h(\sigma) - g(\sigma) + (1-\sigma)(1-\xi_r) g(\sigma)] A \\
-m_a &= (\pi/2)[(1-\xi_r)(1-\sigma^2)^2(1-\sigma) f(\sigma) - g(\sigma)] A \\
-m_{\dot{a}} &= (\pi/2)(1-\xi_r)^2(1-\sigma^2)^2(1-\sigma)^2 f(\sigma) A \\
-m_{\ddot{a}} &= (\pi/2)[j(\sigma) - 2h(\sigma) + g(\sigma) + \\
&\quad + 2(1-\sigma)(1-\xi_r)(h(\sigma) - g(\sigma)) + (1-\sigma)^2(1-\xi_r)^2 g(\sigma)] A
\end{aligned}\right\} \quad . \quad (38)$$

The functions $f(\sigma)$, $g(\sigma)$, $h(\sigma)$, $j(\sigma)$ are given by expressions identical in form to equations (35), except that $F_1(r)$ is everywhere replaced by $(F_1(r))^2$: the functions g, h, j are shown in Fig. 4.

The position of the aerodynamic centre of the control, expressed as a fraction of the root chord of the control, is shown in Fig. 6, together with the aerodynamic centre position for the control when the body is treated as a reflecting surface. In evaluating $g(\sigma)$ in the region $0{\cdot}8 < \alpha < 1$, the approximation (36) is not sufficiently accurate for the determination of ξ_r and a Taylor expansion of $(F_1(r))^2$ about $r=1$ was used.

The control derivatives may be based on the area of the control surface by dividing the expressions (38) by $(1-\sigma)^2$. Based on this area, the ratio of the lift on the control to that when the body is treated as a reflecting surface is

$$(1+\sigma)^2 f(\sigma).$$

This ratio is plotted in Fig. 6.

The ratio of the lift carried by the control to that carried by the combination is simply $F(\sigma)$; hence, for small control surfaces, the lift carried by the control approaches one half of that carried by the combination.

References

1. Milne, R. D. The Unsteady Aerodynamic Forces on Deforming, Low Aspect Ratio Wings and Slender Wing-Body Combinations. College of Aeronautics Report No. 94, July 1955.
2. Miles, J. W. *The Potential Theory of Unsteady Supersonic Flow*, pp. 8 and 160. Cambridge University Press, 1959.
3. Mirels, H. Gap Effect on Slender Wing-Body Interference. *Journal of the Aeronautical Sciences*, Vol. 20, No. 8, Readers' Forum, p. 574. August 1953.
4. Mirels, H. Lift Effectiveness of Slender Wings on Cylindrical Bodies. *Journal of the Aeronautical Sciences*, Vol. 20, No. 7, Readers' Forum, p. 504. July 1953.
5. Lamb, H. *Hydrodynamics*. Sixth edition, p. 46. Cambridge University Press, 1952.

The Reliability of Multiple Rocket Engines*

GILLIAN RUSTON

(Rocket Propulsion Establishment, Westcott)

SUMMARY: In assessing the merits of multiple versus single engines the possibility of a loss in reliability due to the use of more working parts must be considered. This paper gives a mathematical treatment of this problem and numerical examples illustrate the method.

1. Introduction

Suppose that it is required to supply, within a given limited time, a rocket engine of given thrust and of acceptable reliability. Will the best solution be a single or a multiple engine? Clearly, consideration of weight, efficiency and the control system for the missile are among the major issues but this paper is confined to a study of the appropriate reliabilities. A simple mathematical treatment of the problem is first propounded and then the theory is modified to bring it more nearly into line with current knowledge. Each modification is considered separately, and the necessary parameters estimated, and then the merits of multiple versus single engines are considered on the basis of the suggested modifications taken in conjunction.

NOTATION

a parameter of thrust-time equation (equation (18))

b parameter of development rate equation (equation (19))

c parameter of man-power needs equation (equation (21))

$f(n) = (1 - C' \log_e n)\, n^{a-1}$

n number of units in multi-unit engine

p_1 probability of failure of single engine giving thrust T

p_n probability of failure of single engine giving thrust T/n

$p(n, t)$ probability of failure of single engine giving thrust T/n after development time t

$p(T, t)$ probability of failure of single engine giving thrust T after development time t

---

Correspondence on this paper is especially invited by the Editor.

Paper received August 1960.

$q_1 = 1 - p_1$, reliability of single engine giving thrust T

q_c reliability of combining mechanism

t development time

t_a actual development time

$t_c(n)$ time needed to combine n sub-engines

t_e effective development time

A parameter of thrust-time equation (equation (18))

B parameter of thrust-time equation (equation (18))

$B' = T^{\alpha} B$

C parameter of multi-engine combining time (equation (8))

$C' = C/t$

E number of men who could usefully be employed on a project

F parameter of man-power needs equation (equation (21))

$$G = \frac{\alpha F}{t_a \eta_p K}$$

H parameter of development rate equation (equation (19))

K number of men available for a project

L parameter of multi-engine combining time (equation (14))

P_n probability of failure of n-tuple engine giving thrust T

$Q_n = 1 - P_n$, reliability of n-tuple engine giving thrust T

T thrust

α parameter of development rate equation (equation (3))

$\beta = \alpha/t$

$\eta = \eta_p \eta_m$ coefficient measuring effort

$m = K/E$, man-power coefficient

$$p = \frac{\text{amount of time spent on project}}{\text{total working time}} = \text{priority coefficient}$$

2. Simple Mathematical Model

Suppose p_1 is the probability of failure during a run of a rocket engine giving thrust T and that p_n is the probability of failure during a run of an engine giving thrust T/n. Then the probability of failure of the multiple unit of n of the smaller identical engines, total thrust T, (*i.e.* the probability of failure of at least one engine) is

$$P_n = 1 - (1 - p_n)^n. \quad . \quad . \quad . \quad . \quad . \quad (1)$$

assuming that the failures are independent.

If np_n is small,

$$P_n \simeq np_n \quad . \quad . \quad . \quad . \quad . \quad (2)$$

(*e.g.* if $p_n = 1/1{,}000$, $n=4$; then $np_n = 4\times10^{-3}$, $np_n - P_n < 6\times10^{-6}$), and therefore the multiple unit is more or less reliable than the single unit according as

$$p_n \lesseqgtr \frac{1}{n}\, p_1.$$

Suppose that t is the time needed to develop a single rocket engine giving thrust T and having probability of failure $p(T, t)$. If T is to be the total thrust of n identical engines, the thrust of each is T/n and we may write $p(n, t)$ as the probability of failure of one such engine when a time t has been spent on its development. A suggested functional form for $p(n, t)$ (to be modified in later sections) is

$$p(n, t) = 1 - \exp\left(\frac{-\alpha}{tn^a}\right), \quad . \quad . \quad . \quad . \quad . \quad (3)$$

where α and a are constants. We note that

(*i*) for fixed n, $p(n, t)$ decreases with increasing t; $p(n, 0) = 1$; $p(n, t) \longrightarrow 0$ as $t \longrightarrow \infty$,

(*ii*) for fixed t, $p(n, t)$ decreases with increasing n, *i.e.* with decreasing engine size,

(*iii*) for a given probability level $t \propto (1/n)^a$, *i.e.* $t \propto (\text{thrust})^a$.

If the development time t is fixed we have, from equation (3),

$$p_n = 1 - \exp\left(\frac{-\beta}{n^a}\right), \quad . \quad . \quad . \quad . \quad . \quad (4)$$

where $\beta = \alpha/t$ is a constant. Using the expression (1), the probability of failure of the multiple unit of n engines is

$$P_n = 1 - \exp\left(\frac{-\beta}{n^{a-1}}\right). \quad . \quad . \quad . \quad . \quad (5)$$

Taking survival chance as the measure of reliability,

the reliability of the single engine $\quad q_1 = \exp(-\beta)$,

the reliability of the n-multiple unit $Q_n = \exp\left(\frac{-\beta}{n^{a-1}}\right)$,

so that $\quad Q_n = (q_1)^{n^{1-a}} \quad . \quad . \quad . \quad . \quad . \quad (6)$

Since $q_1 < 1$, $Q_n \lesseqgtr q_1$ according as $a \lesseqgtr 1$; that is,

if $a < 1$, the reliability of the multiple unit decreases with increasing n,

if $a > 1$, the reliability of the multiple unit increases with increasing n.

The validity of this conclusion depends, of course, on the validity of equation (3) and this may be questioned. Equation (3) may be written more generally in terms of thrust as

$$p(T, t) = 1 - \exp\left(\frac{-BT^a}{t}\right), \quad . \quad . \quad . \quad (7)$$

where $p(T, t)$ is the probability of failure of an engine giving thrust T after a time t has been spent on its development; in later sections modifications to equation (7) are considered.

3. Development of a Composite Engine

In Section 2 it was assumed that to develop a multiple unit it is necessary simply to develop the individual engines making up the composite engine; the relation

$$P_n = 1 - (1 - p_n)^n \quad . \quad . \quad . \quad . \quad . \quad (1)$$

given there implies that the individual engines are completely independent. It has been suggested that the simple product rule is unduly pessimistic and that the logarithm of reliability should be used in the product rule, instead of the actual reliability. This may be accounted for by the human element, perhaps because research workers are expected to rise to the challenge of a more complex system, but, in the absence of mathematical justification for this supposition, the simple product rule is used in this discussion.

For a multi-engined piloted aircraft it is essential that the engines should be completely independent, since failure of one or more engines without loss of the aircraft is contemplated and the failure of one engine must not, as far as practicable, increase the probability of failure of another. Here this consideration does not hold, since failure of one unit means failure of the whole missile to achieve its goal. Nevertheless, bearing in mind the need for economy in development, the present discussion is limited to a composite engine in which each unit is complete in itself.

It will still be necessary to construct the n-tuple engine from the single units and no allowance was made for this in Section 2, nor for the time needed for solving such problems as the synchronising of the firing of the engines. Some of the development work for combining units might be carried on simultaneously with the development of the individual engines (assuming the necessary man-power to be available (Section 6)) but the nature of the work is essentially different and perhaps the fairest way of accounting for the development of the combination of units is on the time scale. It is suggested that the time needed to develop to an acceptably high

level of reliability the composite n-tuple unit from the n smaller units is proportional to the logarithm of n,

$$t_c(n) = C \log_e n, \quad . \quad . \quad . \quad . \quad . \quad (8)$$

where C is a function of the reliability required. We note that

(*i*) $t_c(1) = 0$,

(*ii*) $t_c(n)$ is an increasing function of n,

(*iii*) the extra time needed for development in changing from 1 to 2 engines is greater than that needed in changing from 2 to 3 engines and so on.

The expression (8) assumes that, for instance, the mechanism required for 8 engines is more than a simple extension of that required for 4 engines, and is perhaps pessimistic for the larger multiples.

If the total time available for development is t, the time left for the development of a single sub-engine is

$$t - t_c(n) = t - C \log_e n$$

and the probability of failure of such an engine is, from equation (3),

$$p(n, t - t_c(n)) = 1 - \exp\left\{\frac{-\alpha}{(t - C \log_e n)\, n^a}\right\}. \quad . \quad . \quad . \quad . \quad (9)$$

Assuming that the combining mechanism is completely reliable, the probability of survival of the composite engines (assuming independence) is

$$Q_n = \exp\left\{\frac{-\alpha}{(t - C \log_e n)\, n^{a-1}}\right\}$$

$$= \exp\left\{\frac{-\beta}{(1 - C' \log_e n)\, n^{a-1}}\right\}, \quad . \quad . \quad . \quad (10)$$

where $\beta = \alpha/t$, $C' = C/t$. We still have the reliability of the single engine giving the required thrust as

$$q_1 = \exp(-\beta)$$

and so $$Q_n = (q_1)^1 / f(n), \quad . \quad . \quad . \quad (11)$$

where $$f(n) = (1 - C' \log_e n)\, n^{a-1}. \quad . \quad . \quad . \quad (12)$$

Since $q_1 < 1$, $Q_n \lesseqgtr q_1$ according as $f(n) \lesseqgtr 1$; that is,

the multiple unit is more reliable than the single unit if $f(n) > 1$,

the multiple unit is less reliable than the single unit if $f(n) < 1$.

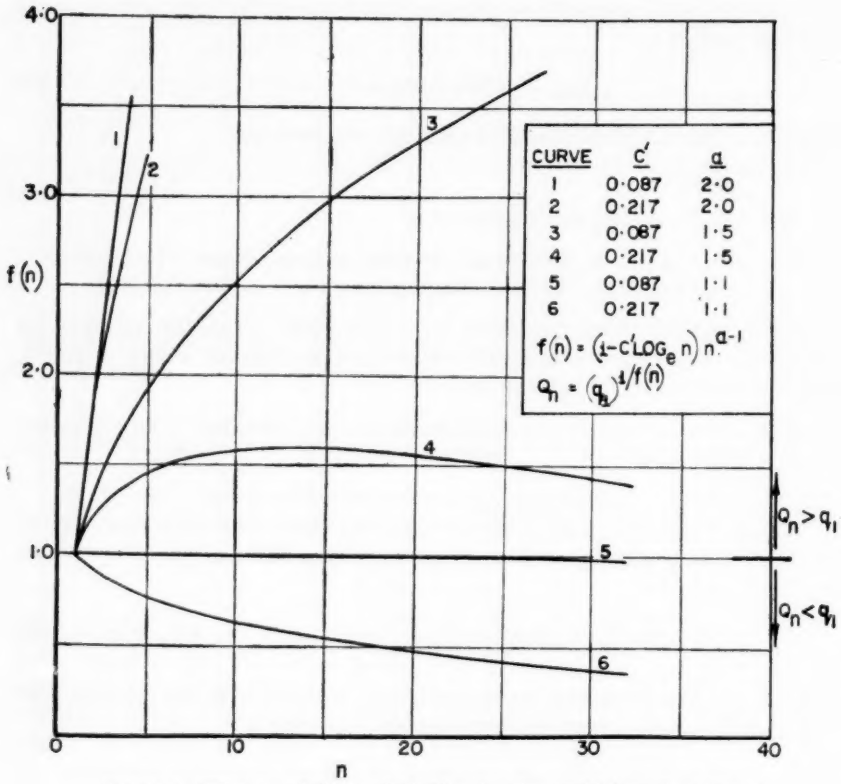

FIGURE 1. Effect on reliability of allowing time for combining sub-engines.

Values of $f(n)$ are plotted against n for various values of a and C' in Fig. 1. For increased reliability with the multiple engines we must have $a > 1$.

It is found, by differentiating (12), that Q_n has a maximum value when

$$\log_e n = \frac{a-1-C'}{(a-1)C'} \quad . \quad . \quad . \quad . \quad . \quad (13)$$

Imposing the condition that $a > 1$, equation (13) gives a solution for $n > 1$ only if

$$a > 1 + C'.$$

If $a < 1 + C'$, then $f(n)$ is a continuously decreasing function for $n > 1$ and therefore in this case a single engine will always give higher reliability than a multiple unit.

To give an idea of the significance of the value of C', suppose the total time

allowed for development is 10 years; then, if $C'=0{\cdot}1$,

$$t_c(2) = 0{\cdot}7 \text{ years}$$
$$t_c(4) = 1{\cdot}4 \text{ years}$$
$$t_c(32) = 3{\cdot}5 \text{ years.}$$

The main problem of the multi-engine unit will be that of starting the unit and, although it may be expected that little in the way of extra equipment liable to failure would be needed, it may be thought that the preceding analysis may have been unduly optimistic in assuming that the combining mechanism can be made absolutely reliable in a limited time. The degree of reliability will depend on the time expended on it, and time for development of the combining mechanism may, for the purposes of this assessment, be assumed to be obtained at the expense of the development of the individual engines. To allow for some degree of unreliability in the combining mechanism we may replace (8) by

$$t_c(q_c, n) = \frac{L \log_e n}{\log_e q_c} , \qquad . \quad . \quad . \quad . \quad . \quad (14)$$

where q_c is the reliability of the combining mechanism and L is a constant. The behaviour of the expression (14), as n varies while q_c is kept constant, is the same as that of expression (8) with C replaced by $L/\log_e q_c$, (since $0 < q_c < 1$, L will be negative). We note that

(*i*) $t_c(0, n) = 0$,

(*ii*) as $q_c \longrightarrow 1$, $t_c(q_c, n) \longrightarrow \infty$,

(*iii*) for constant n we have

$$t_c(q_c, n) \propto \frac{-1}{\log_e q_c}$$

$$\text{whence} \qquad q_c = \exp\left(\frac{-\lambda}{t_c}\right)$$

$$\text{or} \qquad p_c = 1 - \exp\left(\frac{-\lambda}{t_c}\right) ,$$

where λ is a positive constant, in agreement with the rate of development given in relation (3) for individual engines.

The probability of failure of a single engine is now, from relation (3),

$$p\,[n, t - t_c(q_c, n)] = 1 - \exp\left\{\frac{-\alpha}{\left[t - \frac{L \log_e n}{\log_e q_c}\right] n^{\alpha}}\right\}$$

and the survival chance for the composite engine is

$$Q_n = q_c \exp\left\{\frac{-\alpha}{\left[t - \frac{L \log_e n}{\log_e q_c}\right] n^{\alpha - 1}}\right\} . \qquad . \quad . \quad (15)$$

It is necessary to find the best division of development time between the individual engines and the combining mechanism by maximising Q_n with respect to q_c. Purely as an illustration, Fig. 2 shows how Q_n varies with q_c, taking as values of the relevant parameters

$$t=10,\ n=4,\ a=1{\cdot}2,\ \alpha=1{\cdot}0,\ L=-0{\cdot}09.$$

These values give $q_1=0{\cdot}905$ and, for $q_c=0{\cdot}9$, then $t_c=1{\cdot}2$.

Differentiating equation (15),

$$\frac{dQ_n}{dq_c}=\frac{Q_n}{q_c}\left\{1+\frac{\alpha}{\left[t-\dfrac{L\log_e n}{\log_e q_c}\right]^2 n^{\alpha-1}}\cdot\frac{L\log_e n}{(\log_e q_c)^2}\right\},$$

and Q_n is a maximum when

$$(t\log_e q_c - L\log_e n)^2=\frac{-L\alpha\log_e n}{n^{\alpha-1}} \quad . \quad . \quad . \quad . \quad (16)$$

The quantity in the bracket on the left is negative, since $t > L\log_e n/\log_e q_c$ and $\log_e q_c$ is negative. The optimum value of q_c given by equation (16) is plotted against n in Fig. 2, taking the same values of the parameters as before in this section.

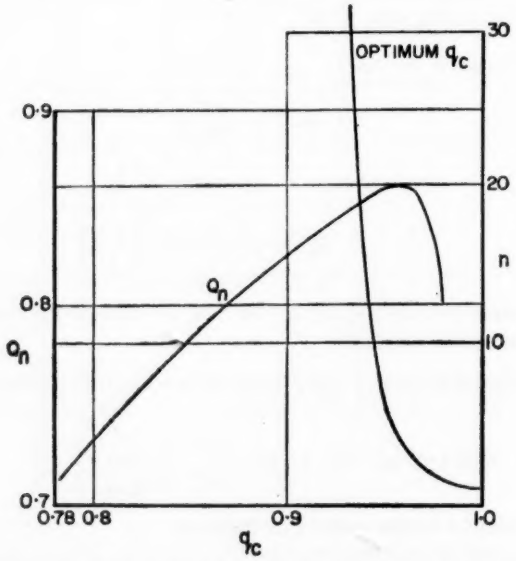

FIGURE 2. Variation of the reliability of a 4-unit engine with q_c, the reliability of the combining mechanism; and of optimum q_c with the number of units in a multi-unit engine.

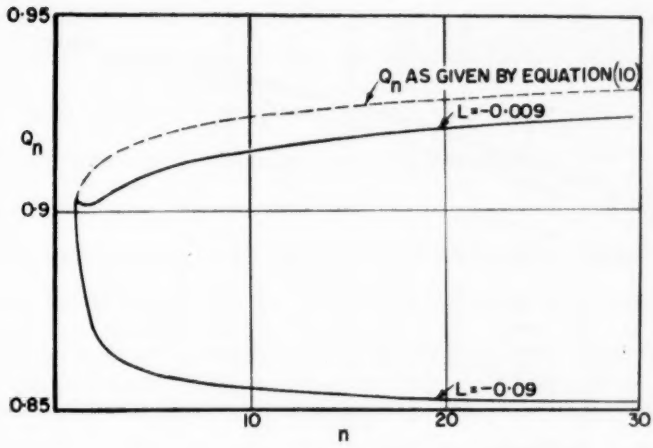

FIGURE 3. Variation of maximum reliability of an n-fold engine with n.

The maximum value of the reliability is obtained by substituting in equation (15) the value of q_c obtained from equation (16). Since the reliability of the multiple unit is sensitive to the reliability that can be achieved for the combining mechanism, two values of the appropriate parameter, L, have been chosen:—

$L=-0{\cdot}09$ corresponding to $q_c=0{\cdot}9$ and $t_c(2)=0{\cdot}6$

$L=-0{\cdot}009$ corresponding to $q_c=0{\cdot}99$ and $t_c(2)=0{\cdot}6$.

The curves of reliability against number of units are shown in Fig. 3 and, for comparison, the broken line is the curve given by equation (10), taking $\alpha=1{\cdot}0$, $C=0{\cdot}87$, so that $t_c(2)=0{\cdot}6$, $q_1=0{\cdot}905$ and the combining mechanism is assumed to be perfectly reliable. The figure demonstrates the importance of the reliability of the combining mechanism if multiple units are to be acceptable.

4. Dependence of Development Time on Size of Projects

Equation (7) gives the relation

$$t \propto T^a, \qquad . \quad . \quad . \quad . \quad . \quad (17)$$

where t is the development time needed to bring an engine giving thrust T to a given level of reliability. The implication of the value of a is suggested by the following values:—

If it takes 10 years to develop a 200,000 lb. thrust engine to an acceptable level of reliability, the time needed to develop a 50,000 lb. engine to the same level of reliability is, from relation (17),

2 months if $a=3$, $2\frac{1}{2}$ years if $a=1$,

$1\frac{1}{4}$ years if $a=3/2$, 5 years if $a=\frac{1}{2}$.

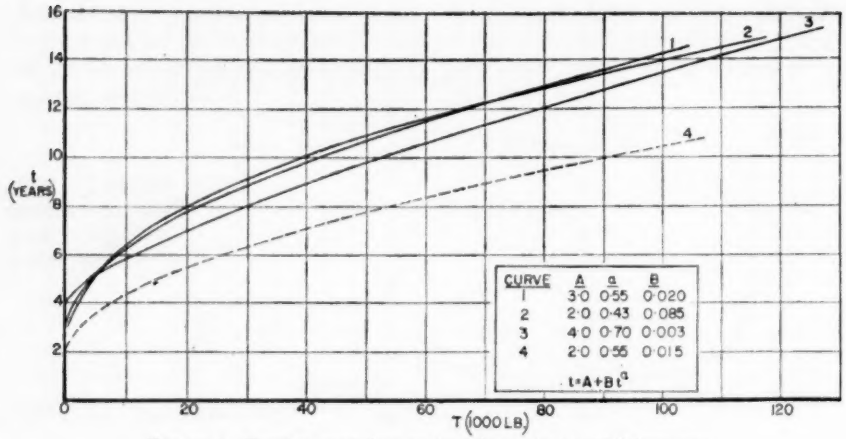

FIGURE 4. Development time against thrust for 1/100 failure rate.

The value $a=1$ is the "break even" value of a for which, on the simple theory of Section 2, there is neither loss nor gain in reliability for the development of a multi-unit engine. For $a<1$ the single unit is more reliable than the composite engine.

A comparison of these values with such data on development time as is available suggests that the simple power relation

$$t \propto T^a$$

is not a fair representation of the facts: there would seem to be a "dead weight" of time spent in development irrespective of the size of the project. We therefore suggest the relation

$$t = A + BT^a, \qquad . \quad . \quad . \quad . \quad . \quad (18)$$

where the values of A and B will depend on the level of reliability required and also, to some extent, on when the project is begun, that is, on how much past experience is available. Fig. 4 shows curves of time against thrust for three suggested sets of values applicable to a given failure rate of 1/100, namely

$$\left.\begin{aligned} A &= 4{\cdot}0 \\ a &= 0{\cdot}7 \\ B &= 0{\cdot}003 \end{aligned}\right\} \qquad \left.\begin{aligned} A &= 3{\cdot}0 \\ a &= 0{\cdot}55 \\ B &= 0{\cdot}02 \end{aligned}\right\} \qquad \left.\begin{aligned} A &= 2{\cdot}0 \\ a &= 0{\cdot}43 \\ B &= 0{\cdot}085 \end{aligned}\right\}$$

For a project starting at a later date we might expect the values of A and B to be less while that of a remains constant. The set

$$\left.\begin{aligned} A &= 3{\cdot}0 \\ a &= 0{\cdot}55 \\ B &= 0{\cdot}02 \end{aligned}\right\}$$

might be modified to

$$\left.\begin{aligned} A &= 2{\cdot}0 \\ a &= 0{\cdot}55 \\ B &= 0{\cdot}015 \end{aligned}\right\}$$

The resulting curve is shown as a broken line in Fig. 4.

5. Dependence of Reliability on Development Time

It seems likely that the rate of development given by equation (7) could be improved upon in practice, but that the exponential form is satisfactory. The development of any engine will, of course, proceed by steps (if not by leaps and bounds) and the functional form can only be expected to represent a mean of development of projects of similar size. It is suggested that equation (7) be replaced by the expression

$$p(T,t) = 1 - \exp\left\{-H\left(\frac{BT^a}{t}\right)^b\right\}, \quad . \quad . \quad . \quad . \quad (19)$$

where b is a constant greater than 1. The relationship between thrust and development time is then unchanged, but the rate of improvement in reliability is increased. Suppose B and a are chosen to relate t and T for a probability of failure of 1/100: then $H \simeq 0{\cdot}01$ in equation (19). If a certain project has a probability of failure of 1/100 after 5 years development, Fig. 5 shows the development rate for various values of b.

6. Effect of Limitation of Available Effort

It would be expected that the time taken to develop a project to a given level of reliability would depend on the effort put into the development. This suggests that the value of t to be used in equation (7) should be the effective time t_e given by

$$t_e = \eta t_a \quad . \quad . \quad . \quad . \quad . \quad (20)$$

where t_a is the actual time, η is a coefficient measuring the effort put into development and $0 < \eta \leqslant 1$.

We further define $\eta = \eta_p \eta_m$

where η_p = priority coefficient = $\dfrac{\text{amount of time spent on project}}{\text{total working time}}$

η_m = manpower coefficient = $\dfrac{\text{number of men working on project}}{\text{number of men who could usefully be employed on project}}$

and $0 < \eta_p \leqslant 1$, $0 < \eta_m \leqslant 1$.

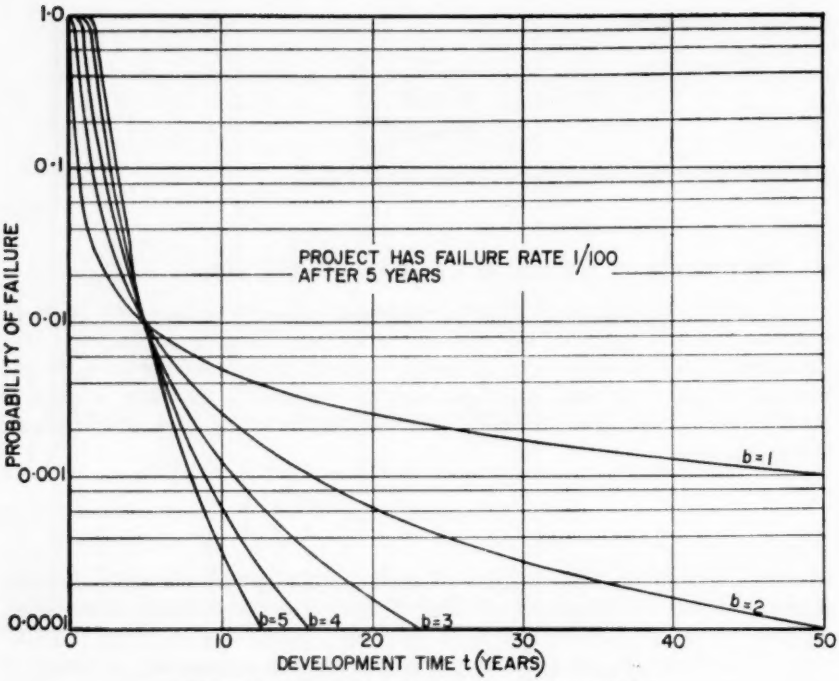

FIGURE 5. Increase in reliability with development time.

Let E be the number of men who could usefully be employed on the project; E may be expected to be a slowly increasing function of the thrust that the engine is designed to produce, say

$$E(n)=F\left(\frac{1}{n}\right)^{c}, \qquad (21)$$

where F and c are constants. For example, if the total thrust to be provided by n engines is 200,000 lb. we may have $F=100$, $c=0{\cdot}3$; the resulting curve for E is shown in Fig. 6. In practice t_a, η_p and η_m E, number of men available ($=K$), will be fixed, so that

$$\begin{aligned} t_e=\eta_p\eta_m t_a=\eta_p\,\frac{K}{E(n)}\,t_a \quad &\text{where} \quad E(n)\geqslant K \\ =\eta_p t_a \quad &\text{where} \quad E(n)\leqslant K. \end{aligned} \qquad (22)$$

In Fig. 6, t_e is plotted against n for parameter values $K=56$, $\eta_p=0{\cdot}9$, $t_a=20$.

In the region for which $E(n)\geqslant K$, we have, from equation (3),

$$p(n,t)=1-\exp\left(\frac{-G}{n^{a+c}}\right), \qquad (23)$$

where $$G=\frac{\alpha F}{t_a \eta_p K},$$

and when $$E(n) \leqslant K$$

$$p(n, t)=1-\exp\left(\frac{-\alpha}{t_a p n^a}\right). \quad . \quad . \quad . \quad . \quad . \quad (24)$$

Comparison of equations (23) and (24) with equation (3) shows that the placing of some limit on available effort has, in effect, increased the value of α. This indicates a decrease in reliability of an engine of any size at any stage of its development. However, the decision as to whether the single or the multiple engine is better depends on the value of the parameter a (Section 2).

Equation (23) shows that, when less men are available than could usefully be employed, the power to which n is raised is increased (in effect, a is increased). We now have the criterion:—the multiple unit is more or less reliable than the single engine according as $a+c \gtrless 1$, which should be compared with that given just after equation (6).

7. Modified Mathematical Theory

Each of the modifications introduced in the preceding sections requires a change in the form of the relation (7) and the estimation of the values of one or more parameters—it seems that the simple theory of Section 2 with its two parameters has little but its elegance to commend it.

Omitting the question of development effort (Section 6) which introduces a discontinuity very special to the conditions of the particular project, we may combine

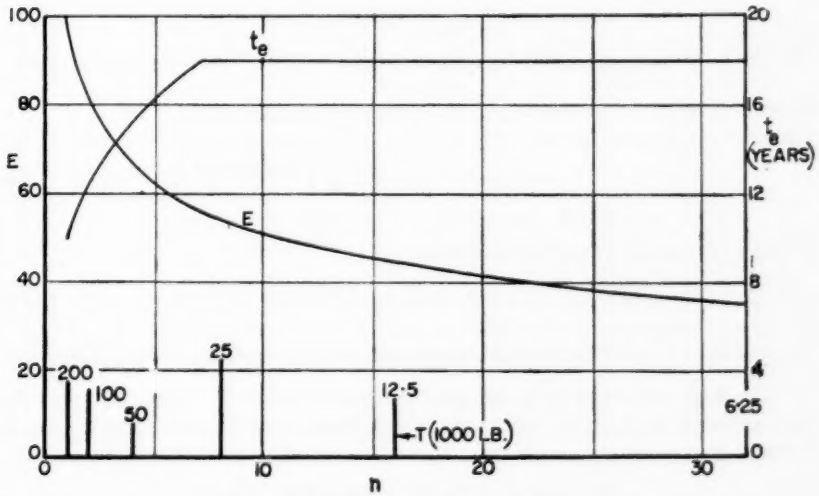

FIGURE 6. Illustration of effect of limitation of effort.

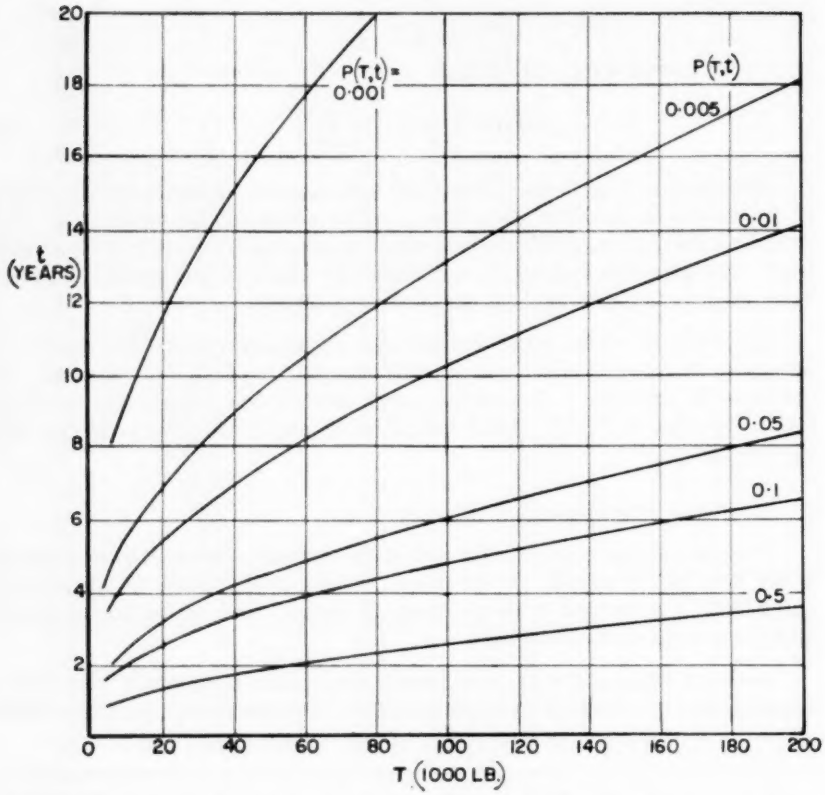

FIGURE 7. Contours of reliability for a single engine of thrust T after development time t.

the modifications of Sections 4 and 5 and replace equation (7) by

$$p(T,t)=1-\exp\left\{-H\left(\frac{A+BT^a}{t}\right)^b\right\} \quad . \quad . \quad (25)$$

Taking a representative set of parameters

$$H=0{\cdot}01,\ A=2{\cdot}0,\ a=0{\cdot}55,\ B=0{\cdot}015,\ b=3{\cdot}0,$$

contours of $p(T,t)$ against T and t have been calculated and are shown in Fig. 7.

The final consideration is the modification of Section 3: if it is assumed that the combining mechanism can be made absolutely reliable, equation (25) can be replaced by

$$p(T,t)=1-\exp\left\{-H\left[\frac{A+BT^a}{t-C\log_e n}\right]^b\right\} \quad . \quad . \quad . \quad (26)$$

or, setting thrust in terms of n,

$$p(n,t)=1-\exp\left\{-H\left[\frac{An^a+B'}{(t-C\log_e n)\,n^a}\right]^b\right\} \quad . \quad . \quad . \quad (27)$$

where $B'=T^aB$ and T is the total thrust of n engines. Then

$$Q_n=\exp\left\{-H\left[\frac{An^a+B'}{(t-C\log_e n)\,n^{a-1/b}}\right]^b\right\} \quad . \quad . \quad . \quad (28)$$

and $$q_c=\exp\left\{-H\frac{(A+B')^b}{t}\right\} \quad .$$

Clearly the behaviour of Q_n as a function of n depends on the values assumed for the various parameters. Fig. 6 shows $P_n=1-Q_n$ plotted against n for the sets of values given in Table I.

TABLE I

Curve	*Total Thrust (lb.)*	H	A	a	B	B'	t *(years)*	C'	C	b
1	200,000	0·01	2·0	0·55	0·015	9·348	10	0·13	1·3	3·0
2	200,000	0·01	2·0	0·55	0·015	9·348	20	0·13	2·6	3·0
3	200,000	0·01	2·0	0·55	0·015	9·348	10	0·087	0·87	3·0
4	,200,000	0·01	2·0	0·55	0·015	9·348	10	0·13	1·3	2·0
5	200,000	0·01	3·0	0·7	0·002	10·274	10	0·13	1·3	3·0

If allowance is made for some degree of unreliability in the combining mechanism, equation (28) must be modified to give

$$Q_n=q_c\exp\left\{-H\left[\frac{An^a+B'}{\left(t-\dfrac{L\log_e n}{\log_e q_c}\right)n^{a-1/b}}\right]^b\right\} \quad . \quad . \quad . \quad (29)$$

Differentiation of this equation shows that Q_n will take its maximum value with respect to variation in q_c when

$$\frac{(t\log_e q_c-L\log_e n)^{b+1}}{(\log_e q_c)^{b-1}}=\frac{-bHL\,(An^a+B')^b\log_e n}{n^{ab-1}} \quad . \quad . \quad (30)$$

(which may be compared with equation (16), where b was unity). The optimum value of q_c, obtained from equation (30), is substituted in equation (29) to give Curves 6 and 7 in Fig. 8 with the sets of parameters given in Table II.

TABLE II

Curve	*Total Thrust (lb.)*	H	A	a	B	B'	t *(years)*	L	b
6	200,000	0·01	2·0	0·55	0·015	9·348	10	−0·09	3·0
7	200,000	0·01	2·0	2·0	0·015	9·348	10	−0·009	3·0

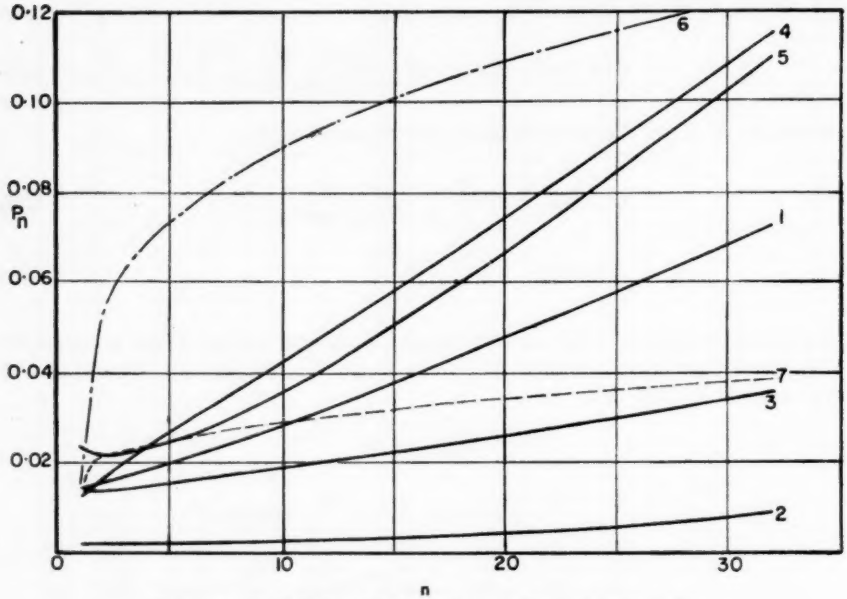

FIGURE 8. Probability of failure of composite engine of n units.

These two curves should be compared with Curve 3 in Fig. 8, for which the combining mechanism was assumed to be perfectly reliable.

8. Conclusions

It is clear from equation (2) that for a composite engine to reach a given level of reliability the sub-engines will each individually have to be more reliable than would a single engine designed to give the required thrust. When only a limited time is available for development, however, the composite engine may have some advantage.

While these conclusions may seem too obvious to justify the mathematical structure presented, it is considered that such a method should enable useful predictions on the reliability of future rocket-propelled missiles to be made from an analysis of the growth of reliability of past projects.

The Quasi-Cylinder of Specified Thickness and Shell Loading in Supersonic Flow

H. PORTNOY

(Department of Mechanical Engineering, Royal Technical College, Salford)

SUMMARY: The methods of the operational calculus are used to obtain a linear approximation to the shape of the mean camber surface of a quasi-cylinder in a supersonic flow in terms of its shell thickness and loading distributions. The analysis deals with a generalised quasi-cylinder; that is one which, although lying close to a mean cylinder, need not possess axial symmetry. The quasi-cylinder is also permitted to be within the small disturbance field of other separate components, *e.g.* a centre-body. Because the linearised theory is inadmissable for internal duct flows close to and beyond the first reflected characteristic cone, the present solution is likewise invalid close to and beyond the position where this characteristic meets the mean cylinder. The work given here enables the camber shapes of "ring-wings", which have been used theoretically to reduce or even nullify the wave-drag of a central slender-body, to be found. An example illustrates the general method.

1. Introduction

The theory of quasi-cylinders is due to Lighthill[1] and Ward[2]. Both dealt with the external and internal flow problems for axisymmetric quasi-cylinders. It should be noted that Ward's[2] internal flow analysis forms a correction to that in Ref. 1. Ward[2] also considered small-incidence effects.

The concept of a quasi-cylinder has been extended by Nielsen and Pitts[3] to include non-axisymmetric shapes lying close to a mean cylinder and they have dealt with the external flow past such bodies.

In this paper a generalised quasi-cylinder of this kind is considered. In general it can be subject to the perturbation field of other separate components together with the main stream, which is parallel to its mean cylinder axis in the undisturbed state. Its own perturbation field must be such as to satisfy the linearised equation of supersonic flow, the conditions at infinity and on the Mach surface from the intake edge and, when combined with the other two component flows mentioned, it must produce a resultant flow tangential to the outer and inner surfaces of the quasi-cylinder.

Received July 1960.

This paper deals with the problem of finding the shape of the mean camber surface of a quasi-cylinder of this kind when the thickness and loading distributions of the shell are specified, together with the variation of the intake opening radius with angular position. The mean camber surface lies midway between the outer and inner surfaces. Apart from the usual conditions to be satisfied in quasi-cylinder theory[2, 3], the flow must remain supersonic inside the duct for as far downstream of the inlet as the solution is used. Ward[2] has observed that the internal flow results of linearised theory are of doubtful validity as the first reflected characteristic cone (which meets the mean cylinder at a distance $2Ba$ from the inlet) is approached, even if the flow is still supersonic. Thus the present work, which assumes the linearised supersonic solution to apply within the duct, is valid, at most, for a distance somewhat less than $2Ba$ from the inlet.

The relationships required are obtained, in operational form, from the standard solutions of the transformed linearised equation[4]. On inversion, the thickness and loading distributions are seen to enter into the solution through separate superposition integrals and with different influence functions, each of which can be expressed in terms of complete elliptic integrals. Their effects are therefore simply additive.

An example of the use of the method is given in Section 4. The mean camber surface shape is found for an axisymmetric duct with a conical centre-body, the duct having constant shell loading per unit area and linearly increasing shell thickness from the inlet onwards. Loading and thickness are interrelated by making the inner surface at the inlet lip have zero streamwise slope. Thus the loading at the forward edge (and hence everywhere) can be readily found, because two-dimensional theory is applicable at the lip.

The work given here finds, perhaps, its most interesting use in the design of "ring-wing"-body combinations of small or even zero theoretical wave-drag. In Ref. 5, the method of designing the correct combination of central body of revolution with shell thickness and loading distributions of the ring-wing surrounding it is considered. The present method enables the mean camber surface shape of the ring-wing corresponding to the required distributions of thickness and loading to be found.

Notation

a radius of mean cylinder

$a_n(z)$ Fourier coefficient of $R(\theta, z) - R(\theta, 0)$

$A_n(p)$ arbitrary function of p in operational solution for $\bar{\phi}$ outside the cylinder

$b_n(z)$ Fourier coefficient of $R(\theta, z) - R(\theta, 0)$

$B = \sqrt{(M^2 - 1)}$

$B_n(p)$ arbitrary function of p in operational solution for $\bar{\phi}$ outside the cylinder

$c_n(z)$ Fourier coefficient of $v(\theta, z)/U$

$C_n(p)$ arbitrary function of p in operational solution for $\bar{\phi}$ inside the cylinder

$d_n(z)$ Fourier coefficient of $v(\theta, z)/U$

$D_n(p)$ arbitrary function of p in operational solution for $\bar{\phi}$ inside the cylinder

$e_n(z)$ Fourier coefficient of $t(\theta, z)$

E complete elliptic integral of the second kind

$f_n(z)$ Fourier coefficient of $t(\theta, z)$

$F(z)$ any function of z

$\bar{F}(p)$ the Laplace transform of $F(z)$

$g_n(z), h_n(z)$ Fourier coefficients of $l(\theta, z)$

$H(z)$ the Heaviside unit function. $H(z)=1$ for $z>0$ and zero for $z<0$

I_n the modified Bessel function of the first kind of order n

K complete elliptic integral of the first kind

K_n the modified Bessel function of the second kind of order n

$l(\theta, z)$ radially outward load per unit area of the shell divided by $\frac{1}{2}\rho U^2$

M Mach number

p the Laplace transform variable

$q_n(z)$ function whose Laplace transform is $p\, I_n(p)\, K_n(p)$

$Q_n(z)$ function whose Laplace transform is $\frac{1}{2}p\, I_n'(p)\, K_n'(p)$

$R(\theta, z)$ radius of mean camber surface

$R_n(z)$ function whose Laplace transform is $-\frac{1}{2}p\,\frac{d}{dp}[I_n(p)\, K_n(p)]$

$\mathbf{u}$ perturbation velocity vector

U free stream velocity magnitude

$v(\theta, z)$ radial velocity produced by other components at mean cylinder

$y=z/(Ba)$

α semi-cone angle of centre-body in example

ε constant value of dt/dz in example

ϕ velocity potential such that $\mathbf{u}=U\nabla\phi$

ρ free stream density

∇ gradient operator

2. Operational Solution for the Mean Camber Surface Shape

The quasi-cylinder is immersed in a stream of initial velocity U, Mach number M and density ρ. Cylindrical polar co-ordinates (r, θ, z) are taken, with the axis Oz lying along the mean cylinder axis parallel to the undisturbed stream and the origin at the centre of its nose section. The mean cylinder radius is a and the symbol B denotes $\sqrt{(M^2-1)}$. The sharp edged intake opening has a radius $R(\theta, 0)$, the mean camber surface radius being $R(\theta, z)$, where

$$R(\theta, z)=\sum_{n=0}^{\infty}[a_n(z)\cos n\theta + b_n(z)\sin n\theta] + R(\theta, 0). \quad . \quad . \quad (1)$$

Other components besides the quasi-cylinder may produce a radial velocity distribution at the mean cylinder given by

$$v(\theta, z) = U \sum_{n=0}^{\infty} [c_n(z) \cos n\theta + d_n(z) \sin n\theta]. \quad . \quad . \quad . \quad . \quad (2)$$

The specified thickness of the shell is

$$t(\theta, z) = \sum_{n=0}^{\infty} [e_n(z) \cos n\theta + f_n(z) \sin n\theta], \quad . \quad . \quad . \quad . \quad (3)$$

while the radially outward load per unit area of the shell, divided by $\frac{1}{2}\rho U^2$, is

$$l(\theta, z) = \sum_{n=0}^{\infty} [g_n(z) \cos n\theta + h_n(z) \sin n\theta]. \quad . \quad . \quad . \quad . \quad (4)$$

If ϕ is the perturbation velocity potential of the quasi-cylinder, so that its perturbation velocity vector $\mathbf{u}$ is given by

$$\mathbf{u} = U\nabla\phi, \quad . \quad . \quad . \quad . \quad . \quad . \quad . \quad (5)$$

then the linear approximation to the pressure coefficient produced by the cylinder's field[4] is $-2\partial\phi/\partial z$. Since the pressure due to the other components is continuous across the quasi-cylinder, it follows that

$$l(\theta, z) = 2\left[\left(\frac{\partial\phi}{\partial z}\right)_{r=a+} - \left(\frac{\partial\phi}{\partial z}\right)_{r=a-}\right] \quad . \quad . \quad . \quad . \quad (6)$$

to a first approximation.

ϕ satisfies the linearised equation[4], vanishes far away from the cylinder and also on the wave fronts emanating from the inlet edge, and satisfies the tangency conditions at the duct surfaces[2].

The one-sided Laplace transform is now introduced[4, 6].

The relationship between a function $F(z)$ and its transform $\bar{F}(p)$ is indicated by the symbolism of van der Pol and Bremmer[6] thus:—

$$F(z) \fallingdotseq \bar{F}(p). \quad . \quad . \quad . \quad . \quad . \quad . \quad (7)$$

In Chapter 8 of Ref. 4, it is shown that the operational solution of the linearised equation suitable for the region outside a quasi-cylinder is

$$\bar{\phi} = \sum_{n=0}^{\infty} [A_n(p) \cos n\theta + B_n(p) \sin n\theta] K_n(Bpr). \quad . \quad . \quad . \quad (8)$$

where A_n, B_n are arbitrary functions of p, and K_n is the modified Bessel function[7] of the second kind of order n.

The type of operational solution suitable for the internal region is shown to be

$$\bar{\phi} = \sum_{n=0}^{\infty} [C_n(p) \cos n\theta + D_n(p) \sin n\theta] I_n(Bpr), \quad . \quad . \quad . \quad (9)$$

C_n and D_n being again arbitrary functions, while I_n is the modified Bessel[7] function of the first kind of order n.

The boundary conditions of tangency at the outer and inner surfaces are, respectively, to first order,

$$\left(\frac{\partial \phi}{\partial r}\right)_{r=a+} + \frac{v(\theta, z)}{U} = \frac{\partial R}{\partial z} + \tfrac{1}{2}\frac{\partial t}{\partial z} \quad . \quad . \quad . \quad . \quad (10)$$

and

$$\left(\frac{\partial \phi}{\partial r}\right)_{r=a-} + \frac{v(\theta, z)}{U} = \frac{\partial R}{\partial z} - \tfrac{1}{2}\frac{\partial t}{\partial z} \quad . \quad . \quad . \quad . \quad . \quad (11)$$

If the operational forms of these are taken and the appropriate series (1), (2), (3), (8) and (9) are used, equation of corresponding Fourier coefficents yields

$$Bp\, A_n(p)\, K_n'(Bpa) + \bar{c}_n(p) = p\,\bar{a}_n(p) + \tfrac{1}{2}p\,\bar{e}_n(p), \quad . \quad . \quad (12)$$

$$Bp\, B_n(p)\, K_n'(Bpa) + \bar{d}_n(p) = p\,\bar{b}_n(p) + \tfrac{1}{2}p\,\bar{f}_n(p), \quad . \quad . \quad (13)$$

$$Bp\, C_n(p)\, I_n'(Bpa) + \bar{c}_n(p) = p\,\bar{a}_n(p) - \tfrac{1}{2}p\,\bar{e}_n(p) \quad . \quad . \quad (14)$$

and

$$Bp\, D_n(p)\, I_n'(Bpa) + \bar{d}_n(p) = p\bar{b}_n(p) - \tfrac{1}{2}p\,\bar{f}_n(p) \quad . \quad . \quad (15)$$

Also (4) and (6), with (8) and (9), yield similarly

$$\bar{g}_n(p) = 2p\,[A_n(p)\, K_n(Bpa) - C_n(p)\, I_n(Bpa)] \quad . \quad . \quad (16)$$

and

$$\bar{h}_n(p) = 2p\,[B_n(p)\, K_n(Bpa) - D_n(p)\, I_n(Bpa)]. \quad . \quad . \quad (17)$$

If A_n, B_n, C_n and D_n are now eliminated from (16) and (17) by substitution from equations (12) to (15), the following relationships result:—

$$\tfrac{1}{2}B\bar{g}_n(p) I_n'(Bpa)\, K_n'(Bpa) = [p\bar{a}_n(p) - \bar{c}_n(p)]\,[I_n'(Bpa)\, K_n(Bpa) - I_n(Bpa)\, K_n'(Bpa)] + \tfrac{1}{2}\,p\bar{e}_n(p)\,[I_n'(Bpa)\, K_n(Bpa) + I_n(Bpa)\, K_n'(Bpa)] \quad (18)$$

and

$$\tfrac{1}{2}B\bar{h}_n(p)\, I_n'(Bpa)\, K_n'(Bpa) = [p\bar{b}_n(p) - \bar{d}_n(p)][I_n'(Bpa)\, K_n(Bpa) - I_n(Bpa)\, K_n'(Bpa)] + \tfrac{1}{2}p\bar{f}_n(p)\,[I_n'(Bpa)\, K_n(Bpa) + I_n(Bpa)\, K_n'(Bpa)]. \quad (19)$$

If use is made of the Wronskian determinant[7] for I_n and K_n and the formula for derivative of a product, these simplify to

$$\bar{a}_n(p) = \frac{1}{p}\,\bar{c}_n(p) + \tfrac{1}{2}B^2a\bar{g}_n(p)\, I_n'(Bpa)\, K_n'(Bpa) - \tfrac{1}{2}p\bar{e}_n(p)\frac{d}{dp}[I_n(Bpa)\, K_n(Bpa)] \quad . \quad . \quad . \quad (20)$$

and

$$\bar{b}_n(p) = \frac{1}{p}\,\bar{d}_n(p) + \tfrac{1}{2}B^2a\bar{h}_n(p)\, I_n'(Bpa)\, K_n'(Bpa) - \tfrac{1}{2}p\bar{f}_n(p)\frac{d}{dp}[I_n(Bpa)\, K_n(Bpa)]. \quad . \quad . \quad . \quad (21)$$

Writing $$Q_n(z) \fallingdotseq \tfrac{1}{2}p\, I_n'(p)\, K_n'(p) \quad . \quad . \quad . \quad . \quad (22)$$

and $$R_n(z) \fallingdotseq -\tfrac{1}{2}p \frac{d}{dp}[I_n(p)\, K_n(p)]. \quad . \quad . \quad . \quad (23)$$

equations (20) and (21) may be formally inverted, using certain standard operational rules[6], to yield

$$a_n(z) = \int_0^z c_n(u)\, du + B \int_0^z Q_n\left(\frac{z-u}{Ba}\right) g_n(u)\, du + \int_0^z R_n\left(\frac{z-u}{Ba}\right) f_n'(u)\, du \qquad (24)$$

and $$b_n(z) = \int_0^z d_n(u)\, du + B \int_0^z Q_n\left(\frac{z-u}{Ba}\right) h_n(u)\, du + \int_0^z R_n\left(\frac{z-u}{Ba}\right) f_n'(u)\, du. \qquad (25)$$

These are the required relationships determining the slope of the mean camber surface from equation (1). It remains to perform the actual inversions of $\overline{Q}_n(p)$ and $\overline{R}_n(p)$ in (22) and (23).

3. The Functions $Q_n(z)$ and $R_n(z)$

If a subsidiary function $q_n(z)$ is defined by

$$q_n(z) \fallingdotseq p\, I_n(p)\, K_n(p), \quad . \quad . \quad . \quad . \quad . \quad (26)$$

then it follows from (23) directly, using a standard operational rule[6], that

$$R_n(z) = \tfrac{1}{2}z\, q_n(z). \quad . \quad . \quad . \quad . \quad . \quad (27)$$

To invert $\overline{Q}_n(p)$ we observe that

$$\begin{aligned}
\tfrac{1}{2}p \frac{d^2}{dp^2}[I_n(p)\, K_n(p)] &= \tfrac{1}{2}p\,[I_n(p)\, K_n''(p) + 2I_n'(p)\, K_n'(p) + I_n''(p)\, K_n(p)] \\
&= \tfrac{1}{2}pI_n(p)\left[-\frac{1}{p}K_n'(p) + \left(1+\frac{n^2}{p^2}\right)K_n(p)\right] + \tfrac{1}{2}pI_n'(p)\, K_n'(p) + \\
&\quad + \tfrac{1}{2}pK_n(p)\left[-\frac{1}{p}I_n'(p) + \left(1+\frac{n^2}{p^2}\right)I_n(p)\right] \\
&= -\tfrac{1}{4}\frac{d}{dp}\left[I_n(p)\, K_n(p)\right] + \tfrac{1}{2}\left(1+\frac{n^2}{p^2}\right)p\, I_n(p)\, K_n(p) + \\
&\quad + \tfrac{1}{2}p\, I_n'(p)\, K_n'(p), \quad . \qquad (28)
\end{aligned}$$

where the differential equation for the modified Bessel functions has been used.

Rearranging and inverting the terms:—

$$Q_n(z) = (\tfrac{1}{2}z^2 - \tfrac{1}{2})\, q_n(z) - \tfrac{1}{2}\int_0^z (n^2 z - n^2 u + \tfrac{1}{2}u) q_n(u)\, du. \quad . \quad . \quad (29)$$

Now, by a formula given in Watson (Ref. 7, p. 441),

$$p\,I_n(p)\,K_n(p)=\frac{2(-)^n}{\pi}\int_0^{\frac{1}{2}\pi} p\,K_0(2p\cos\theta)\cos 2n\theta\,d\theta \quad . \quad . \quad (30)$$

and so, by inversion under the integral sign[6],

$$q_n(z)=\frac{2(-)^n}{\pi}\int_0^{\frac{1}{2}\pi}\frac{H\left(\frac{z}{2\cos\theta}-1\right)\cos 2n\theta}{2\cos\theta\sqrt{\left(\frac{z^2}{4\cos^2\theta}-1\right)}}\,d\theta, \quad . \quad . \quad . \quad (31)$$

where H is the Heaviside unit function. Thus

$$q_n(z)=\frac{(-)^n}{\pi}\int_{H(1-\frac{1}{2}z)\cos^{-1}(\frac{1}{2}z)}^{\frac{1}{2}\pi}\frac{\cos 2n\theta}{\sqrt{\{(\frac{1}{2}z)^2-\cos^2\theta\}}}\,d\theta. \quad . \quad . \quad (32)$$

It is readily shown from (32) that $q_n(z)$ is expressible in finite series of elliptic integrals with modulus $\frac{1}{2}z$ for $z<2$ and modulus $2/z$ for $z>2$. In particular

$$q_0(z)=\frac{1}{\pi}K(\tfrac{1}{2}z)\,H(2-z)+\frac{2}{\pi z}K\left(\frac{2}{z}\right)H(z-2), \quad . \quad . \quad . \quad (33)$$

K being the complete elliptic integral of the first kind with modulus as indicated.

Hence, from (29) and (27),

$$Q_0(z)=\frac{1}{\pi}\left[\tfrac{1}{2}K(\tfrac{1}{2}z)-E(\tfrac{1}{2}z)\right]H(2-z)+\frac{1}{\pi}\left[\left(\tfrac{1}{2}z-\frac{1}{z}\right)K\left(\frac{2}{z}\right)-\tfrac{1}{2}zE\left(\frac{2}{z}\right)\right]H(z-2), \quad (34)$$

(E being the complete integral of the second kind) and

$$R_0(z)=\frac{z}{2\pi}K(\tfrac{1}{2}z)\,H(2-z)+\frac{1}{\pi}K\left(\frac{2}{z}\right)H(z-2). \quad . \quad . \quad . \quad (35)$$

In practice, owing to the limitations on the theory mentioned in Section 1, the functions are only needed for $z<2$.

In general it can be shown readily, from (32), that $q_n(z)$ has one singularity, at $z=2$, of the form $\{(-)^{n+1}/(2\pi)\}\log|2-z|$ and so, from (27), $R_n(z)$ has precisely the same form of singularity at $z=2$ only and, from (29), $Q_n(z)$ has a single singularity of the form $\{(-)^{n+1}/(4\pi)\}\log|2-z|$.

Series for Q_n and R_n for small z and for very large z may be established easily by standard operational methods[4, 6].

4. Example

The method is now used to find the camber surface shape of an axisymmetric quasi-cylinder with a conical centre-body whose semi-cone angle is α and which starts at $z=-Ba$, so that the Mach wave from its nose just meets the intake lip (*see* Fig. 1).

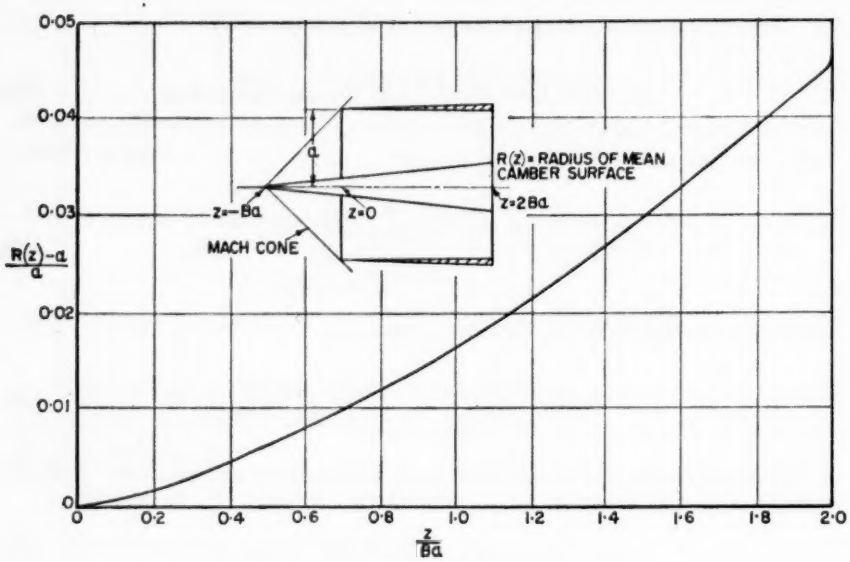

FIGURE 1.

The inlet radius $R(0)$ is taken as the radius of the mean cylinder and is denoted as usual by a; the thickness of the shell $t(z)$ is given by

$$t(z)=\varepsilon z, \qquad (36)$$

where ε is a small positive constant and the shell loading is constant, being fixed by making the internal duct surface have zero streamwise slope at the inlet. Since, close to the inlet, the flow is two-dimensional it follows that

$$l(z)=-\frac{2\varepsilon}{B}. \qquad (37)$$

It is readily shown[4] that at the mean cylinder the radial velocity induced by the central cone for $z>0$ is

$$v(z)=U\alpha^2 B\sqrt{\left[\left(\frac{z}{Ba}+1\right)^2-1\right]}. \qquad (38)$$

As the system is axisymmetric, equation (1) gives $R(z)-R(0)=a_0(z)$ and so, from (24), (36), (37) and (38),

$$R(z)-a=\int_0^z \alpha^2 B\sqrt{\left[\left(\frac{u}{Ba}+1\right)^2-1\right]}\,du+B\int_0^z Q_0\left(\frac{z-u}{Ba}\right)\left(-\frac{2\varepsilon}{B}\right)du+\int_0^z R_0\left(\frac{z-u}{Ba}\right)\varepsilon\,du. \qquad (39)$$

For the present simple case the superposition integrals can be evaluated analytically, as can the first integral too.

The result of performing these integrations when $z < 2Ba$ is

$$R(z) = a + \tfrac{1}{2}\alpha^2 B^2 a\left\{\left(\frac{z}{Ba}+1\right)\sqrt{\left[\left(\frac{z}{Ba}+1\right)^2 - 1\right]} - \cosh^{-1}\left(\frac{z}{Ba}+1\right)\right\} + \frac{\varepsilon z}{\pi}E\left(\frac{z}{2Ba}\right) +$$

$$+ \frac{2\varepsilon Ba}{\pi}\left[E\left(\frac{z}{2Ba}\right) - \left(1 - \frac{z^2}{4B^2a^2}\right)K\left(\frac{z}{2Ba}\right)\right]$$

$$= a\left\{1 + \tfrac{1}{2}\alpha^2 B^2\left[(y+1)\sqrt{[(y+1)^2-1]} - \cosh^{-1}(y+1)\right] + \frac{\varepsilon B}{\pi}\left[(y+2)E(\tfrac{1}{2}y) - \right.\right.$$

$$\left.\left. - 2(1-\tfrac{1}{4}y^2)K(\tfrac{1}{2}y)\right]\right\} . \quad . \quad . \quad (40)$$

where y has been written for $z/(Ba)$.

This has been shown in Fig. 1 for $\varepsilon B = 0{\cdot}1 \alpha B = 0{\cdot}01$, as a graph of $\{R(z)-a\}/a$ against $z/(Ba)$. The slope of the line has a logarithmic singularity when $z/(Ba)=2$ (which is barely discernible with the scale used). This corresponds, of course, to the breakdown of the theory mentioned in Section 1.

References

1. Lighthill, M. J. Supersonic Flow past Bodies of Revolution. R. & M. 2003, 1945.
2. Ward, G. N. The Approximate External and Internal Flow past a Quasi-Cylindrical Tube Moving at Supersonic Speeds. *Quarterly Journal of Mechanics and Applied Mathematics*, Vol. 1, No. 2, June 1948.
3. Nielsen, J. N. and Pitts, W. C. Wing-Body Interference at Supersonic Speeds with an Application to Combinations with Rectangular Wings. N.A.C.A. Technical Note 2677, 1952.
4. Ward, G. N. *Linearized Theory of Steady High-Speed Flow*. Cambridge University Press, 1955.
5. Graham, E. W., Beane, B. J. and Licher, R. M. The Drag of Non-Planar Thickness Distributions in Supersonic Flow. *The Aeronautical Quarterly*, Vol. VI, No. 2, May 1955.
6. Van der Pol, B. and Bremmer, H. *Operational Calculus Based on the Two-Sided Laplace Integral*. Second Edition, Cambridge University Press, 1955.
7. Watson, G. N. *The Theory of Bessel Functions*. Second Edition, Cambridge University Press, 1944.

Review

Progress in Solid Mechanics, Volume I. I. N. Sneddon and R. Hill (Editors). North Holland Publishing Co., Amsterdam, 1960. 448 pp. Diagrams. £5.

The time has long passed since the classical theory of elasticity formed an adequate basis for the solution of all of the practical problems of solid mechanics. However, knowledge of the progress that has taken place in recent years in the fields of plasticity, large deflection elasticity, viscoelasticity and thermoelasticity is not so widespread as it ought to be. The series of books of which this is the first volume is therefore very welcome indeed.

This book contains eight short monographs of the highest standard and of great scientific interest. The titles are as follows:— I—Viscoelastic Waves by S. C. Hunter. II—Matrices of Transmission in Beam Problems by K. Marguerre. III—Dynamic Expansion of Spherical Cavities in Metals by H. G. Hopkins. IV—General Theorems for Elastic-Plastic Solids by W. T. Koiter. V—Dispersion Relations for Elastic Waves in Bars by W. A. Green. VI—Thermoelasticity: The Dynamical Theory by P. Chadwick. VII—Continuous Distributions of Dislocations by B. A. Bilby. VIII—Asymmetric Problems of the Theory of Elasticity for a Semi-Infinite Solid and a Thick Plate by R. Muki.

It is not, of course, possible to do justice to this wealth of material in a short review, but a few brief indications of content may stimulate interest in particular topics. The material basis of Chapter I is expressed by a stress-strain equation in which the modulus is complex and frequency-dependent. This is applied to uni-axial stress pulses, compared with experiment and generalised to three dimensions. Chapter II presents a systematic development of the Holzer-Myklestad method for the analysis of the vibration of (say) a continuous beam composed of segments of differing elasticity, with concentrated masses and supports of various kinds. Chapter III surveys existing knowledge concerning the explosive expansion of cavities and the resulting elastic-plastic waves. This difficult subject is treated with great mathematical elegance. Chapter IV gives a very thorough account of the whole field of small deflection plasticity theory and of limit design. It will be invaluable to anyone wishing to do work in this field. Chapter V deals with the important and difficult problem of wave propagation in bars and throws much light on the adequacy of approximate calculation and on the way in which the basic elastic waves combine to give signal velocities of different magnitude. Chapter VI discusses the basic principles of thermoelasticity, following Biot, and applies the results to wave propagation in elastic solids, determining quasi-elastic and quasi-thermal waves. Readers should notice the misprint in equation (2.1). Chapter VII contains a profound study of continuously dislocated crystals and related non-Riemannian spaces, which the author believes will lead to a theory of macroscopic plasticity. Finally Chapter VIII deals with the solution of elastic problems for plates and half-spaces.—W. S. HEMP.

Applied Mathematics

FIELD COMPUTATIONS IN ENGINEERING AND PHYSICS

A. Thom, Professor of Engineering Science, University of Oxford, and

C. J. Apelt, Senior Lecturer in Civil Engineering, University of Queensland

A fast, versatile squaring method of obtaining numerical solutions to partial differential equations in two dimensions, ideally suited to digital computation. "The pioneer work carried out by Thom and by his fellow workers . . . has given the world of mathematics, physics and engineering a splendid series of exact numerical solutions of various outstanding problems of great interest and significance."—PROF. G. TEMPLE IN THE FOREWORD.

viii + 168 *pp.*, 73 *diags.*, 30*s.*

LINEAR DIFFERENTIAL OPERATORS

Cornelius Lanczos, Senior Professor, Department of Theoretical Physics, Dublin Institute for Advanced Studies

A thorough treatment of the General Theory of Green's Functions, and Orthogonal Expansions on the basis of eigenvalue methods, with many examples and about 150 problems, of considerable interest to pure and applied mathematicians, mathematical physicists and engineers, honours and postgraduate students. (*In the press*).

ORDINARY DIFFERENTIAL EQUATIONS AND THEIR SOLUTIONS

G. M. Murphy, Professor of Chemistry, New York University

The co-author of Margenau & Murphy's *Mathematics of Physics and Chemistry* presents a comprehensive collection of methods for solving ordinary differential equations with a compilation of some 2,000 differential equations and their solutions. This book is said to be easier to use than the German language work by Kamke. *ix* + 451 *pp.*, 64*s.*

STATISTICAL PROCESSES AND RELIABILITY ENGINEERING

Prof. Dr. D. N. Chorafas, I.B.M. World Trade Corporation

A complete treatment of statistics for the engineer, in which the principles and methods are explained and then applied to engineering design, computer programming and calculation, cybernetics, quality control and reliability testing. *xiv* + 438 *pp.*, *illus.*, 96*s.*

APPLIED MATHEMATICS FOR ENGINEERS AND SCIENTISTS

S. A. Schelkunoff, Bell Laboratories Series

Readers should have mathematical maturity gained either through use of undergraduate calculus in various subjects or through courses in either advanced calculus or differential equations. The contents have been arranged in order of increasing difficulty. The explanations are thorough with a large number of examples and problems.

472 *pp.*, *illus.*, 71*s.* 6*d.*

INTERNATIONAL DICTIONARY OF APPLIED MATHEMATICS

Edited by W. F. Freiberger, Assoc. Prof. of Applied Maths., Brown University

A key to the terms and the use of mathematics as applied in 32 major fields of science and engineering. Each definition or essay is written by an expert in that particular field—some 40 contributors from both sides of the Atlantic—who, between them, ensure a compilation of great worth and merit. Send for special brochure.

1315 *pages*, 315 *illus.*, 8000 *definitions*, £9 7*s.* 6*d.* **OR** £8 5*s.* 0*d. if ordered by Dec.* 22, 1960.

VAN NOSTRAND

358 KENSINGTON HIGH STREET - LONDON W14 - PUBLISHERS SINCE 1848

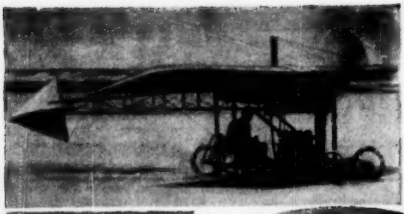

50

50 years of experience are behind the Blackburn Buccaneer

1909 Robert Blackburn designed, built and flew his first aircraft at Marske Sands in Yorkshire.

1960 Latest of a long line, the Blackburn Buccaneer Strike Aircraft, which first flew on its target date in April, 1958, is now in production. Of this aircraft the Ministry of Defence has stated: "In the low-level strike role, the NA.39 (Buccaneer) is ahead of any aircraft in the world"

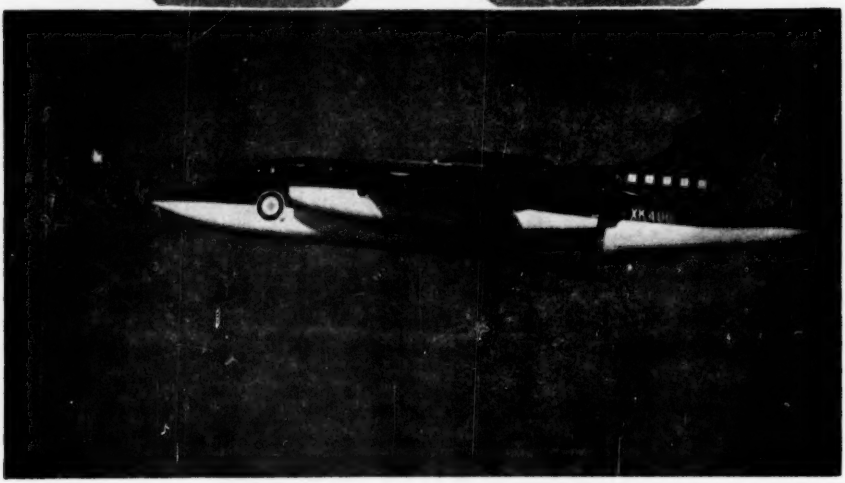

If you are an A.F.R.Ae.S. or possess an equivalent qualification, please write to the Technical Staff Manager, when we shall be pleased to give you details of the opportunities available to experienced men within our technical organisation.

Blackburn Aircraft Limited, Brough, Yorkshire

Member Company of the Hawker Siddeley Group.

A128/d

BRISTOL Aircraft

OPPORTUNITIES FOR WORK ON NEW PROJECTS AT BRISTOL

Bristol Aircraft Limited offer excellent and progressive careers with their research, development and design teams at FILTON to young men or women who have a degree or a Higher National Certificate or Diploma.

Bristol are known throughout the world for their successful turboprop BRITANNIA and the BLOODHOUND Guided Missile.

They can offer interesting and challenging careers on the projects of the future.

Structures Design Engineers
Mechanical Engineers
Dynamics Engineers
Mathematicians **Draughtsmen**
Physicists **Designers**
Aerodynamicists
Systems Engineers
Electrical/Electronic Engineers

If you are interested, write to:–

J. Raimes, Personnel Manager,
Room FW/10/AQ
Bristol Aircraft Limited, FILTON, Bristol,

giving full details of your education, experience and position in which you are interested.

MEMBER COMPANY OF BRITISH AIRCRAFT CORPORATION

LIFT and THRUST from ONE ENGINE— the Revolutionary BS 53 Turbofan

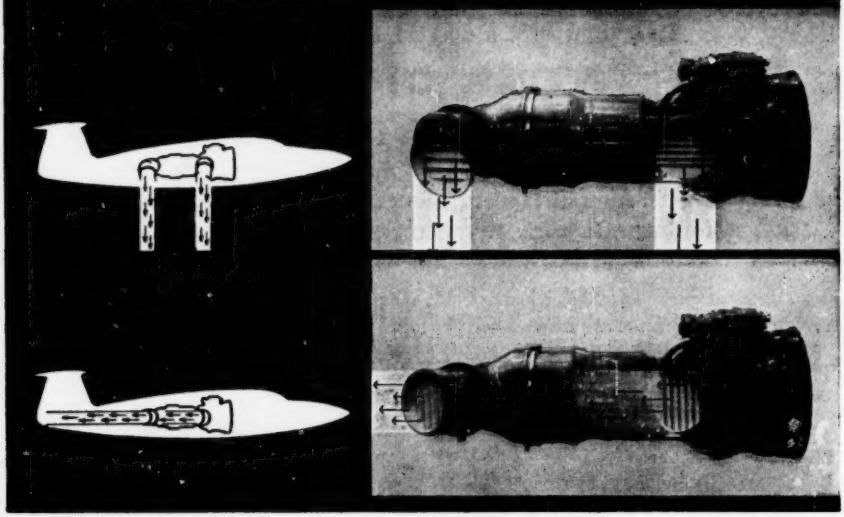

...ANOTHER ENGINEERING ADVANCE BY BRISTOL SIDDELEY

The new Bristol Siddeley BS 53 high-ratio turbofan represents a major engineering breakthrough in the field of aircraft propulsion. Because the BS 53 can be fitted with movable nozzles evenly disposed around the centre of gravity which give directional control to its total thrust, this remarkably versatile engine provides the airframe designer with a *single power source for all conditions of flight.*

VTOL, STOL and normal take-off capability in the same aircraft. Suitable for subsonic or supersonic applications.

High cold-flow ratio gives high thrust for low weight, low fuel consumption and low noise level.

Conventional installation. Operational simplicity. Independent of all fixed ground installations.

Problems of ground erosion, recirculation and ingestion of debris reduced to a minimum.

The Bristol Siddeley BS 53 has already been selected for the Hawker P 1127 VTOL light strike fighter and is supported by the Mutual Weapons Development Programme for NATO.

BRISTOL SIDDELEY ENGINES LIMITED

NOTICE TO CONTRIBUTORS

1. All communications should be addressed to the Editor, The Aeronautical Quarterly, 4 Hamilton Place, London, W.1.

2. Papers for consideration should be typewritten with double spacing and be accompanied by a summary of not more than 250-300 words. *Papers must be as short as possible*, otherwise considerable delay in publication will result, and in any case they should not be longer than twenty foolscap pages. Full descriptions and complete results of work, as written for an internal report, are not suitable for publication in *The Aeronautical Quarterly*, and such reports need to be rewritten in concise form. Only necessary equations should be included in the text; routine mathematics should be omitted or given as an Appendix to the paper. Illustrations should be reduced to a minimum. The titles of papers should be kept short—with sub-titles if necessary.

3. Only simple symbols and formulae should be typewritten. All others should be written clearly in ink. Greek letters should be indicated and a clear distinction drawn between capital and small letters. Particular attention should be paid to the use of alpha and *a*, kappa and *k*, mu and *u*, nu and *v*, eta and *n*. The letter *l* must be distinguished from the numeral 1, and the letter *O* from the zero 0.

   The use of dots, bars, and so on, over letters, or the use of dots as multiplication signs and bars for brackets should be avoided as far as possible.

   Suffixes and prefixes must be indicated clearly and complicated suffixes and prefixes should be avoided.

4. A list of *all* symbols used, both in the illustrations and text, *must* be given whether they are standard or not.

5. *Clear* diagrams or sketches must be submitted for redrawing by the Society's draughtsman.

   Photographs must be not less than half plate size and must be clear black and white glossy prints.

6. References should be given in the form:—
   WARD, G. N. Calculation of Downwash Behind a Supersonic Wing. *The Aeronautical Quarterly*, Vol. I, pp. 35-38, May 1949.

7. The copyright of every paper printed in *The Aeronautical Quarterly* is the property of The Royal Aeronautical Society. Permission to reprint or to use any paper will not be unreasonably refused.

8. It is a condition of publication that the author shall have obtained consent where necessary to use any material in his paper which is copyright or the property of any other person or his employers.

9. Authors will be entitled to 20 reprints of their papers free of charge. This number will be shared between joint authors.

The Aeronautical Quarterly is published at the Offices of The Royal Aeronautical Society, 4 Hamilton Place, Piccadilly, London, W.1, at 15s. 0d. net for a single number to non-members and 7s. 6d. net for a single number to members of The Royal Aeronautical Society. Instructions for Contributors are given above. None of the papers must be taken as expressing the opinion of the Council of The Royal Aeronautical Society unless such is definitely stated to be the case. All communications for publication or advertisement in The Quarterly should be addressed to—The Editor, The Aeronautical Quarterly, 4 Hamilton Place, W.1.

Telephone: Grosvenor 3515 (5 lines). Telegraphic Address: Didaskalos, Audley, London

LIFT and THRUST from ONE ENGINE— the Revolutionary BS 53 Turbofan

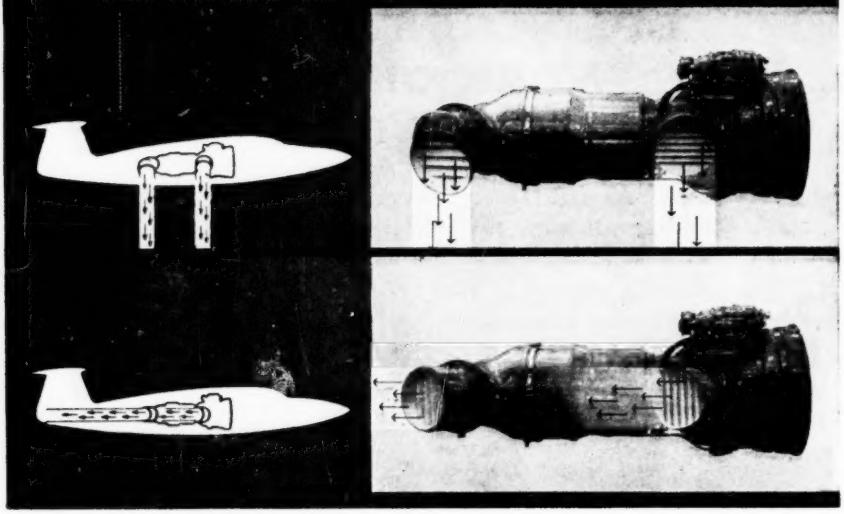

...ANOTHER ENGINEERING ADVANCE BY BRISTOL SIDDELEY

The new Bristol Siddeley BS 53 high-ratio turbofan represents a major engineering breakthrough in the field of aircraft propulsion. Because the BS 53 can be fitted with movable nozzles evenly disposed around the centre of gravity which give directional control to its total thrust, this remarkably versatile engine provides the airframe designer with a *single power source for all conditions of flight.*

VTOL, STOL and normal take-off capability in the same aircraft. Suitable for subsonic or supersonic applications.

High cold-flow ratio gives high thrust for low weight, low fuel consumption and low noise level.

Conventional installation. Operational simplicity. Independent of all fixed ground installations.

Problems of ground erosion, recirculation and ingestion of debris reduced to a minimum.

The Bristol Siddeley BS 53 has already been selected for the Hawker P 1127 VTOL light strike fighter and is supported by the Mutual Weapons Development Programme for NATO.

BRISTOL SIDDELEY ENGINES LIMITED

NOTICE TO CONTRIBUTORS

1. All communications should be addressed to the Editor, The Aeronautical Quarterly, 4 Hamilton Place, London, W.1.

2. Papers for consideration should be typewritten with double spacing and be accompanied by a summary of not more than 250-300 words. *Papers must be as short as possible*, otherwise considerable delay in publication will result, and in any case they should not be longer than twenty foolscap pages. Full descriptions and complete results of work, as written for an internal report, are not suitable for publication in *The Aeronautical Quarterly*, and such reports need to be rewritten in concise form. Only necessary equations should be included in the text; routine mathematics should be omitted or given as an Appendix to the paper. Illustrations should be reduced to a minimum. The titles of papers should be kept short—with sub-titles if necessary.

3. Only simple symbols and formulae should be typewritten. All others should be written clearly in ink. Greek letters should be indicated and a clear distinction drawn between capital and small letters. Particular attention should be paid to the use of alpha and *a*, kappa and *k*, mu and *u*, nu and *v*, eta and *n*. The letter *l* must be distinguished from the numeral 1, and the letter *O* from the zero 0.

   The use of dots, bars, and so on, over letters, or the use of dots as multiplication signs and bars for brackets should be avoided as far as possible.

   Suffixes and prefixes must be indicated clearly and complicated suffixes and prefixes should be avoided.

4. A list of *all* symbols used, both in the illustrations and text, *must* be given whether they are standard or not.

5. *Clear* diagrams or sketches must be submitted for redrawing by the Society's draughtsman.

   Photographs must be not less than half plate size and must be clear black and white glossy prints.

6. References should be given in the form:—
   WARD, G. N. Calculation of Downwash Behind a Supersonic Wing. *The Aeronautical Quarterly*, Vol. I, pp. 35-38, May 1949.

7. The copyright of every paper printed in *The Aeronautical Quarterly* is the property of The Royal Aeronautical Society. Permission to reprint or to use any paper will not be unreasonably refused.

8. It is a condition of publication that the author shall have obtained consent where necessary to use any material in his paper which is copyright or the property of any other person or his employers.

9. Authors will be entitled to 20 reprints of their papers free of charge. This number will be shared between joint authors.

The Aeronautical Quarterly is published at the Offices of The Royal Aeronautical Society, 4 Hamilton Place, Piccadilly, London, W.1, at 15s. 0d. net for a single number to non-members and 7s. 6d. net for a single number to members of The Royal Aeronautical Society. Instructions for Contributors are given above. None of the papers must be taken as expressing the opinion of the Council of The Royal Aeronautical Society unless such is definitely stated to be the case. All communications for publication or advertisement in The Quarterly should be addressed to—The Editor, The Aeronautical Quarterly, 4 Hamilton Place, W.1.

Telephone: Grosvenor 3515 (5 lines). Telegraphic Address: Didaskalos, Audley, London

THE AERONAUTICAL QUARTERLY

It is the aim of *The Aeronautical Quarterly* to attract not only original papers contributing to aeronautical science and engineering, and papers developing new or improved methods of analysis and experimental techniques, but also papers on allied sciences which have a bearing on aeronautical problems. *The Aeronautical Quarterly* is open to authors of any nationality and is not restricted to members of the Society.

Most papers can be published within nine months of receipt. Short papers, of not more than 2,000 words, are published much more quickly.

A selection of the more specialised papers read before the Society during the current lecture session will be published in *The Aeronautical Quarterly*.

VOLUME XI

Volume XI of *The Aeronautical Quarterly* is published in four parts, in February, May, August and November 1960. The prices, *including postage and packing*, are:—

	To Members of the Society		*To Non-Members*	
	£ s. d.		£ s. d.	
Per Part	8 0	($1.15)	15 6	($2.20)
Subscription (4 parts)	1 12 0	($4.50)	3 2 0	($8.70)

PRINTED BY THE LEWES PRESS WIGHTMAN & CO. LTD., LEWES, SUSSEX, ENGLAND, AND PUBLISHED BY THE ROYAL AERONAUTICAL SOCIETY, 4 HAMILTON PLACE, LONDON W.1, ENGLAND.